PEOPLE'S DEMOCRATIC REPUBLIC OF ALGERIA

MINISTRY OF HIGHER EDUCATION AND SCIENTIFIC RESEARCH

AMAR TELIDJI UNIVERSITY- LAGHOUAT

FACULTY OF TECHNOLOGY

Dissertation Master Degree in Microelectronic Engineering

Presented by: GUEDDOUDA Mustapha Kamal

Performance enhancement of a novel tandem CZTSe structure based solar cells: A numerical simulation

Board of Examiners:

Chairman:	**MAA**	VILBOIS Leila	**UATL**
Examiner:	**MCA**	MOUHOUB Abdelhafid	**UATL**
Supervisor:	**MCA**	SELMANE Naceur	**UATL**
Co-supervisor:	**Prof**	CHEKNANE Ali	**UATL**

2022/2023

Acknowledgments

First of all, I would like to express my gratitude to ALLAH the Almighty and Merciful, who has bestowed upon me the strength and patience to complete this modest work. Secondly, I extend my sincere thanks to my supervisor, Dr. Naceur Selmane, for his invaluable guidance and support throughout the duration of this project. I am deeply grateful for his precious advice and assistance. I would like to thank sincerely Pr. Ali Cheknane for being a role model and a leader to this institution, and for us the students.

I would also like to Convey my sincere appreciation to the members of the jury for their interest in my research and for agreeing to evaluate and enhance my work with their valuable suggestions. Their contribution is highly valued and appreciated.

Furthermore, I would like to express my thanks to all the individuals who have contributed, whether directly or indirectly, to the completion of this work. Your participation, no matter how near or far, has played a significant role in its realization.

Finally, I would like to express my profound gratitude to Dr. Marc Burgelman and his team of development.

إهداء

أهدي هذا العمل القيم لوالدي الغالي، ولأمي
العزيزة التي كانت سندًا لي طوال هذه الرحلة
وقد أنارت لي الطريق الى ان توفاها الله،
رحمهما الله برحمته الواسعة.

أود أيضًا أن أهدي هذا العمل الثمين لزوجتي
العزيزة التي صبرت ووقفت بجانبي
وساعدتني، ولابني عبدالله، ولابنتي بيان

وأرغب أيضًا في تقديم هذا العمل لأختي
الغالية وإخوتي الأعزاء.


بسم الله الرحمن الرحيم

List of figures

Chapter I:

Chapter II:

Chapter III:

List of tables

Chapter II

Chapter III

List of Symbols

- **CIGS=** Copper Indium Gallium Selenide
- **AM=** Air Mass
- **PV=** Photovoltaic
- **PC=** Photochemical
- **PB=** Photobiological
- **UV=** Ultraviolet
- **IR=** Infrared
- **CET=** Coal Equivalent Tons
- **kWh=** Kilowatt-hour
- **n_r=** Refractive Index
- **P-N=** Semiconductor type P-type N
- **R_s=** Series Resistance
- **R_{sh}=** Shunt Resistance
- **SUS=** Swiss Units of Solar
- **kWhr=** Kilowatt-hour
- **CPV=** Concentration Photovoltaics
- **DSC=** Dye-Sensitized Solar Cell
- **TiO_2=** Titanium Dioxide
- **J-V=** Current Density-Voltage
- **V_{oc}=** Open-Circuit Voltage
- **I_{sc}=** Short-Circuit Current
- **J_{sc}=** Short-Circuit Current Density
- **I_{mp}=** Maximum Power Point Current
- **V_{mp}=** Maximum Power Point Voltage
- **FF=** Fill Factor
- **η=** Efficiency
- **QE=** Quantum Efficiency
- **Si=** Silicon
- **CdTe=** Cadmium Telluride
- **CIS=** Copper Indium Selenide
- **GaAs=** Gallium Arsenide
- **AlGaAs=** Aluminium Gallium Arsenide
- **UHV=** Ultra-High Vacuum
- **SIMS=** Secondary Ion Mass Spectrometer
- **ESCA=** Electron Spectroscopy for Chemical Analysis
- **LEED=** Low-Energy Electron Diffraction
- **HEED=** High-Energy Electron Diffraction
- **SCAPS=** Solar Cell Analysis and Performance Simulation
- **ELIS=** Electronics and Information Systems
- **MB=** Megabytes

- **a-Si=** Amorphous Silicon
- **LW/CVI=** Lab Windows of National Instruments developer
- **IV=** Current-Voltage
- **C=** Capacitance
- **G=** Conductance
- **C-V=** Capacitance-Voltage
- **C-f=** Capacitance-Frequency
- **RbGeI3=** Rubidium Germanium Iodide
- **CZTS=** Copper Zinc Tin Sulphide
- **Fn=** Fermi level
- **Eg=** Band gap
- **µm=** Micrometre
- **ABX_3=** Perovskite structure notation (A = organic cation, B = metal cation, X = halide anion)
- **HTL=** Hole Transport Layer
- **ETL=** Electron Transport Layer
- **n-ZnO=** n-Type Zinc Oxide
- **n-CZTSe=** n-Type Copper Zinc Tin Selenide
- **p-CZTS=** p-Type Copper Zinc Tin Sulphide
- **n-CdS=** n-Type Cadmium Sulphide
- **p-CIGS=** p-Type Copper Indium Gallium Selenide
- **AM=** Air Mass
- **I-V=** Current-Voltage
- **Ev=** Valence Band
- **Ec=** Conduction Band
- **eV=** Electron Volt

Contents:

General introduction

General introduction

Since ancient times, energy has served as the driving force behind human activities. It continues to hold immense importance in daily life and the progress of nations. Among the various energy sources, the sun stands out for its unique qualities. Unlike other sources, it is renewable, abundant, and clean. Additionally, on an annual basis, the sun generously bestows the Earth with an energy surplus that surpasses the world's total consumption.

Electricity, renowned for its non-polluting and silent nature, is a prime example of energy conversion through solar means. This conversion is facilitated by a device known as a "Solar cell," functioning based on the "Photovoltaic effect." Presently, significant research efforts are dedicated to solar cells, striving to achieve an ideal balance between energy efficiency and cost-effectiveness. To enhance practicality, lightweight, and affordability, innovative thin-layered cells have been manufactured. These advancements aim to amplify surface area while simultaneously reducing weight and overall expense.

The energy conversion efficiency of CIGS modules which is the core of our research, is in the range of 12-15%, but for small area laboratory cells, the efficiency milestone of > 20% was achieved in 2010. In 2014, Solar Frontier has achieved 20.8% energy conversion efficiency for small area CIGS cells[1].

The aim of this study, is to conduct a numerical simulation study on a novel and previously unexplored combination of a CIGS/CZTSe double absorber and a inorganic perovskite $RbGeI_3$ layer in the form of a tandem solar cell. The objective is to explore the performance and characteristics of this unique tandem solar cell design using computational modelling techniques.

The first chapter is dedicated to theoretical study of the conversion of light to electricity, by taking a glance on the sun and photons, continuing with understanding the effect of the light conversion, that leads us to viewing the technologies that achieve this type of conversion, then understanding the fundamental material of our solar cell to slowly work our way through understanding the tandem structure that can achieve efficiencies close to 40%.

The second chapter we will describe the simulation program used in this study, continuing to explore more materials like the CZTSe and the $RbGeI_3$ inorganic perovskite

that captivated many scientists in the field of solar cell fabrication, after that we will glimpse at the three structures that will be used in this study, and the data that will be added as material properties.

Finally, the last chapter is for the simulation and discussion of the results, commencing by CIGS absorber layer, continuing by adding additional absorber layer CZTSe achieve even higher efficiency, completing with a tandem structure. All this while optimising the new cell created each step of the way to achieve high efficiency.

The aim of this study is to explore the performance and characteristics of a novel tandem solar cell design combining a CIGS/CZTSe double absorber and an inorganic perovskite RbGeI3 layer. Through numerical simulations and computational modelling techniques, the researchers seek to optimize the new cell structure at each step and achieve efficiencies close to 40%. However, several issues need to be addressed in order to overcome the existing challenges:

1. How can the energy conversion efficiency of CIGS modules be improved to reach the desired 40% of efficiency?
2. Can the materials CZTSe and RbGeI3 be integrated into the novel solar cell? If so, how can they be integrated?
3. What are the best optimized properties for the overall solar cell?

Chapter I

General notions about

solar cells

I.1. Introduction:

This chapter aims to provide a theoretical exploration of tandem solar cells. To begin with, we will delve into comprehending the sun and its intricate workings. Specifically, we will examine the nature of photons and solar radiation, laying a foundation for understanding the operation of solar cells.

In order to gain insights into the functioning of solar cells, it becomes imperative to study their basic structure and the corresponding band diagram. This analysis will enable us to grasp how electrons and holes behave upon exposure to solar radiation, shedding light on the underlying mechanisms.

Moving forward, our attention will shift towards investigating the absorber materials employed in our simulation, namely CIGS and perovskite materials. By studying their properties and characteristics, we can gain a deeper understanding of their role in the overall performance of tandem solar cells.

Consequently, these fundamental studies and explorations will pave the way for an in-depth examination of the configuration of tandem solar cells.

I.2. Solar energy

I.2.1. The sun

The sun has played a dominant role since time immemorial for different natural activities in the universe at large and in the earth in particular for the formation of fossil and renewable energy sources. It will continue to do so until the end of the earth's remaining life, which is predicted to be about 5×10^9 years. Deposited fossil fuels, in the form of coal, that are used through combustion are expected to last for approximately the next 300 years at the most, and from then onward human beings will be left with renewable energy resources only.

The diameter of the sun is R = 1.39 $\times10^6$ km. The sun is an internal energy generator and distributor for other planets such as the earth. It is estimated that 90% of the energy is generated in the region between 0 and 0.23R, which contains 40% of the sun's mass. The core temperature varies between 8 $\times10^6$ K and 40 $\times10^6$ K and the density is estimated at about 100 times that of water. At a distance 0.7R from the centre the temperature drops to about 130,000 K where the density is about 70 kg/m^3. The space from 0.7R to 1.0R is known as the convective zone with a temperature of about 5000 K and the density is about 10−5 kg/m^3.

An account of the earth's energy sources and demand cannot be regarded as complete without a discussion of the sun, the solar system, and the place of the earth within this system. In general, the sun supplies the energy absorbed in the short term by the earth's atmosphere and oceans, but in the long term by the lithosphere where the fossil fuels are embedded. Conversion of some of the sun's energy into thermal energy derives the general atmospheric circulation (Becquerel 1839). A small portion of this energy in the atmosphere appears in the form of the kinetic energy of the winds, which in turn drive the ocean circulations. Some of the solar energy is intercepted by plants and is transformed by photosynthesis into biomass. In turn, a large portion of this is ultimately converted into heat energy by chemical oxidation within the bodies of animals and by the decomposition and burning of vegetable matter.
On the other hand, a very small proportion of the photosynthetic process produces organic residues, which may eventually be transformed into fossil fuels. It is estimated that the solar radiation intercepted by the earth in 10 days is equivalent to the heat that would be released by the combustion of all known reserves of fossil fuels on earth.

The sun radiates electromagnetic energy in terms of photons which are light particles. Almost one third of this incident energy on the earth is reflected back, but the rest is absorbed

and is, eventually, retransmitted to deep space in terms of long-wave infrared radiation. Today, the earth radiates just as much energy as it receives and sits in a stable energy balance at a temperature suitable for life on the earth. In fact, solar radiation is in the form of white light and it spreads over a wider spectrum of wavelengths from the short-wave infrared to ultraviolet. The wavelength distribution is directly dependent on the temperature of the sun's surface.

The total power that is incident on the earth's surface from the sun every year is 1.73×10^{14} kW and this is equivalent to 1.5×10^{18} kWh annually, which is equivalent to 1.9×10^{14} coal equivalent tons (CET). Compared to the annual world consumption of almost 10^{10} CET, this is a very huge and unappreciable amount. It is approximately 10,000 times greater than that which is consumed on the earth annually. In engineering terms, this energy is considered to be uniformly spread all over the world's surface and, hence, the amount that falls on one square meter at noon time is about 1 kW in the tropical regions. The amount of solar power available per unit area is known as irradiance or radiant-flux density. This solar power density varies with latitude, elevation, and season of the year in addition to time in a particular day. Most of the developing countries lie within the tropical belt of the world where there are high solar power densities and, consequently, they want to exploit this source in the most beneficial ways. On the other hand, about 80% of the world's population lives between latitudes 35° N and 35° S. These regions receive the sun's radiation for almost 3000 – 4000 h/year. In solar power density terms, this is equivalent to around 2000 kWh/year, which is 0.25 CET/year.[2]

Additionally, in these low latitude regions, seasonal sunlight hour changes are not significant. This means that these areas receive the sun's radiation almost uniformly throughout the whole year. Apart from the solar radiation, the sunlight also carries energy. It is possible to split the light into three overlapping groups:

1. Photovoltaic (*PV*) group: produces electricity directly from the sun's light

2. Photochemical (PC) group: produces electricity or light and gaseous fuels by means of non-living chemical processes

3. Photobiological (PB) group: produces food (animal and human fuel) and gaseous fuels by means of living organisms or plants.

The last two groups also share the term “photosynthesis”, which means literally the building (synthesizing) by light.

I.2.2. Photons and light

Electromagnetic radiation can be viewed as being composed of electromagnetic waves, or as consisting of massless energy quanta called photons. Radiation, in either view, can be classified according to its wavelength, λ, or frequency ν. These quantities hold the relationship:

$$\boldsymbol{\lambda = \frac{c_\gamma}{\nu}} \qquad \text{(I. 1)}$$

where cγ is the speed of light, which depends on the refractive index of the medium, n_r, through which the radiation travels, as:

$$\boldsymbol{c_\gamma = \frac{c}{n_r}} \qquad \text{(I. 2)}$$

The angular frequency is ω = 2πν. h is Planck’s constant and ħ = h/2π. The photon energy can be converted to wavelength using the formula:

$$\lambda(\text{nm}) = \frac{1240}{h\nu\ (\text{eV})} \qquad \text{(I. 3)}$$

The parts of the electromagnetic spectrum are indicated in Figure I. 1. The optical region, which is the wavelength region of interest for solar energy conversion and lighting, is the long-wave portion comprising the ultraviolet region (UV), the visible-light region extending from approximately λ = 0.4–0.7 μm, and the infrared region (IR) from beyond the red end of the visible spectrum to about λ = 1000 μm. We denote light the part of the electromagnetic spectrum that provokes a visual response in humans. The solar spectrum shows two different fashions: the number of photons arriving at the top of the earth’s atmosphere, and at the earth’s surface, per interval of wavelength. Approximately 50% of solar irradiation occurs outside the visible range, especially in the IR; therefore, this part provides radiant energy and heat but not light. The spectral differences above and below the atmosphere are due to the filtering of certain wavelengths[3].

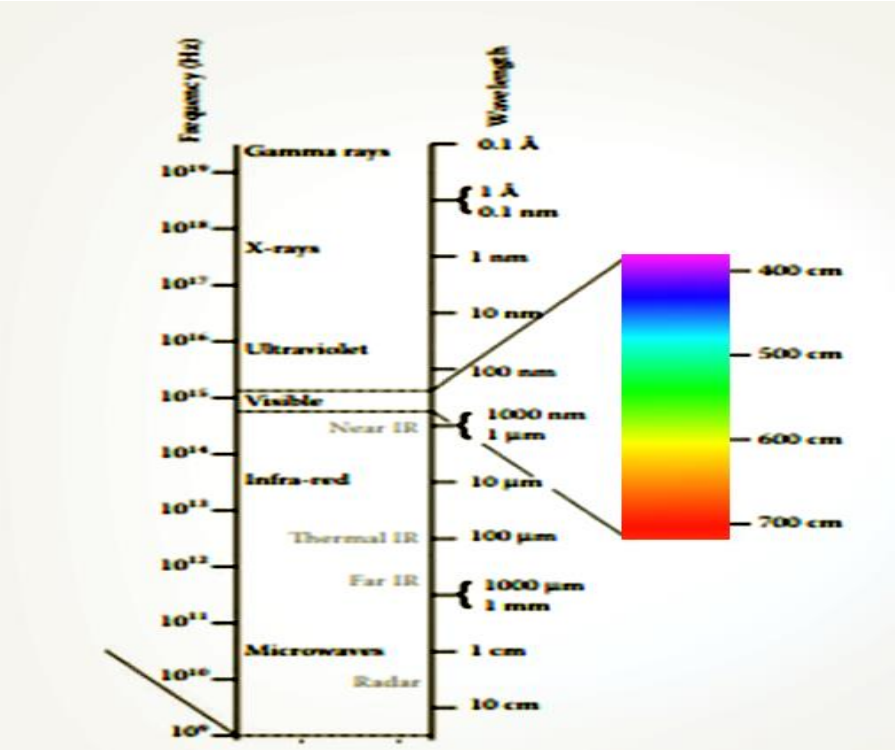

Figure I. 1:Electromagnetic spectrum in the range between microwaves and gamma rays.[2]

I.2.3. Notions on solar radiation

The radiation emitted by the sun corresponds to that of a black body at a temperature of 5900°K. Above the atmosphere, the radiation intensity measures 1.35 kW/m^2, with a spectrum centred around lambda=0.48 µm.

However, at the ground surface, the power density reduces to only 0.9 kW/m^2. This reduction is primarily due to absorption by substances like ozone, water, and carbon dioxide. Additionally, the spectrum undergoes changes, exhibiting absorption bands instead of a continuous pattern.

To account for the atmospheric effects, the concept of air mass (AM) is employed. The air mass is defined as AM=1/cos(alpha), where alpha represents the angle between the sun's direction and the vertical. Specifically, AM1.5 represents sunlight reaching the ground under clear weather conditions, with a surface area of one square meter making an angle of 48° with the equator. It's worth noting that AM1.5D and AM1.5G spectra are distinguished, representing direct and global fluxes, respectively (direct + diffuse).

Furthermore, different air mass values indicate specific sun positions. For instance, AM1 corresponds to the sun directly overhead (alpha=0), while AM4 signifies the sun near the horizon (alpha=75°). On the other hand, AM0 specifies conditions above the atmosphere [4].

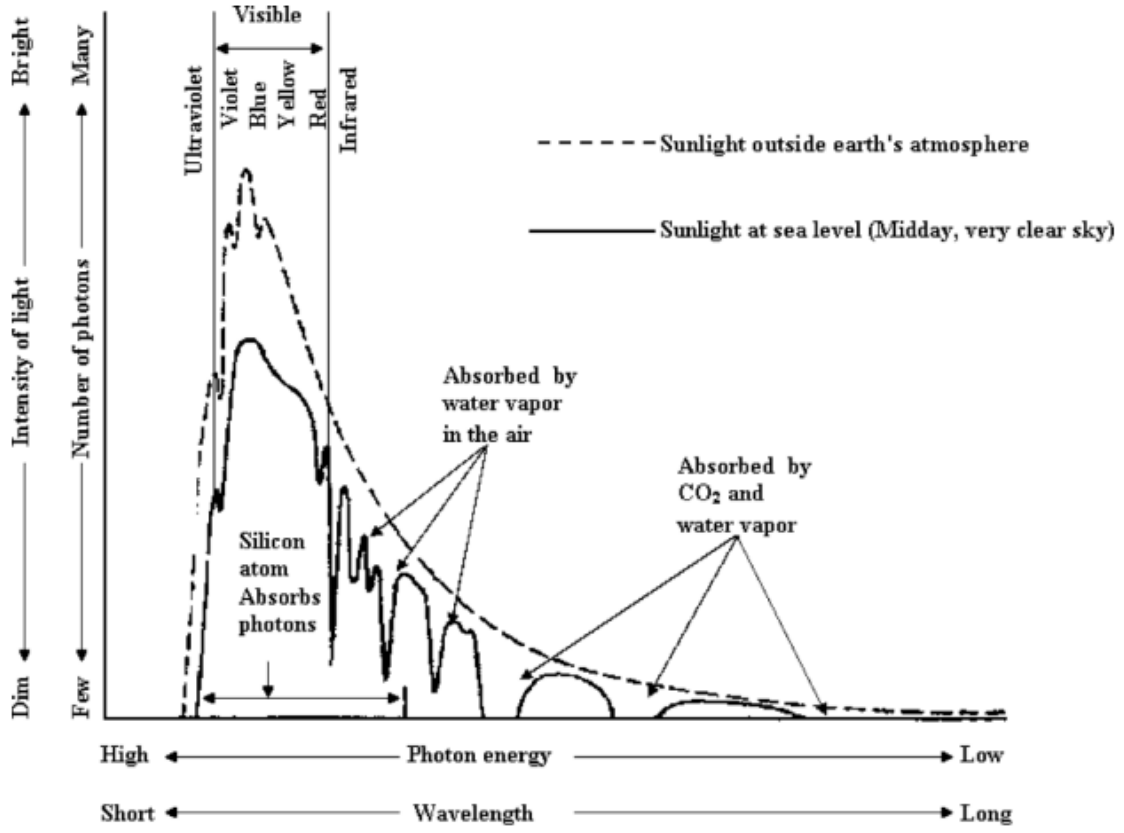

Figure I. 2: Solaire spectre at the earth atmosphere [2]

I.3. Basic structure of a photovoltaic cell:

Solar power is the most reliable source of electricity in the world today. Photovoltaic *PV* modules generate electricity when they are exposed to sunlight. The actual creation of usable electrical current in a solar cell takes place at the atomic level. The most commonly available solar cells are made from high-grade silicon that is treated with negatively and positively charged semiconductors, phosphorous and boron. This process is called "doping. When light energy (photons) strikes the face of the cell, it excites the electrons within the cell. This flow of electrons (current) from the negative semi-conductor (phosphorous) to the positive semi-conductor (boron) is what we call the photovoltaic effect.

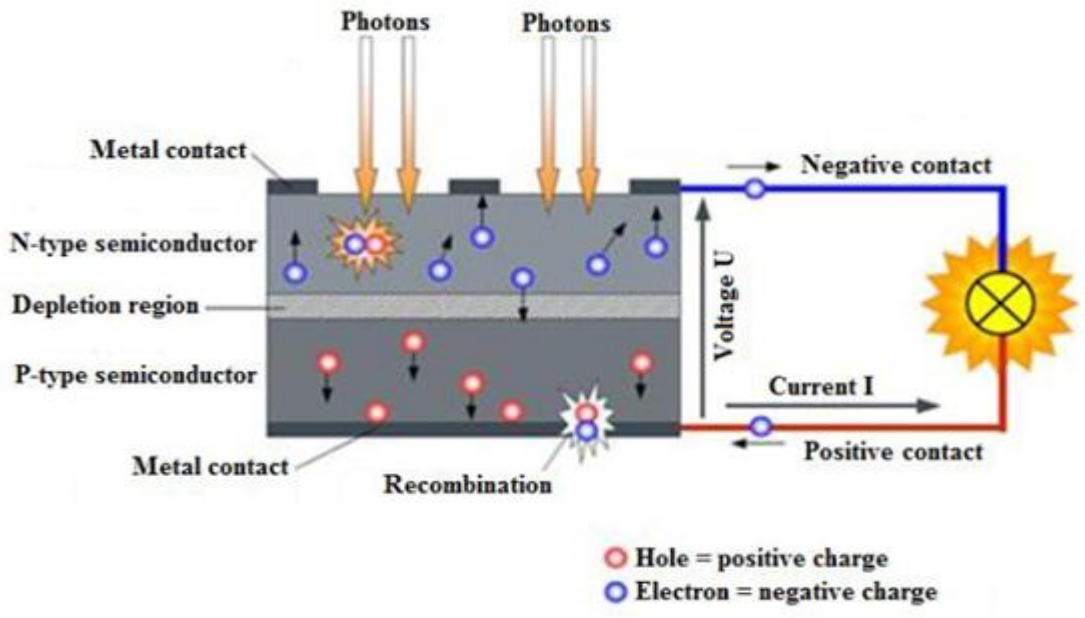

Figure I.3: Working principle of solar cell [5]

Therefore, in the field of solar energy, the material used in photovoltaic cells must have two energy levels and be conductive enough to allow the flow of current. This is why semiconductors are highly valued in the solar industry.

To efficiently gather the produced electron/hole pairs, an electric field is needed to separate them. The most common method is to use a P-N junction, although other structures like heterojunctions and Schottky diodes can also be used. This explains how photovoltaic cells operate. The incident photons create carriers in the N and P region and in the space charge region[6].

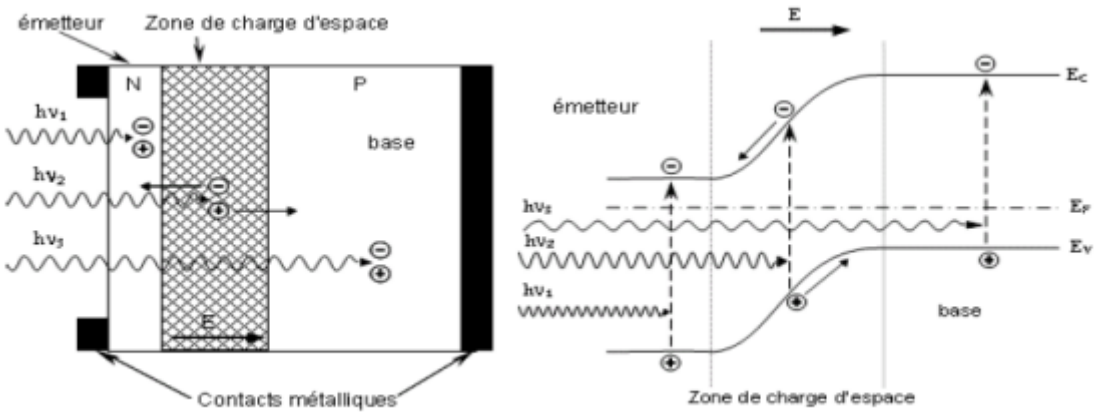

Figure I. 4: Schematic diagrams of the operation of a solar cell (left image) is band diagram (right image) of a Photovoltaic cell. [7]

I.4. Equivalent Diagram for the solar cell:

a) Single Junction solar cell:

The corresponding schematic can be depicted as an ideal diode linked in parallel with a current source, while incorporating series resistances R_s and shunt resistance R_{sh} to account for losses resulting from layer resistivity and leakage currents.

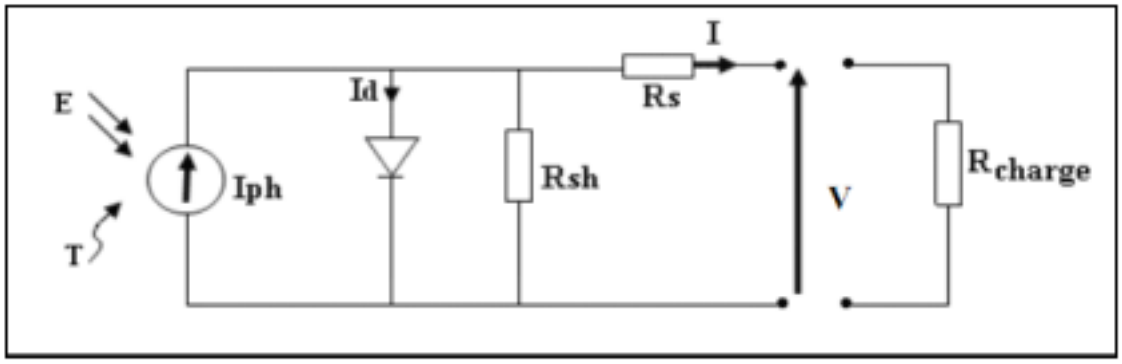

Figure I. 5: Equivalent diagram for the solar cell

b) Double-junction tandem solar cell:

This is an example of a tandem solar cell equivalent circuit. It is similar to the previous one, but it includes an additional stage. As it was demonstrated previously the shunt resistor and series resistance can be used to model the electrical losses in the solar cell.

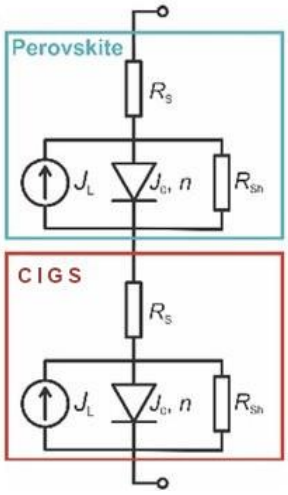

Figure I. 6. Equivalent diagram for the tandem solar cell [8]

I.5. Historical background of the solar cell development

Solar cell technology, which directly converts sunlight into electricity using suitable materials, has undergone significant development in recent decades. Originally a curiosity in laboratories for over a century, solar cells initially provided power for spacecraft and have more recently been adopted for terrestrial systems. This progress stems from the realization that traditional fossil energy resources like coal, oil, and gas are not only limited but also contribute to unpredictable climate changes through carbon dioxide emissions. Concerns about environmental pollution have also discredited nuclear power as a long-term alternative. In light of these challenges, utilizing sunlight presents a viable solution to global energy problems.

Solar cells operate based on the photovoltaic effect, first discovered by Becquerel in 1839 when studying the behaviour of solids in electrolyte solutions. Becquerel noticed that metal plates immersed in an electrolyte, when exposed to sunlight, produced a small voltage and current. Subsequently, selenium (in 1876) and later cuprous oxide (in the 1900s) exhibited light-dependent voltages, indicating that semiconductors would be promising for photovoltaic energy conversion. Technological development began with the diffused silicon p-n junction in 1954, a precursor to modern silicon solar cells, which efficiently converted light into electricity. Concurrently, the development of cuprous sulphide/cadmium sulphide heterojunctions paved the way for thin film solar cell devices. Initially, solar cells found applications in small-scale settings, but their true impact was realized with the advent of space exploration, where the need for a reliable and durable power source drove their deployment. By 1958, silicon solar cells were being used in spacecraft.

Interest in solar cells as an alternative energy source for terrestrial applications grew in the mid-1970s following the Middle East political crisis and oil embargo, coupled with the recognition of fossil fuel limitations. Increased research efforts led to improved efficiencies of silicon solar cells, significant reduction in energy costs, and the development of new photovoltaic materials and devices. These advancements, combined with increased production volume and cost-effective solar cell technologies, allowed the achievement of key milestones. The target set in 1986 aimed for the cost of electricity from a photovoltaic plant operating for 30 years to be around 0.06 SUS/kWhr. Attaining this target required module efficiencies of 15-20% for flat plate panel systems and 25-30% for systems operating under concentrated sunlight. Throughout the 1980s, pilot production stages evaluated new

solar cell materials and innovative device concepts, presenting several promising options for future development. However, the breakthrough of solar technology as a competitive energy source has not been fully realized, primarily due to the current limitations in achieving laboratory-level efficiencies. Additionally, the high cost of fossil and nuclear power acts as a barrier to wider adoption of photovoltaic technology.

A comprehensive comparison of alternative energy systems is complex and must consider the full costs to society, including environmental and climatic effects, hidden subsidies, and the production of intermediate goods. While these external costs are just beginning to be considered, they have already influenced the energy policies of various European countries. Despite solar cell technology not yet reaching maturity, it is expected to contribute around 5-7% of total energy consumption in the next decade, offering a realistic and promising energy solution for the future.

A photovoltaic system comprises multiple components, starting from the solar cell itself to the module, the array of modules, and the entire plant. Among these components, the solar cell remains the primary challenge for technological feasibility. Therefore, research into photovoltaic alternatives is crucial to enhance the competitiveness of the technology. This research encompasses the development of low-cost techniques, higher efficiency cells utilizing new materials and concepts, and thin films that require less material. Essential to any option is successful customization of the semiconductor material and precise control of the electro-optical properties during each processing step. The following discussion will explore various cell concepts, with a particular focus on the material properties that ultimately determine solar cell performance [9].

I.6. Technologies of solar cells

There have been many generations of solar cells in the past decades, and we will briefly mention them [10], also There are my categorisation of solar cell technologies I should precise that the classification of the technology are taken from a lecture from [11] :

I.6.1. First generation Silicone based solar cells

I.6.1.1. Mono-crystalline silicon cells

These cells are made from pure mono-crystalline silicon. The silicon has a single and continuous crystal lattice structure with almost no defects or impurities. The principal advantage of mono-crystalline cells is their high efficiency, typically around 15 %, although

the manufacturing process required to produce mono-crystalline silicon is complicated, resulting in slightly higher costs than other technologies. Different manufacturing methods are used, depending largely upon the Czochralski method of growing, or pulling a perfect crystal that has a solid, cylindrical shape. EFG (Edge-defined Film-fed Growth) has become popular, where the cells are cut from an octagon, to allow higher packing densities in modules. Another approach deposits grown films of crystalline silicon onto a low- cost substrate. The cost of silicon ingot sawing is eliminated and the quantity of silicon per solar module can be reduced significantly. A third approach is a string ribbon technique, where two high temperature strings are pulled vertically through a shallow silicon melt and the molten silicon expands and freezes between the strings.

Figure I. 7: Monocrystalline silicon cell and photovoltaic module [3]

I.6.1.2.Poly- or multi-crystalline silicon cells

Poly-crystalline (also called multi-crystalline) cells are produced using ingots of multi-crystalline silicon. In the manufacturing process, molten silicon is cast into ingots, which are square or rectangular in shape, and allowed to cool so as to form large crystals. These ingots are then cut into very thin wafers and assembled into complete cells. New manufacturing methods also use the approach of grown films of poly-crystalline silicon on a low-cost substrate. Such substrates have included a metallurgical- grade silicon sheet, stainless steel, ceramics and quartz glass, using a variety of growth techniques to deposit silicon films onto these substrates. Poly-crystalline cells are cheaper to produce than mono-crystalline cells, due to the simpler manufacturing process. They tend to be slightly less efficient however, with average efficiencies of around 12 %.

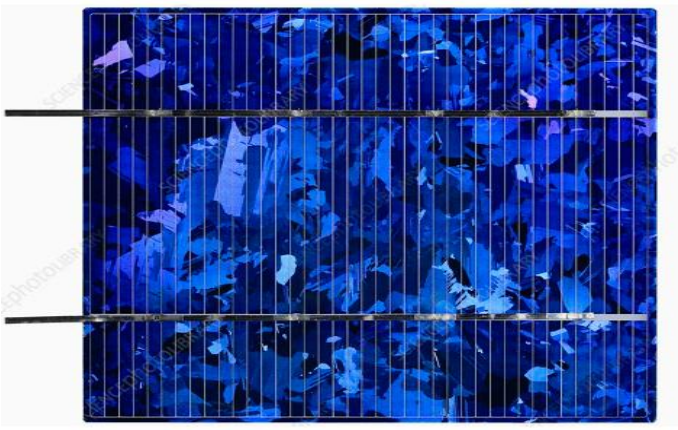

Figure I. 8: Polycrystalline solar cell [4]

I.6.1.3.Amorphous silicon cells

Amorphous silicon cells are composed of silicon atoms in a thin homogenous layer, rather than a crystal structure. Amorphous silicon is produced by deposition onto a substrate, rather than wafer sawing, so the cells can be thinner. For this reason. amorphous silicon is also known as a 'thin film' *PV* technology. Amorphous silicon can be deposited on a wide range of substrates, both rigid and flexible, which makes it ideal for curved surfaces and 'fold-away' modules. Amorphous cells are. however, less efficient than crystalline-based cells, with typical efficiencies of around 6%, but they require less material and are therefore cheaper to produce. Their low cost makes them ideally suited for many applications where high efficiency is not required and low cost is important. For instance, their early market has been in appliances such as calculators and watches.

I.6.2. Second generation of solar cell

Thin films solar cell and number of other promising materials such as copper indium diselenide (CIS), and cadmium telluride (CdTe), are now being used for *PV* modules. The attraction of these technologies is that they can be manufactured using relatively inexpensive industrial processes, certainly in comparison to crystalline silicon technologies, and typically offer higher module efficiencies than amorphous silicon. Some of the raw materials required, however, are less abundant than silicon and there are lingering concerns over the environmental toxicity of some of the elements used, although it appears possible to overcome these, with careful manufacturing, recycling and disposal processes.

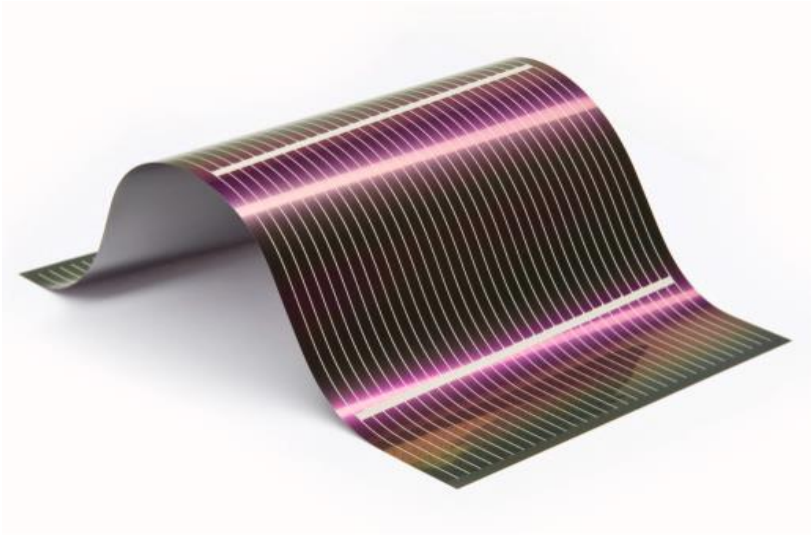

Figure I. 9: Thin film solar cell [5]

I.6.3. Third generation of solar cell

I.6.3.1. Perovskite solar cells

They are the new generation of solar cells that appear to have a very good chance of contributing to large scale solar energy production based on their high EFFICIENCY and compatibility with scalable processes and are therefore included in this newsletter. Perovskite solar cells warrant discussion because never before in the history of solar cell research has such rapid progress in increasing the efficiency been witnessed as that which has occurred for these solar cells[15].

I.6.3.2. Polymer collar cells

these solar cells are fabricated from solution-processing techniques and have unique prospects for achieving low-cost solar energy harvesting, owing to their material and manufacturing advantages. The potential applications of polymer solar cells are broad, ranging from flexible solar modules and semi-transparent solar cells in windows, to building applications and even photon recycling in liquid-crystal displays [16].

I.6.4. Future generation of solar cells:

I.6.4.1. Multijunction solar cells

Multijunction solar cells were first introduced by the Research Triangle Institute and by Varian Research Centre in the late 1970s to mid-1980s when dual-junction (2-junction)

devices were formed from an AlGaAs junction stacked or grown on top of a GaAs junction, and interconnected by a semiconductor tunnel junction [17]. Multijunction solar cell can achieve maximum theoretical efficiency limit of 86.8% [18].

I.6.4.2. Concentration photovoltaics

Concentration photovoltaics *CPV* seems to be the much-needed breakthrough enabling the solar energy industry to be competitive in the power generation market. Although, discovered more than three decades ago, this technology did not gain the needed momentum due to several reasons. Today, with increasing solar cells efficiencies and their associated high costs for manufacture, *CPV* technology is back into business to make the best use of the technology advancement and the solar cell materials [19].

I.6.5. Other form of solar cell technologies

Dye-sensitised Solar Cell *DSC* technology is best considered as artificial photosynthesis. It performs well under indirect radiation, during cloudy conditions, and when temporarily or permanently partially shaded. *DSC* technology has been dominated by the Grätzel titanium dioxide TiO, cell. Particles of titanium dioxide are coated with a photosensitive dye and suspended between two electrodes in a solution containing iodine ions. When this dye is exposed to light energy, some of its electrons jump on to the titanium dioxide particles, which are then attracted to one of the electrodes. At the same time, the iodine ions transport electrons back from the other electrode to replenish the dye particles. This creates a flow of electrons around the circuit. Efficiencies over time are still to be established but technically could achieve around 10% or more, and are very effective over a wide range of sunlight conditions[10].

I.7. Performance characterization of solar cells

The main method for measuring the performance of a solar cell is the measurement of the current (density) as a function of voltage, providing I or (J)-V characteristics. In this method, a time varying bias voltage is applied to the device and at the time the current is recorded. Typically, the time varying voltage is swept from a negative value or zero to a positive value. The output J-V characteristics can be measured while the device under test is in dark conditions or under illumination. In the case of illumination, the device is illuminated by a light source, which is usually a solar simulator. Such a light source is designed to generate the solar radiation spectrum. a typical J-V of a solar cell in dark condition and under

illumination. The dark J-V characteristic of a solar cell equals the J-V characteristic of a diode, which, for a classical p-n junction[20].

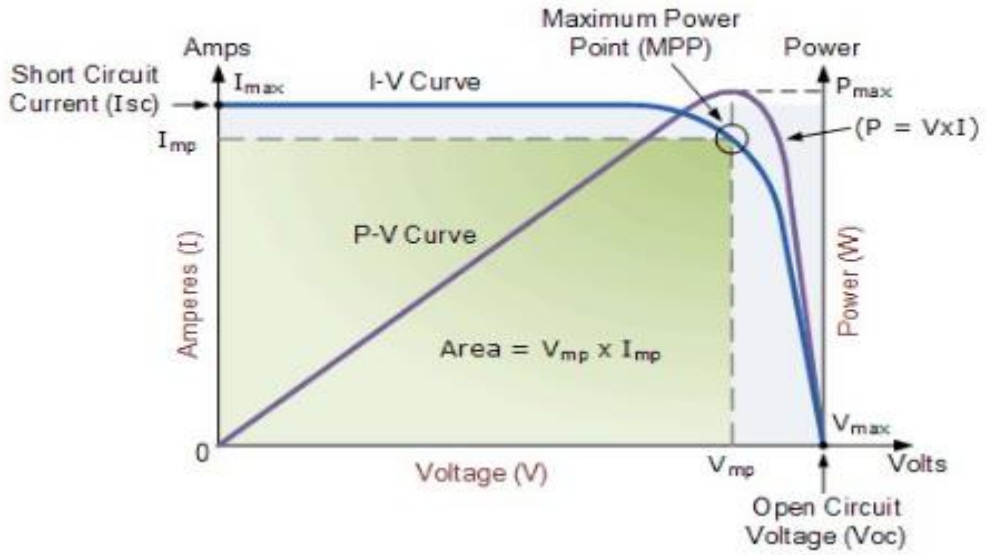

Figure I. 10: Electrical characteristics of photovoltaic cell [16]

The electrical characteristics of a photovoltaic array are summarized in the relationship between the output current and voltage. The amount and intensity of solar insolation (solar irradiance) controls the amount of output current I or J to refer to current density, and the operating temperature of the solar cells affects the output voltage V of the PV array. Solar cell J-V (I-V) characteristic curves that summaries the relationship between the current and voltage are generally provided by the panels manufacturer and are given as[22]:

• **Open-circuit voltage** (V_{oc}) This is the maximum voltage that the array provides when the terminals are not connected to any load (an open circuit condition). This value is much higher than V_{mp} which relates to the operation of the PV array which is fixed by the load. This value depends upon the number of PV panels connected together in series. The equation for open circuit voltage is:

$$Voc = \frac{KT}{q} \ln \left(\frac{I_{sc} + I_s}{I_s}\right) \quad \text{(I. 4)}$$

• **Short-circuit current** (I_{sc} or J_{sc}) The maximum current provided by the PV array when the output connectors are shorted together (a short circuit condition). This value is much higher than I_{mp} which relates to the normal operating circuit current.

The current density J delivered by an ideal single-junction photovoltaic cell operated at a voltage V is commonly described by an adaptation of Shockley's diode equation, which considers photogenerated carriers by application of the superposition principle, that is

$$J = Jsc - J_s(e^{\frac{qV}{KT}} - 1) \quad \text{(I. 5)}$$

where J_{sc} is the short-circuit current density of the cell, q is the elementary charge, k is Boltzmann's constant, and T is the cell temperature. The parameter Js is the reverse saturation current in the dark [23].

• **Maximum power point** (P_{mp}) This relates to the point where the power supplied by the array that is connected to the load (batteries, inverters) is at its maximum value, where

$$V_{mp} = Voc - \frac{KT}{q}\ln\left(1 + \frac{qV_m}{KT}\right) \quad \text{(I. 6)}$$

$$I_{mp} = I_s\left(e^{\frac{q\,Vm}{KT}} - 1\right) - I_{sc} \quad \text{(I. 7)}$$

$$P_{mp} = \mathrm{I_{mp}\ xV_{mp}} \quad \text{(I. 8)}$$

The maximum power point of a photovoltaic array is measured in Watts (W) or peak Watts (W_p).

• **Fill factor** (FF) The fill factor is the relationship between the maximum power that the array can actually provide under normal operating conditions and the product of the open-circuit voltage multiplied by the short-circuit current, this fill factor value gives an idea of the quality of the array and the closer the fill factor is to 100 % the more power the array can provide. Typical values are between 0.7 and 0.8. the fill factor is calculated using these equations:

$$FF = \frac{V_m I_m}{V_{oc} I_{sc}} = \frac{\text{Area of inner rectangle}}{\text{Area of outer rectangle}} \quad \text{(I. 9)}$$

• **Efficiency (η %)** The efficiency of a photovoltaic array is the ratio between the maximum electrical power that the array can produce compared to the amount of solar irradiance hitting the array. The efficiency of a typical solar array is normally low at around 10-12%, depending on the photovoltaic type (monocrystalline, polycrystalline, amorphous or thin film) of cell being used[22].

The efficiency can be calculated using these equations where P_{in} is the incident solar power:

$$\eta = \frac{V_m I_m}{P_{in}} \qquad \text{(I. 10)}$$

• **Quantum efficiency**: as its formula indicates is quantum efficiency, divide the number of electrons collected by the number of incident photons

$$\text{QE} = \frac{\text{The number of electrons collected}}{\text{Number of incident photons}} \qquad \text{(I. 11)}$$

The figure below provides the efficiency recorded development from 1976 to 2017

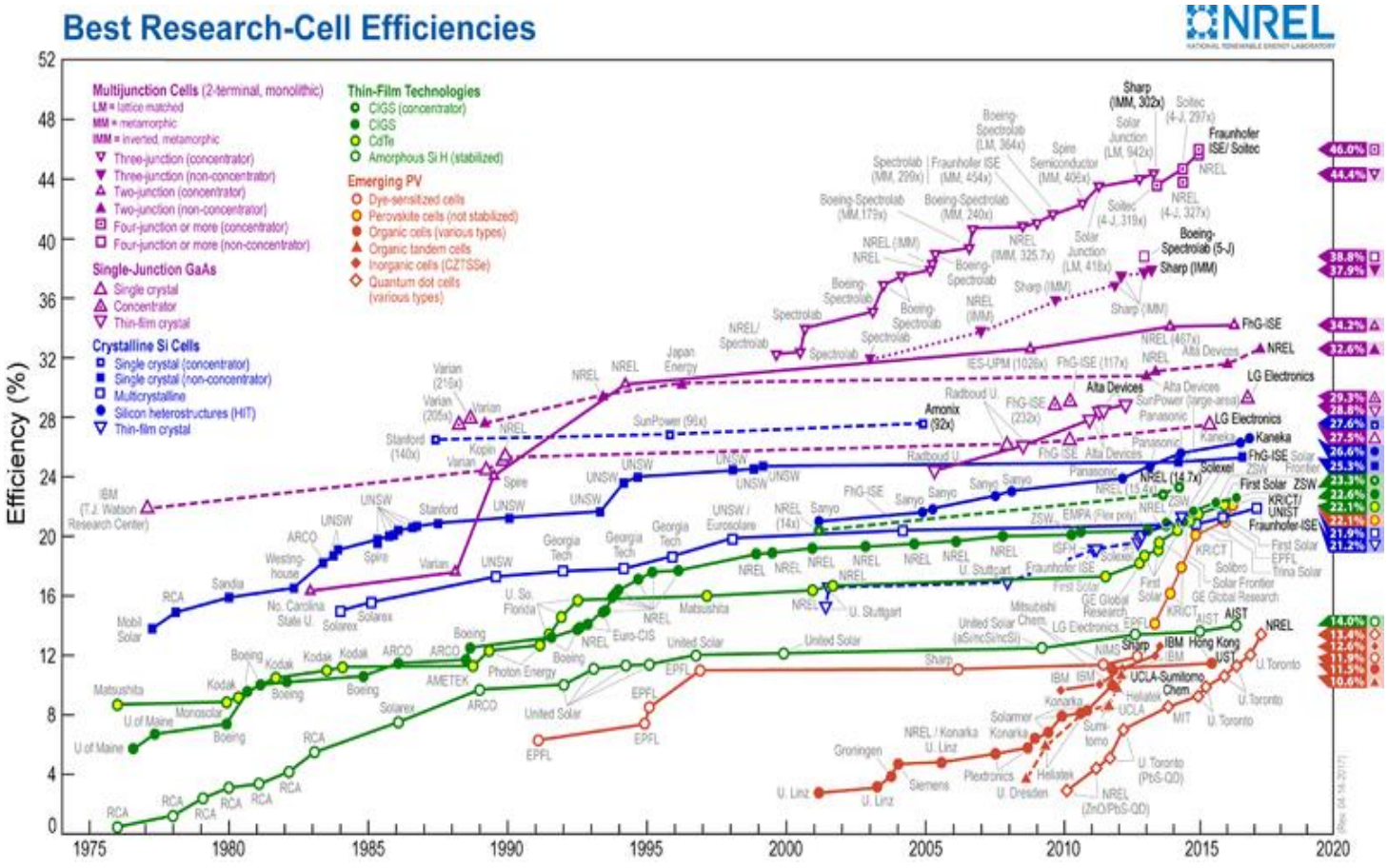

Figure I. 11: best solar cell efficiencies of various types of cells tracked by the National Renewable Energy Laboratory (NREL) from 1976 to 2017 [24]

I.8. Thin film solar cells

In this section, we will closely examine the materials used in thin film solar cells. Thin film solar cells are created by combining different materials to form a new material thus it allows the material to have adjustable band gap by allowing materials, which can be doped to create either P-type or N-type characteristics. Let's delve into these materials and their production methods.

I.8.1. Fundamental material requirements

A well-known feature of all PV devices is that at least some of their constituting materials must have a not-too-wide forbidden gap, say Eg ~ 1–2 eV. The origin of that criterion is that larger band gaps exceeding the energies of most of sun spectra photons would not allow efficient light absorption necessary to produce enough electrons and holes. However, there is also the opposite requirement of those gaps being not too small, so that efficiently absorbing narrow band semiconductors are not good for PV either.

As a result, semiconductors with substantial but not-too-wide forbidden gaps Eg ~ 1–2 eV, such as Si, Ge, CdTe, CIGS and some others are most suitable for PV.

The not-too-narrow gap limitation is less intuitive and may be worth explaining here. It is dictated by PV functionality as a power source. The power is a product of electric current and voltage, P = IV where both I and V components must be not too small. I (current) is proportional to the light induced charge generation rate favouring significant absorption coefficients in the sun spectral region of $\hbar\omega$ ~ 0.5–2 eV. Forbidden gaps Eg ~ 1–2 eV of many semiconductors falls in that region. To the contrary, the typical dielectric gaps Eg $\gtrsim$ 4 eV are too wide for sufficient absorption (for example, window glass that is practically transparent and does not absorb light).

The requirement that undermines the suitability of narrow gap semiconductors (despite their strong absorption coefficients) is related to the voltage component: $V \leq Eg/q$, where q is the electron charge. To explain the latter inequality, we note that V can be related to the difference in Fermi energies in two metal electrodes. the Fermi (quasi-Fermi) energy describes the energy change due to removing one particle from the system. Therefore, $\Delta EF \equiv EF_1 - EF_2$ gives the energy change due to transferring one electron between the two metals, and so does qV. On the other hand, the metal Fermi energies must not overlap with the semiconductor conduction or valence bands because such an overlap would mean that the semiconductor has in reality metal conductivity (no gap between the Fermi level and forbidden gap edges).

Eg presents the upper limit of the difference between the electron and hole Fermi levels allowing their steady state spatial separation. Increasing V beyond Eg/q would shift the Fermi levels beyond the forbidden gap turning the semiconductor into metal thus shorting the built in field and the circuit.

Another wording of the same is that electrons and holes recombine very efficiently when the two Fermi levels are close thus suppressing their spatial separation and the built-in field. Assuming point defect mediated recombination, the electron-hole recombination rate strongly accelerates with decrease of the gap Eg. As a result, there exists a range of gaps optimizing PV performance, Eg $\lesssim$ 2 eV.

It should be remembered however, that the latter optimum gap prediction was derived under certain assumptions about the nature of (defect facilitated) recombination, lack of traps, insignificant leakage due to shunts [25].

I.8.2. CIGS Based Solar Cell and its crystal structure

Copper indium selenide ($CuInSe_2$ or CIS) is a member of the chalcogenide family exhibits a direct band gap of about 1.52 eV, which is very close to the theoretical value of 1.5 eV, and an absorption coefficient of 10^5 cm^{-1} invisible spectrum range. CIS was first chalcopyrite materials synthesized by Hahn et al. in 1953 with the band gap of 1.04 eV. Later in 1976, Kazmersk et al., prepared first $CuInSe_2$/CdS thin film solar cell and achieved efficiency of 4–5%. $CuInGaSe_2$ (CIGS), a promising thin film solar cell material, has gained lots of attention in decades due to its high energy conversion efficiency and potential lower manufacture cost over conventional Si solar cells. CIGS and CIGSSe are ternary I-III-VI2 semiconductors having chalcopyrite structure. By replacing In with Ga in CIS to form Cu(Inx Ga1-x)Se_2 had an profound impact on the defect density of the material exhibiting high cell performance compared to CIS. The unit cell of CIGS is tetragonal have lattice constant ratio (c/a) near to two and any deviation from this value is due to Cu–Se, In–Se or Ga–Se bonds Figure I. 12. High performance photovoltaic material CIGS and CIGSSe thin films have surpassed efficiency of 20% attracting considerable attention in the solar community. Owing to its high absorbing coefficient, CIGS is attractive and promising material for thin film solar cells with direct band (~1.0–1.12 eV) and high absorption coefficient (10^5 cm^{-1}) [26].

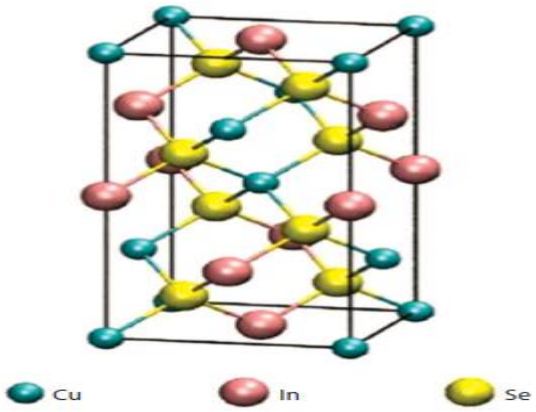

Figure I. 12: Crystal structure of tetragonal chalcopyrite CIGS unit cell. [20]

I.8.3. Elaboration methods and technics

I.8.3.1.Method of epitaxy

Epitaxy refers to the deposition of an overlayer on a crystalline substrate, where the overlayer is in registry with the substrate[28].

I.8.3.1.1. Hot wall epitaxy

In this technique one or two annular vapor sources are used and the vapours are transported through a heated cylindrical enclosure that is held at a temperature higher than the substrate. Thus, deposition of homogenized and equilibrated multicomponent vapours takes place on the substrate.

This technique has been used to obtain good epitaxial films of several IV-VI and II-VI compounds.

I.8.3.1.2. Molecular Beam Epitaxy

Epitaxial growth onto a single crystal substrate obtained by the condensation of one or more directed beams of atoms and/or molecules (in some special cases) from an effusion source in an ultrahigh-vacuum UHV system is called molecular beam epitaxy. The low-density vapor beam is obtained from a high-vapor-pressure Knudsen type (effusion) source.

Basically, a slow evaporation technique, its significant advantages are best derived by making full use of the UHV analytical techniques for obtaining information on the structure, topography, and composition and its depth profile and the chemical state of the surface of the film during its growth. A practical molecular beam epitaxy (MBE) system should therefore include a quadrupole mass spectrometer for analysing vapor species, sputter

ion gun, secondary ion mass spectrometer (SIMS), scanning Auger microprobe (SAM), ESCA, LEED, and HEED. By keeping the deposition rates low (< 1 A^0 S^{-l}) onto ultraclean substrates, we can achieve epitaxial growth of high perfection at relatively lower substrate temperatures. In the case of multicomponent compounds, kinetics of condensation and thermodynamic reactions of the various ad-atoms can be monitored and controlled literally monolayer-by-monolayer.

Very slow deposition rates allow MBE to obtain multilayer structures of one or more material in a predetermined sequence with variable layer thicknesses ranging from about 10 A^0 to several micrometres, enabling the formation of quantum-well superstructures, heterostructures, heterojunctions, and graded composition/property structures. The surface of a film may be terminated with a desired material so that passivation, protection, or work-function alteration may be achieved. Further, three-dimensional geometrical structuring of thin films is possible by using appropriate masks/shutters, or simply by "writing" masked patterns utilizing fine vapor beams (~ 10 μm or less).

MBE is obviously a very sophisticated and expensive setup and has thus been used primarily for basic epitaxial growth studies and for specialized microelectronic applications. No doubt, the idea of using fine vapor beams under controlled condensation conditions is attractive for the study of novel structures and concepts in multijunction solar cells. MBE and its less sophisticated versions have been used extensively for the deposition of II-VI and III-V compounds, in particular, GaAs-based ternary (e.g., Al1-xGaxAs and Inl-xGaxAs, $GaSb_1$-yAsy) and quaternary (GaxIn(1-x)Asy P(1-y)/InP) heterojunction structures. The MBE technique has been used to deposit solar cell structures of the type Gal-x Alx As/GaAs.

I.8.3.1.3. Graphoepitaxy

Vapor-deposited films on amorphous substrates are generally poly-crystalline. Partially textured or oriented films are obtained under suitable deposition conditions. Recently, Smith and co-workers have shown that by depositing textured films (of Si in their case) on an amorphous substrate ($Si0_2$ in their case) having a relief pattern of grating lines with the right periodicity and profile, and subsequent crystallization by a laser (6 W) in a repeated raster pattern results in complete orientation of the film over the grating relief along the grating direction. The required grating spacing, according to this Lincoln laboratory group, should be less than the characteristic grain size of the film to be deposited. By creating a 3.8 μm grating of square-well profile through a photolithographic technique on Cr coated

$Si0_2$ substrate, 5000-A^0-thick CVD deposited Si films were oriented with (100)-plane parallel to the substrate and (001) directions parallel to the grating direction. A (111)-plane orientation would require a difficult-to-fabricate sawtooth grating profile. Although the technique continues to be an academic curiosity with doubts regarding the orientation processes, it nevertheless is an attractive possibility for growing large-area crystalline films from vapor deposited silicon on X-ray lithographically textured amorphous carbon or other conducting substrates for solar cell applications [29].

I.8.3.2.Sputtering technique

When a material is bombarded by energetic entities such as accelerated ions, atoms are ejected from its surface. This phenomenon, as depicted in Figure I. 13 called back sputtering. The simplest kind of a practical sputtering reactor is the so-called diode sputtering system. It is composed of an anode and a cathode facing each other in a vacuum chamber. The sputtering chamber is filled with a gas, most commonly argon. The target material is usually part of the cathode while a substrate is placed at the anode. Applying a potential difference higher than the threshold breakdown voltage between the cathode and the anode results in partial ionization of the gas molecules and the formation of a plasma discharge. The breakdown voltage depends on the gas used, the pressure and the cathode material. The potential of the cathode is kept more negative than the anode, consequently, positively charged gas ions are accelerated towards the target (cathode). If their kinetic energy is higher than the surface binding energy of the target material, usually assumed to be close to the sublimation energy U, atoms will be sputtered away. A large part of them travels towards the substrate facing the target. The accumulation of these particles on the substrate progressively builds up the thin film. The impact of highly energetic ions on the target surface also induces ejection of secondary electrons. They are accelerated towards the anode, ionizing more gas atoms on their path, sustaining the plasma and hence ensuring a continuous sputtering process. Non-inert gases can also be used during sputtering. This deposition process is called reactive sputtering. Atoms sputtered from the target are combined with gas molecules to form a compound thin film. Sputtering a metallic target in nitrogen or oxygen containing atmosphere is commonly used in industrial or research context to form nitride or oxide thin films. The number of atoms back-scattered after collision of one incident ion with the surface defines the sputtering yield S.

$$S = \frac{\text{Atoms removed}}{\text{Incident ion}} \qquad \text{(I. 12)}$$

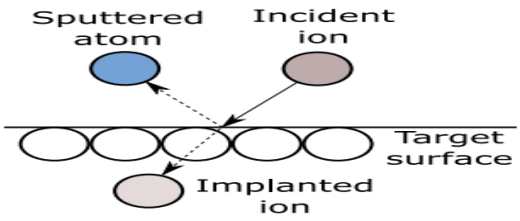

Figure I. 13: The sputtering phenomenon [23]

The energy of incident ions has a strong influence on sputtering yield. If incoming ions have less energy than the target surface threshold energy (several tens of eV), the sputtering yield is obviously very low, in the order of 10^{-5}. In the energy regime where ions have a kinetic energy between 10 eV and 1 keV, it is energetically possible to displace atoms at the target surface. Sputtering through collision-cascade phenomenon can take place. This energy range is particularly useful for thin film deposition as the sputtering yield is in the order of unity. In practical applications, the regime above 1 keV is rarely used due to low energy efficiency, and potential damages caused by ion implantation in the target material. The sputtering yield tends to saturate and even decrease as ions penetrate deeper into the material and more energy is dissipated as heat in the core of the target.

I.9. Perovskite solar cell:

Discovered in 1839 by Gustav Rose and named after Russian mineralogist Lew Alexejewitsch Perovski, perovskites represent a family of crystalline compounds that adopt a similar crystal structure as the parent mineral calcium titanate $CaTiO_3$. This class of materials can be generally described by the ABX_3. In the ideal ABX_3 perovskite structure, the large monovalent cation A occupies 12-fold coordination site in the middle of the cube to form an AX_{12} cuboctahedron, while the smaller divalent cation B forms corner sharing BX_6 octahedra in a 3D perovskite framework Figure I. 14. The ideal cubic perovskite structure is not very common due to the sizes of the cations A and B, and the anion X and the mineral perovskite itself are slightly distorted. Distorted perovskites have reduced symmetry, affecting the crystal structure transition, which is one of the key aspects of the structural stability issue for perovskite materials. Such structural distortions, when reversible, can be used for mechanical energy harvesting purposes as demonstrated for the perovskite barium titanate ($BaTiO_3$)[31].

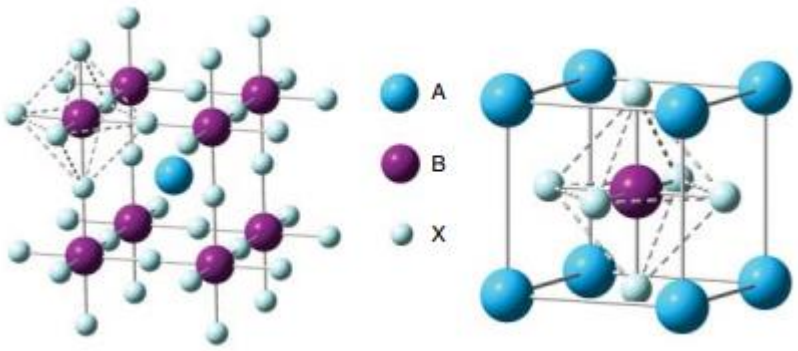

Figure I. 14: Ideal cubic perovskite structure

I.10. Tandem solar cell:

In connection with the heterostructure cells it has already been discussed that the spectrum of the incident sun light can be utilized more effectively if semiconductors with different band gaps are employed. Practical systems differ in the method by which the light is directed towards the semiconductor with the appropriate band gap. One concept separates the light by using spectrally sensitive mirrors before it is directed to the appropriate cell, whereas in the second case, the tandem cell approach, a series of cells is stacked upon each. The cells are arranged from the top side with decreasing band gaps, so that light with longer wavelengths and lower absorption coefficients passes through the upper cells and is absorbed in the bottom cells. The latter concept seems to be more compatible with today's semiconductor thin film technologies and has been mainly pursued in the past. Since the design of a cascade system adds extra complexity to the solar cell it is better suited for concentrator concepts.

Tandem configurations can be completely integrated with two terminals or connected only mechanically, with four terminals, as shown in Figure I. 15. In the first case one has the problem to fabricate a conductive and optically transparent connection between the top and bottom cell. A usual technique is the use of a tunnel junction which sometimes has stability problems.

Numerical programs which incorporate individual cell performance parameters, e.g., current-voltage characteristics and spectral quantum efficiencies, are currently applied to calculate optimal configurations for tandem solar cells. Some calculations of the efficiencies of a tandem structure as a function of the bandgaps for the top and bottom cells. Four terminal designs offer a wider range of bandgaps for maximum efficiencies. The bandgap of the top cell can vary between 1.5-1.9 eV and for the bottom cell between

0.95-1.2 eV. Recently, a tandem cell using a silicon bottom cell and a GaAs top cell was reported with a terrestrial concentrator efficiency of 31%, which is the highest efficiency reported so far for a photovoltaic device.

The number of available semiconductors is significantly larger in the second case and thus allows greater flexibility for this structure. The tandem concept seems especially suitable for thin film solar cells and currently a number of systems such as a-Si: H/a-Si-Ge: H (efficiency 12.7%), a-Si:H/CulnSe$_2$ (efficiency 14.6%) or CuGaSedCulnSe$_2$ are being considered. Calculations of the efficiencies of cascade systems with more than two semiconductors show that for an ideal system the efficiency saturates for about n > 7. In reality one has to consider however additional unavoidable optical losses when connecting the different cells [9].

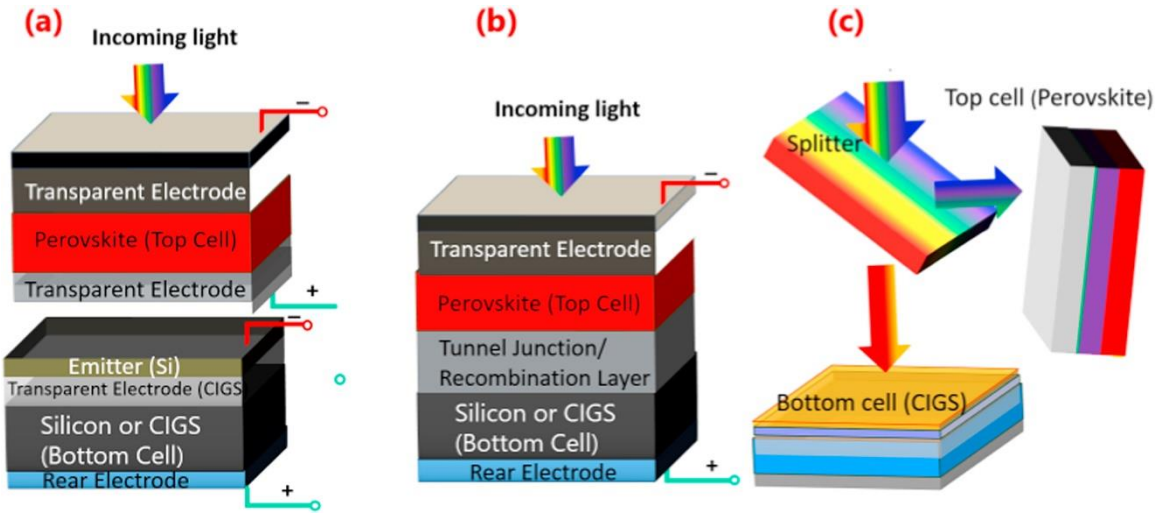

Figure I. 15: Schematic illustration of tandem solar cells, (a) mechanically stacked 4T, (b) monolithically integrated 2T , and (c) optical splitting of solar spectrum [32]

I.11. Conclusion:

In this chapter, we have embarked on a comprehensive study of solar cells, examining their overall functionality and significance. We have observed that the sun emits radiation, and despite potential filtration, a considerable amount can be effectively captured on Earth. These photons possess the ideal energy levels necessary for efficient conversion into electricity.

By delving into the intricate transition process from light to electricity via specially designed light-sensitive semiconductors, we have gained a profound understanding of the underlying mechanisms. Furthermore, we have explored the mathematical model that governs the configuration of solar cells, enabling us to perform accurate calculations and simulations to assess their performance.

Moreover, our study of microelectronics has directed our attention towards comprehending the electrical properties of the materials involved. Consequently, it was imperative to provide a brief overview of the materials to be utilized, as it facilitates the simulation process and aids in the interpretation of results.

Ultimately, our investigation has led us to the fascinating realm of tandem solar cells. These cells hold immense promise in achieving exceptional efficiencies, prompting us to conduct comprehensive simulations in the hopes of manufacturing highly efficient solar cells.

Chapter II

Exploring the Structure and Data

II.1. Introduction

Our focus in this chapter revolves around the evaluation of the simulation program SCAPS 1d. Our main objective is to gain a thorough understanding of its operation and performance, as this knowledge is very important to use it effectively in our simulations. In doing so, we will explore the intricacies of this system, understand how it works and identify its potential applications. Then, we will proceed to properties and features of the material that are used $RbGeI_3$ and CZTSe in the development of the solar cell system under study. In providing an overview of their properties and crystalline structure.

Following the elucidation of the materials, our attention will turn to analysing the initial data at hand. This data forms the initial building blocks upon which we will build our initial design. Through micro-analysis and interpretation of this data, we will lay the foundation for our subsequent simulations, aimed at obtaining more accurate and reliable results.

II.2. Introducing SCAPS 1d software

SCAPS is a one-dimensional solar cell simulation program developed at the department of Electronics and Information Systems (ELIS) of the University of Gent, Belgium. Several researchers have contributed to its development: Alex Niemegeers, Marc Burgelman, Koen Decock, Johan Verschraegen, Stefaan Degrave. A description of the program, and the algorithms it uses, is found in the literature. The program is freely available to the PV research community (universities and research institutes). It runs on PC under Windows 95, 98, NT, 2000, XP, Vista, Windows 7, and occupies about 50 MB of disk space. The program can be freely downloaded (but it can't be sold, distributed further, it must refer when you publish results obtained with SCAPS). SCAPS is originally developed for cell structures of the $CuInSe_2$ and the CdTe family. Several extensions however have improved its capabilities so that it is also applicable to crystalline solar cells (Si and GaAs family) and amorphous cells (a-Si and micromorphous Si). An overview of its main features is given below:

- Up to 7 semiconductor layers
- Almost all parameters can be graded (i.e. dependent on the ocal composition or on the depth in the cell): Eg, χ, ε, N_C, N_V, $vthn$, $vthp$, μn, μp, N_A, N_D, all traps (defects) N_t.
- Recombination mechanisms: band-to-band (direct), Auger, SRH-type
- Defect levels: in bulk or at interface; their charge state and recombination is accounted for.
- Defect levels, charge type: no charge (idealisation), monovalent (single donor, acceptor), divalent (double donor, double acceptor, amphoteric), multivalent (user defined) defect levels, energetic distributions: single level, uniform, Gauss, tail, or combinations
- Defect levels, optical property: direct excitation with light possible (impurity photovoltaic effect, IPV)
- Defect levels, metastable transitions between defects
- Contacts: work function or flat-band; optical property (reflection of transmission filter) filter
- Tunnelling: intra-band tunnelling (within a conduction band or within a valence band); tunnelling to and from interface states
- Generation: either from internal calculation or from user supplied $g(x)$ file
- Illumination: a variety of standard and other spectra included (AM0, AM1.5D, AM1.5G, AM1.5Gedition2, monochromatic, white,) illumination: from either the *p*-side or the *n*-side; spectrum cut-off and attenuation
- Working point for calculations: voltage, frequency, temperature the program calculates energy bands, concentrations and currents at a given working point, *J-V*

- Characteristics, ac characteristics (*C* and *G a*s function of *V* and/or *f*), spectral response (also with bias light or voltage)
- Batch calculations possible; presentation of results and settings as a function of batch parameters.
- Loading and saving of all settings; start-up of SCAPS in a personalised configuration; a script language including a free user function.
- Very intuitive user interface.
- A script language facility to run SCAPS from a 'script file'; all internal variables can be accessed and plotted via the script.
- A built-in curve fitting facility.
- A panel for the interpretation of admittance measurements.

II.3. Basic notions of SCAPS 1d

SCAPS calculations rely on a range of mathematical equations to solve problems related to the movement of charges and photons within the cell. These include Poisson's equation, continuity equations, the Einstein relation, Carrier transport equations, the Shockley-Read-Hall recombination model, and Kirchhoff's law. we will explore the ability to introduce a variety of parameters using the user-friendly interface provided. Specifically, we will examine the manner in which these parameters can be incorporated and the manner they are presented.

II.3.1. Action panel of SCAPS

SCAPS is a Windows-oriented program, developed with Lab Windows/CVI of National Instruments. SCAPS uses here the LW/CVI terminology of a 'Panel' (names used in other softwares are: a window, a page, a popup…). SCAPS opens with the 'Action Panel'.

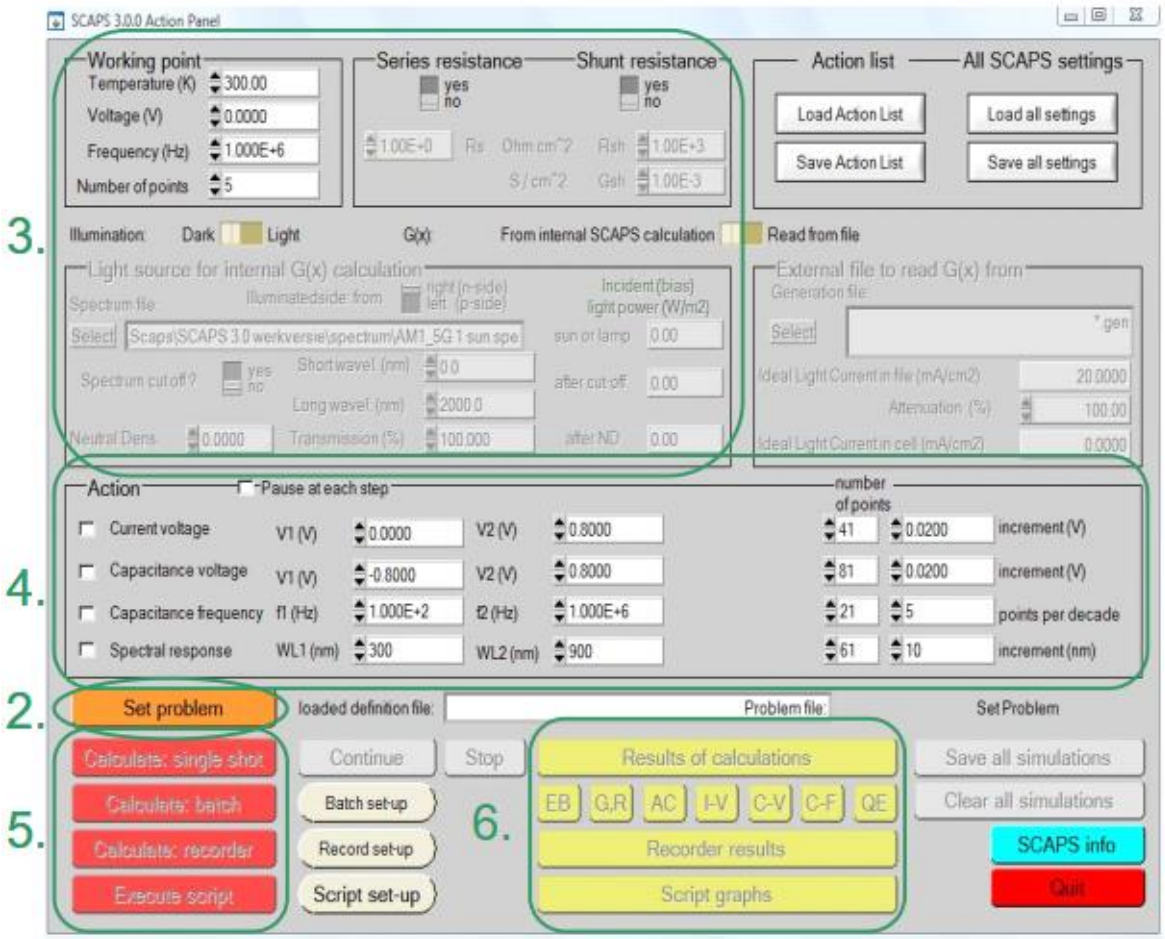

Figure II. 1: The SCAPS start-up panel: the Action panel or main panel.

There are dedicated panels for the basic actions:

1) After Running SCAPS.

2) Define the problem, thus the geometry, the materials, all properties of your solar cell.

3) Indicate the circumstances in which you want to do the simulation, i.e., specify the working point.

4) Indicate what you will calculate, i.e., which measurement you will simulate.

5) Start the calculation(s)

6) Display the simulated curves.

II.3.2. Display the simulated curves

After the calculation(s), SCAPS switches to the Energy band panel (or the AC-band panel). You can now look at your ease to the band diagrams, carrier densities, current

densities, at the last bias point calculated (stop your calculations earlier, or use the pause button on the Action Panel if you want to look at an intermediate state at ease). You can output the results (buttons print, save graphs, show (then the numbers are shown on screen; cut & paste to e.g. Excel is possible), or save (then the numbers are saved to a file). You can switch to one of the specialized output Panels (if you have already simulated at least on corresponding measurement). We only show the example of the IV Panel.

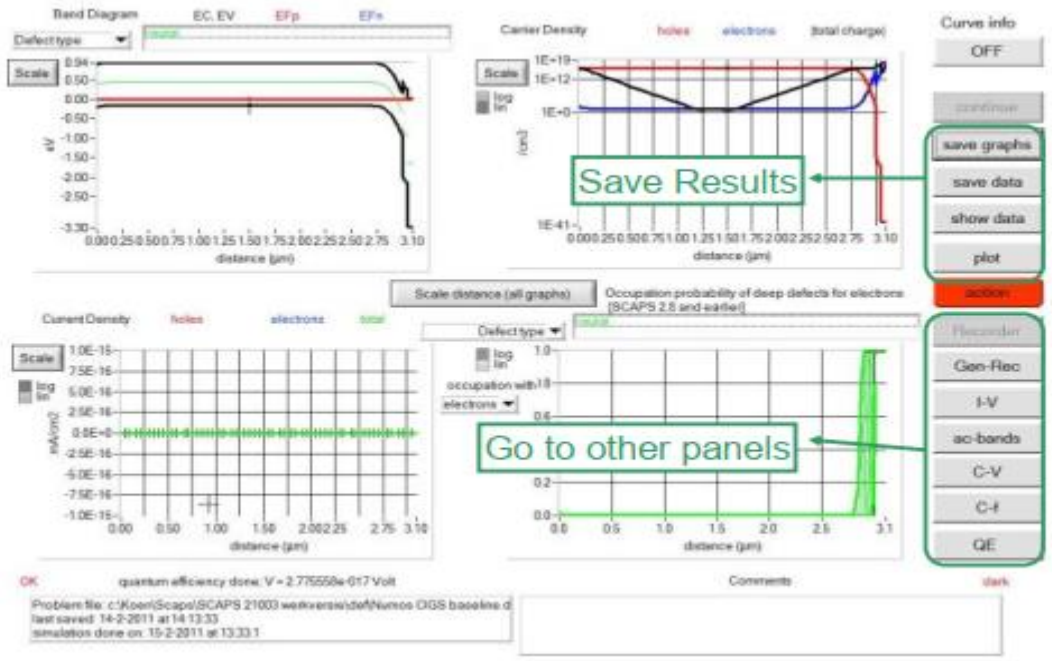

Figure II. 2: simulation curves display

II.3.3. The J-V curves

The meaning of the plot, show or save buttons is as for the Energy Bands Panel. Again, you can switch to the other output panels (energy bands, ac, *C-V, C-f* and *QE*, if already calculated), and to the Action Panel to do a new calculation, or to stop.

Several small remarks: The colour of the last calculated curve is indicated (when the graph gets too crowded, go to the Action Panel and click clear all simulations to clear all graphs). The recombination curves are only shown for the last simulation. The colour of the legend corresponds to the colour of the curve (indicated as 1bis).

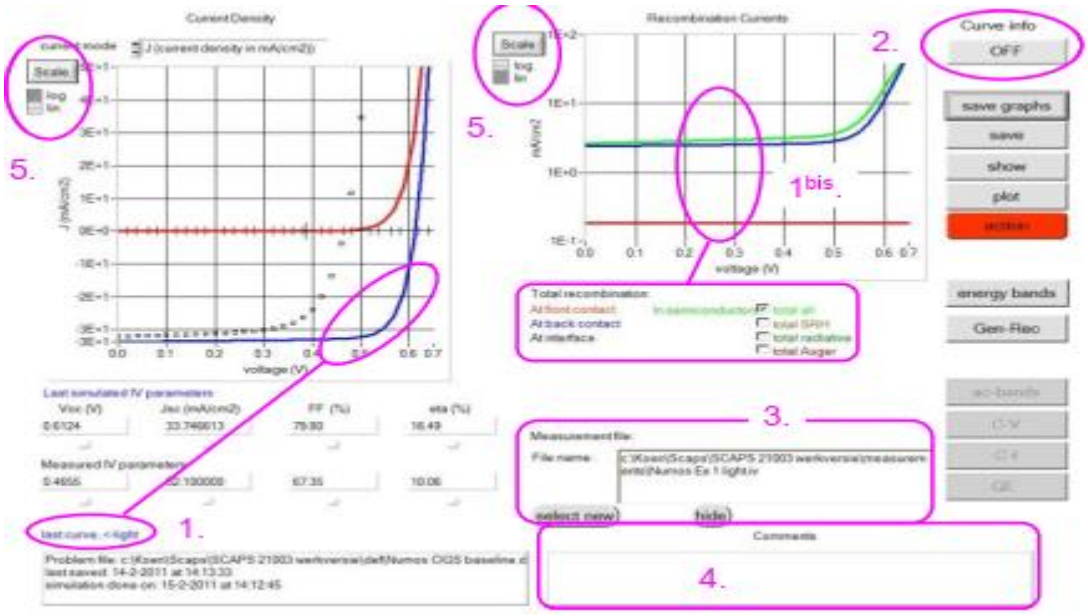

Figure II. 3: The J-V characteristics graphs of SCAPS

You can change the range and scaling of the axes with the Scale button. If you press the CTRL-button and select a rectangular area in a graph, the graph will zoom-in to the selected area. Pressing the CTRL button and clicking the right mouse button results in zooming out.

II.3.4. Editing a solar cell structure

When clicking the ‘Set Problem’-button on the action panel, the ‘Solar cell definition’-panel is displayed. This panel allows to create/edit solar cell structures and to save those to or load from definition files. These definition files are standard ASCII-files with extension ‘*.def’ which can be read with e.g. notepad. Even though the format of these files seems self-explaining it is however strongly advised not to alter them manually.

Layer-, contact-, and interface properties can be edited by clicking on the appropriate box as shown in Figure II. 4. In a similar way, layers can be added by clicking ‘add layer’.

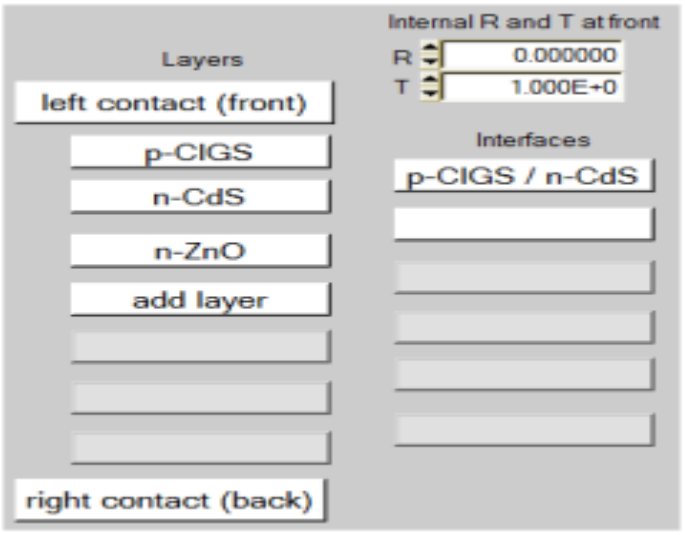

Figure II. 4: Defining a solar cell structure

II.3.5. Contacts

The contact properties can be set by either clicking the front or back contact button on the cell definition panel, which opens the 'contact properties panel'

The metal work function Φ_m (for majority carriers) can be input by the user. However, the user can also choose the option "flat bands". In this case, SCAPS calculates for every temperature the metal work function Φm in such a way that flat-band conditions prevail. In SCAPS versions before 1-1-2014, a simplified algorithm described below was used. When the layer adjacent to the contact is n-type equation II.1 is used, when it is p-type equation II.2 is used, when it can be considered to be intrinsic equation II.3 is used:

$$\Phi_m = \chi + k_B T ln\left(\frac{N_c}{N_D - N_A}\right) \quad \text{(II. 1)}$$

$$\Phi_m = \chi + E_g - k_B T ln\left(\frac{N_c}{N_D - N_A}\right) \quad \text{(II. 2)}$$

$$\Phi_m = \chi + k_B T ln\left(\frac{N_c}{n_i}\right) \quad \text{(II. 3)}$$

As can be seen, only the shallow doping density is taken into account in order to calculate the flat band metal work function. When there is a considerable amount of charge in defects present near the contact however, it is thus possible that the flat band option will not lead to flat bands.

In recent SCAPS versions (after 1-1-2014), also charge in deep defects is considered; an algorithm involving the solution of a non-linear algebraic equation (expressing that total charge = zero) then II.1 should be replaced by equation II.3.

When the layer next to the contact is either n- or p-type (NOT INTRINSIC) a recalculation of the barrier height with respect to the Fermi level and conductance/valence band are calculated and displayed in the contact properties panel. These values however only serve as an indication to the user, they are not used in the simulation. At the contacts a (wavelength dependent) reflection/transmission R(λ) or T(λ) can be set. These can be set either as a constant value (wavelength independent) or as a filter file. These filter files are standard ASCII-files with the extension '*.ftr'. Several files are provided with the SCAPS installation; however, the user can easily make more files. If a line in this file can be interpreted as starting with at least two numeric values, the first value is interpreted as the wavelength (in nm) and the second as the reflection (in %). All other lines are ignored and treated as comment. Often a SCAPS simulation will need R(λ) and T(λ) at a wavelength outside the range specified in the filter file: this is e.g. the case if an R(λ) file was specified between λ = 300 nm and λ = 1100 nm, and a simulation was asked under illumination with the default spectrum AM1_5G 1 (sun.spe) that is specified between 305 nm and 4045 nm. Then extrapolation will be used for the spectrum wavelengths 1100 nm < λ < 4045 nm. For the SCAPS extrapolation rules[33].

II.4. $RbGeI_3$ A Promising Inorganic Material for High-Efficiency Solar Cells:

After the general Perception of the perovskite material, we will glance at the $RbGeI_3$ perovskite material in hops to comprehend the reason behind our choice of material add to our basic structure of (p-CIGS/n-CdS/n-ZnO).

II.4.1. Comprehensive Insight of the $RbGeI_3$ perovskite

$RbGeI_3$ is a perovskite compound with a stable non-magnetic phase, exhibits promising properties for its application in solar cells. Moreover, this material possesses a regular cuboctahedra structure shown in Figure II. 5: crystal structure of cubic perovskites RbGeI3, where the germanium atom is surrounded by iodide atoms, $RbGeI_3$ exhibit a perovskite-type structure with the chemical formula ABX_3 (A = organic cation, B = metal cation, X = halide anion), where X = I. Importantly, with a small, direct optical energy gap of 1.41 eV, $RbGeI_3$ demonstrates its exceptional ability to efficiently absorb light approximately 1.04×10^4 cm^-

[1]. Additionally, it is characterized by its semiconducting behaviour and weak covalent bonding between germanium and iodide atoms. Consequently, these distinctive features make $RbGeI_3$ an extremely attractive candidate for solar cell absorbers, as it can effectively convert sunlight into electricity. Furthermore, its absorption coefficient, which accurately indicates the amount of light it can absorb, aligns perfectly with the specific requirements for efficient solar energy conversion. By harnessing and capitalizing on the unique properties of $RbGeI_3$ researchers aim to not only develop highly stable and efficient solid-state solar cells but also to make significant strides towards creating cost-effective solutions that advance renewable energy technologies [34].

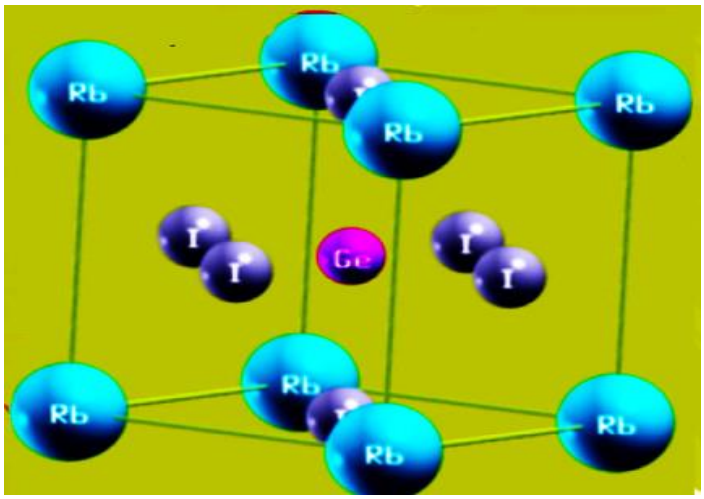

Figure II. 5: crystal structure of cubic perovskites $RbGeI_3$ [35]

II.4.2. $RbGeI_3$ as a Solar Cell Material

$RbGeI_3$, an inorganic material, shows promise as a potential candidate for high-efficiency solar cells due to several desirable properties. Firstly, it exhibits a high absorption coefficient, allowing for efficient capture of sunlight and conversion into electricity. Additionally, $RbGeI_3$ offers easy synthesis and solution processability, enabling cost-effective and scalable manufacturing processes. Furthermore, its bandgap is tenable, allowing for optimization of the solar cell's performance under different light conditions. Moreover, $RbGeI_3$ demonstrates a long diffusion length, which enhances the charge carrier transport within the material, leading to improved efficiency. These properties make $RbGeI_3$ an attractive alternative to lead-based perovskite solar cells, addressing the environmental concerns associated with lead toxicity.

II.5. General study of transport layer of the perovskite cell

II.5.1. Importance of material selection for (HTL) and (ETL) in perovskite Solar cells`

Selecting the right materials for the hole transport layer HTL and electron transport layer ETL is extremely important in perovskite solar cells. These materials play a critical role in helping charge carriers move efficiently within the solar cell, which affects how well the cell performs and how stable it is. Here are the main reasons why it’s crucial to choose the correct HTL and ETL materials.

The HTL and ETL materials are responsible charge for carrier transport by carrying the positive and negative charges, holes, and electrons to where they need to go in the solar cell. It’s important that these charges move easily and quickly to maximize the cell's power conversion efficiency. The right HTL and ETL materials should have properties that allow charges to transfer smoothly and rapidly.

The energy levels alignment of the HTL and ETL materials need to match up properly with the perovskite layer in the solar cell. The HTL material should have a higher energy level than the highest occupied molecular orbital homo of the perovskite to effectively extract holes. On the other hand, the ETL material should have a lower energy level than the lowest unoccupied molecular orbital luminosity of the perovskite to extract electrons. Correct energy level alignment helps minimize energy losses and improves charge extraction efficiency.

The HTL and ETL materials should have the ability to selectively extract charges, preventing unwanted charge recombination. This selectivity allows charges to move freely towards their respective electrodes.

The HTL and ETL materials should have high charge carrier mobilities, enabling charges to move quickly across the solar cell materials with high mobility and minimizing charge trapping and recombination by over doping the material. allowing for efficient charge extraction and transport to the electrodes. Enhanced charge mobility leads to improved efficiency and stability of the solar cell.

The HTL and ETL materials should be chemically stable and compatible with the other layers in the solar cell; they need to withstand operational conditions such as exposure to

light, heat, and moisture without degrading or undergoing structural changes. Stable materials contribute to the long-term reliability and durability of the solar cell.

Choosing HTL and ETL materials that are readily available, affordable, and suitable for large-scale production is important for making perovskite solar cells commercially viable. If these materials can offer comparable or better performance than conventional options while being more cost-effective, it can greatly increase the adoption of PCS [34] [35].

II.5.2. HTL, ETL Energy levels alignment with perovskite

To understand the energy alignment of band in a perovskite solar cell, this diagram summarizes the different layers (metal oxides and organic materials) used in perovskite architecture. Generally, the Electron Transport Layer (ETL) should have a conduction band (CB) aligned or slightly lower than the Perovskite absorber. The Hole Transport Layer (HTL) is expected to have a lower valence band (VB) compared to the perovskite. Additionally, the positions of the conduction band minimum and valence band maximum should be appropriate as well [36].

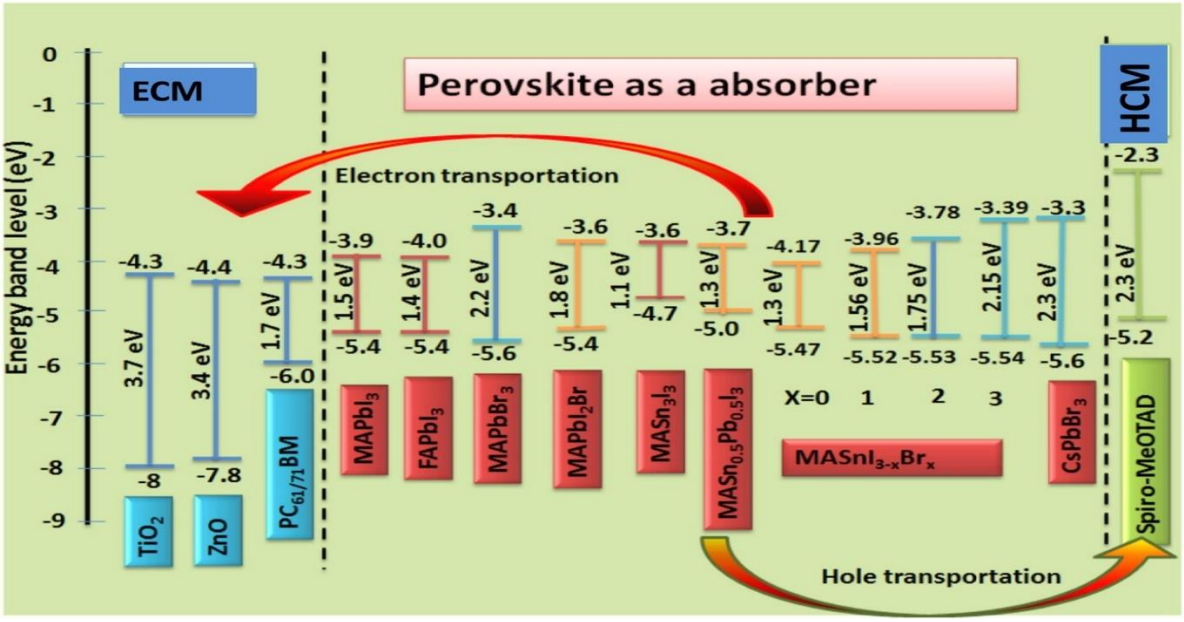

Figure I. 16: Illustration of values of energy levels versus vacuum level of different materials [37]

II.6. Insights about CZTSe as an absorber layer in the solar cell

Kesterite materials, specifically $Cu_2ZnSn(SxSe_1-x)4$ (CZTSe), have attracted attention for solar cell applications. CZTSe offers a tenable band gap with the equation II.4 and II.5,

high absorption coefficient $\alpha > 10^4$ cm^{-1} [38], non-toxicity, and an abundance of earth's natural resources, making it a promising candidate for thin-film photovoltaics. However, CZTSe solar cells have not yet achieved their theoretical conversion efficiencies due to various factors, including grain boundary defects, trap charges, and recombination rates.

Bowing parameter

$$Eg(x) = (1 - x)Eg(CZTSe) + xEg(CZTS) - bx(1 - x) \quad \text{(II. 4)}$$

A linear Eg variation for the material may be obtained as a function of x in cases of small bowing parameter b, using this equation:

$$Eg(x) = (1 - x)Eg(CZTSe) + xEg(CZTSe) \quad \text{(II. 5)}$$

If x = 0, equation II.5 then yields the band gap value for pure CZTSe as 1.0 eV [39].

Defects within the CZTSe material, such as dislocations and distorted bonds, introduce trap states that lead to the recombination of photogenerated carriers, affecting the normal carrier dynamics within the solar cell. Understanding these loss mechanisms is crucial for improving CZTSe solar cell efficiency.

The band alignment at the heterojunction interfaces between CZTSe and CdS plays a crucial role in carrier transport and overall solar cell performance [40].

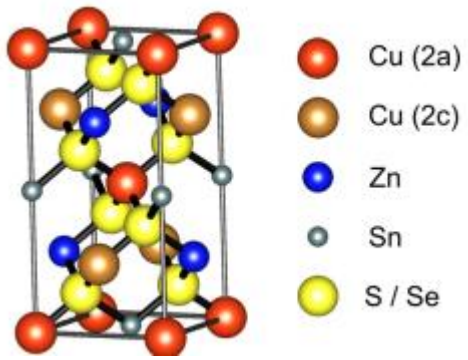

Figure II. 6 Crystalline architecture of CZTSe [41]

II.7. The structure and data of the simulated solar cell

II.7.1. Bottom cell data

This table displays data gathered from prior research that greatly assisted us in our own study.

Table II. 1: bottom sub-cell\data

Properties	p-CIGS [33]	p-CZTSe	n-CdS [33]	n-ZnO[33]
Thickness(µm)	0.5-2	0.8-1.5	0.01-0.1	0.2
Bandgap(eV)	1-1.4	0.9-1.5	2.4	3.3
Affinity(eV)	4.5	4.5[42]	4.2	4.45
Dielec. Perm	13.6	10 [42]	10	9
DOS CB(cm^{-3})	2.20E+18	2.20E+18[42]	2.20E+18	2.20E+18
DOS VB(cm^{-3})	1.80E+19	1.80E+19[39]	1.80E+19	1.80E+19
µe(cm^2/Vs)	1.00E+02	1.00E+02 [43]	1.00E+02	1.00E+02
µh(cm^2/Vs)	2.50E+01	2.50E+01[39]	2.50E+01	2.50E+01
Donor.Con.(cm^{-3}) N_d	1.00E+01	1.00E+01	1e14/5e19	1.00E+18
Accep.Con.(cm^{-3}) N_a	1e13/1e17	2.5e14-1e17	1.00E+01	1.00E+01

Table II. 2 bottom sub-cell defects

Properties	Defect type	Total Density (Nt)	Capture cross section electrons (cm^2)	Capture cross section holes (cm^2)	Energetic distribution	Energy level with respect to reference
p-CIGS	Scaps model	Scaps model	Scaps model	Scaps model	Scaps model	Scaps model
p-CZTSe *[43]*	Donor	1.00E+14	5.00E-13	1.00E-15	Single	0.4 ev
	Acceptor	5.00E+14	1.00E-15	1.00E-15	Single	0.3 ev
n-CdS	Scaps model	Scaps model	Scaps model	Scaps model	Scaps model	Scaps model
n-ZnO	Scaps model	Scaps model	Scaps model	Scaps model	Scaps model	Scaps model
CZTSe/CdS *[43]*	Neutral	2.00E+10	1.00E-14	1.00E-14	Uniform	0.6 ev

II.7.2. Structure of CIGS solar cell

This structure is used in our simulation (p-CIGS/n-CdS/n-ZnO), and that we will try to enhance while keeping the original basic structure, also the research indicated that in a standard CIGS solar cell the need of intrinsic i-ZnO is not necessary [44].

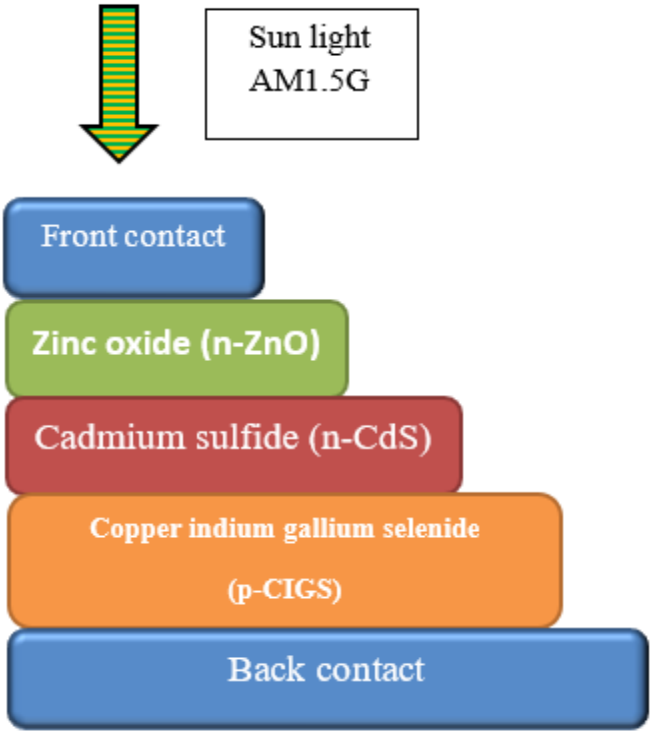

Figure II. 7: Structure of solar cell used

This particular structure corresponds to a thin film solar cell that falls under the second generation of solar cells. We have chosen to utilize this solar cell due to its economical fabrication process and its ability to adjust the band gap. Nevertheless, it is important to acknowledge that this type of cell is not without its drawbacks that we will try to enhance using various steps.

II.7.3. Structure of the new solar cell

we have previously studied a mono absorber layer solar cell consisted of a p-CIGS as the absorber layer, in this section we will introduce a new absorber layer p-CZTSe on top of the CIGS as shown in this figure:

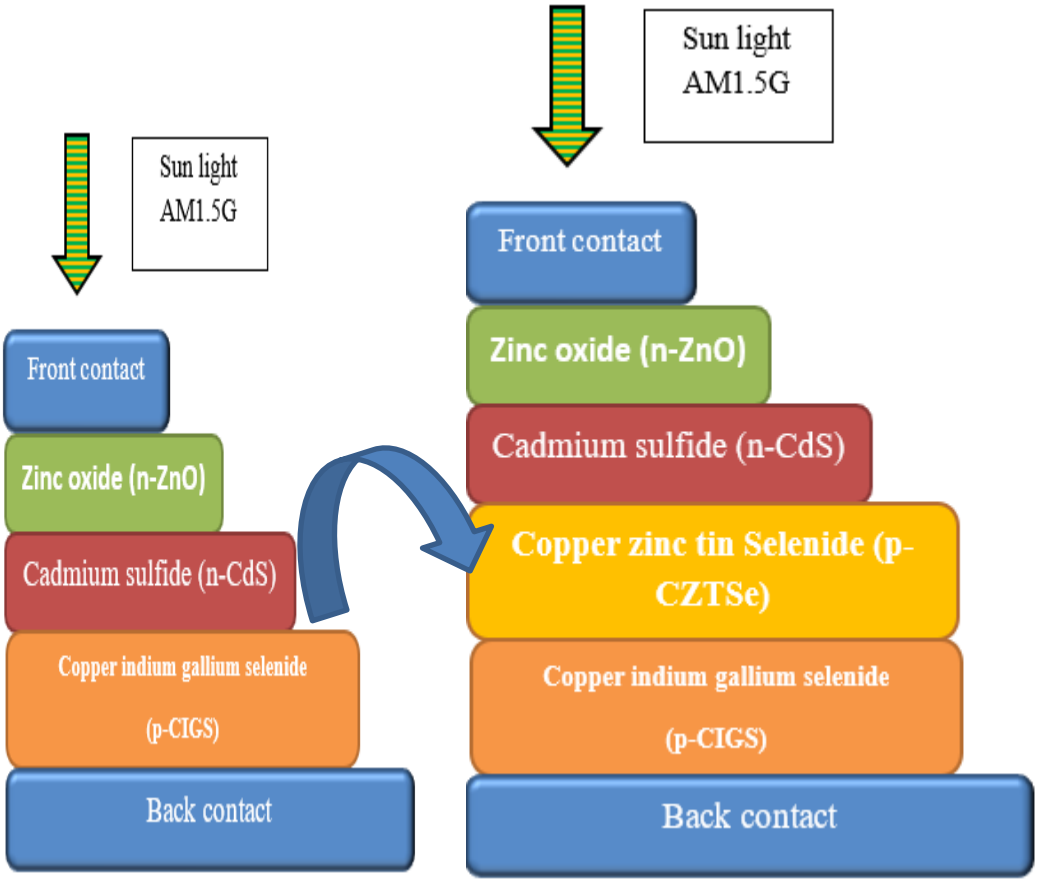

Figure II. 8: new structure of solar cell by adding a new absorber (p-CZTSe) on top of (p-CIGS)

II.7.4. Data of Perovskite solar cell (top sub-cell)

Introducing the data collected from previous studies for the top sub-cell (perovskite layer)

Table II. 3 Perovskite top sun-cell data

Properties	$CuCrO_2$ (HTL) [45]	$RbGEI_3$ [45]	TiO_2 (ETL) [45]
Thickness(µm)	0.05	0.1-0.5	0.05
Bandgap(eV)	3	1.3-1.7	3.2
Affinity(eV)	2.1	3.9[34]	4
Dielec. perm	9.5	23.1[34]	9
Dos cb (cm^{-3})	1.00E+19	2.80E+19[34]	2E+18
Dos vb (cm^{-3})	1.00E+19	1.40E+19[34]	1.8E+18 [46]
µe(cm^2/vs)	1.00E-01	2.86E+01	20
µh(cm^2/vs)	2.53E+00	2.73E+01	10
Donor.con.(cm^{-3}) Nd	1.00E+00	1.00E+00	1E+16
Accep.con.(cm^{-3}) Na	6.40E+15	1.00E+10	1

Table II. 4 top sub-cell defects [46]

Properties	Defect type	Total density (N_t)	Capture cross section electrons (cm^2)	CAPTURE CROSS SECTION HOLES (CM^2)	Energetic distribution	Energy level with respect to reference
$RbGeI_3$	Neutral	1.00E+14	1.00E-15	1.00E-15	Single	0.6 eV
HTL	Neutral	1.00E+14	1.00E-15	1.00E-15	Single	0.6 eV
ETL		1.00E+14	1.00E-15	1.00E-15	Single	0.6 eV
$RbGeI_3$/HTL	Neutral					
ETL/$RbGeI_3$	Neutral	1.00E+12	1.00E-18	1.00E-16	Single	0.6 eV

II.7.5. Tandem solar cell structure:

The structure employed in this study consists of a traditional solar cell configuration, namely p-CIGS* as the absorber layer it has been chosen that the thickness is about 1.2 µm to lower the J_{sc} losses and its band gap about 1 eV to create a multi-level absorption from top with high band gap and bottom with lower band gap, p-CZTSe as the second absorber layer, n-CdS as the electron transport layer, and n-ZnO as the electron contact layer. This well-established structure has demonstrated promising performance in terms of efficiency and stability.

To further enhance the overall efficiency of the solar cell, a perovskite solar cell will be introduced as a tandem component. This perovskite cell will consist of an HTL, $RbGeI_3$-based perovskite absorber layer, and an ETL. The combination of these materials in the perovskite cell aims to harness a broader range of the solar spectrum and increase the overall power output of the tandem solar cell system.

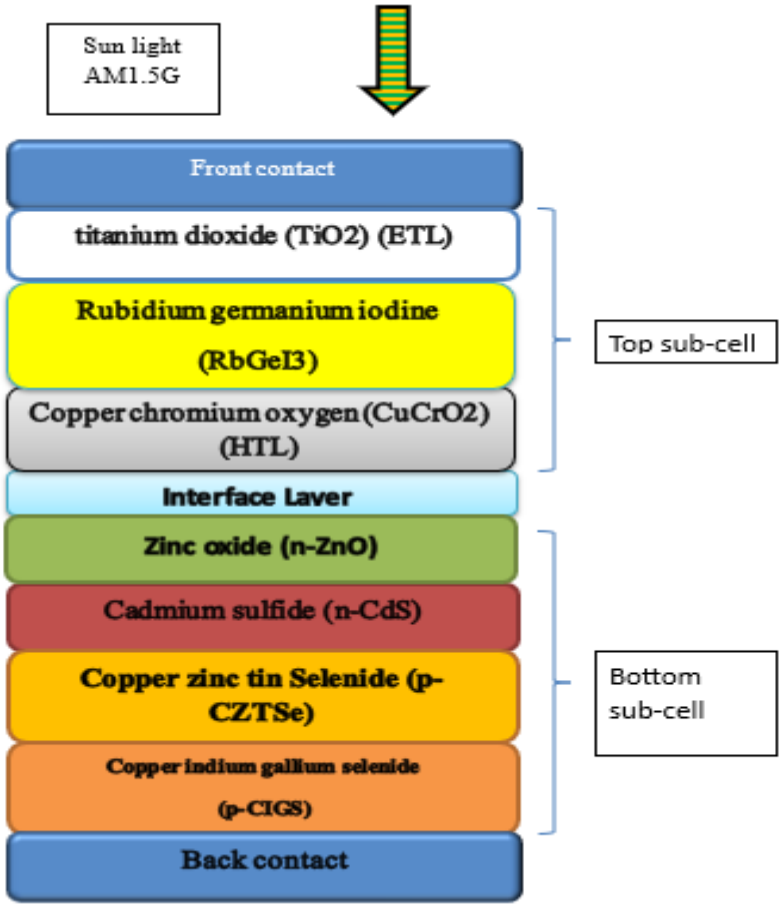

Figure II. 9: Tandem structure of the solar cell

* Note that the CIGS layer in the bottom sub-cell during the simulation of the tandem, is fix and do not variate.

By integrating the perovskite tandem cell with the existing structure, my research aims to explore the synergistic effects and potential performance improvements achievable in this hybrid architecture. The objective is to achieve a higher power conversion efficiency while maintaining the stability and reliability of the solar cell system

.

II.8. Conclusion:

After examining the main features of this program, the ability to simulate a wide range of solar cell structures is obtained. This is done by using scientific theories and mathematical approximations. Among the many programs available, it is clear that this simulation program is the best choice for both beginners and advanced students who want to understand the basics of solar cell technology. It is also beneficial for researchers who want to conduct their primary experiments.

Additionally, we provide a detailed overview by studying the properties and structure of materials like $RbGeI_3$ perovskite and CZTSe. This led us to reach a conclusion in our chapter where we present carefully collected data from different sources. This data will be a valuable reference for simulating our core architecture (p-CIGS/n-CdS/n-ZnO). In the next chapter, we will work to enhance the architecture further to achieve the highest level of efficiency.

Chapter III

Result analysing and discussions

III.1. Introduction

The primary objective of this chapter is to achieve high efficiency through the simulation of a second-generation thin film solar cell. This cell has core structure comprising (p-CIGS/n-CdS/n-ZnO). Following extensive simulations and data analysis, we aim to derive optimal results while incorporating new materials to elevate efficiencies.

Our journey commences with a fundamental and elementary structure, gradually progressing towards a complex tandem solar cell design. This progression involves the reduction of the P-CIGS layer's thickness, but adding a p-CZTSe layer. By integrating this dual absorber layer, we aim to mitigate the toxicity and rarity associated with CIGS cell materials, ultimately enhancing overall performance.

To finish the structure, we introduce an inorganic perovskite layer. This strategic addition aims to surpass the remarkable efficiency of 37%, thereby surpassing the limitations imposed by the Shockley-Quasar principle, which dictates that materials are incapable of surpassing a maximum efficiency of 32%.

Through a step-by-step evolution from a rudimentary framework to a complex tandem structure, we attempt to unlock new frontiers in solar cell efficiency. This scientific pursuit holds the potential to revolutionize the field of photovoltaics, driving advancements in sustainable energy generation beyond previous constraints.

III.2. Simulation results and optimization

In our study, we have examined three parameters that impact the performance of our thin film solar cell. This simulation focuses on analysing the influence of proprieties such as thickness, band gap, and doping on the p-n junction layers, specifically the p-CIGS and n-CdS layers.

III.2.1. Studding of different material properties effect of CIGS layer

III.2.1.1. The effect of thickness on p-CIGS

It is well known that the thickness is one of the major factors that can affect the solar cell performance, this simulation will study the effect of this parameter on the absorber layer, so as to analyse them the typical thickness of CIGS is about 2µm [1] .

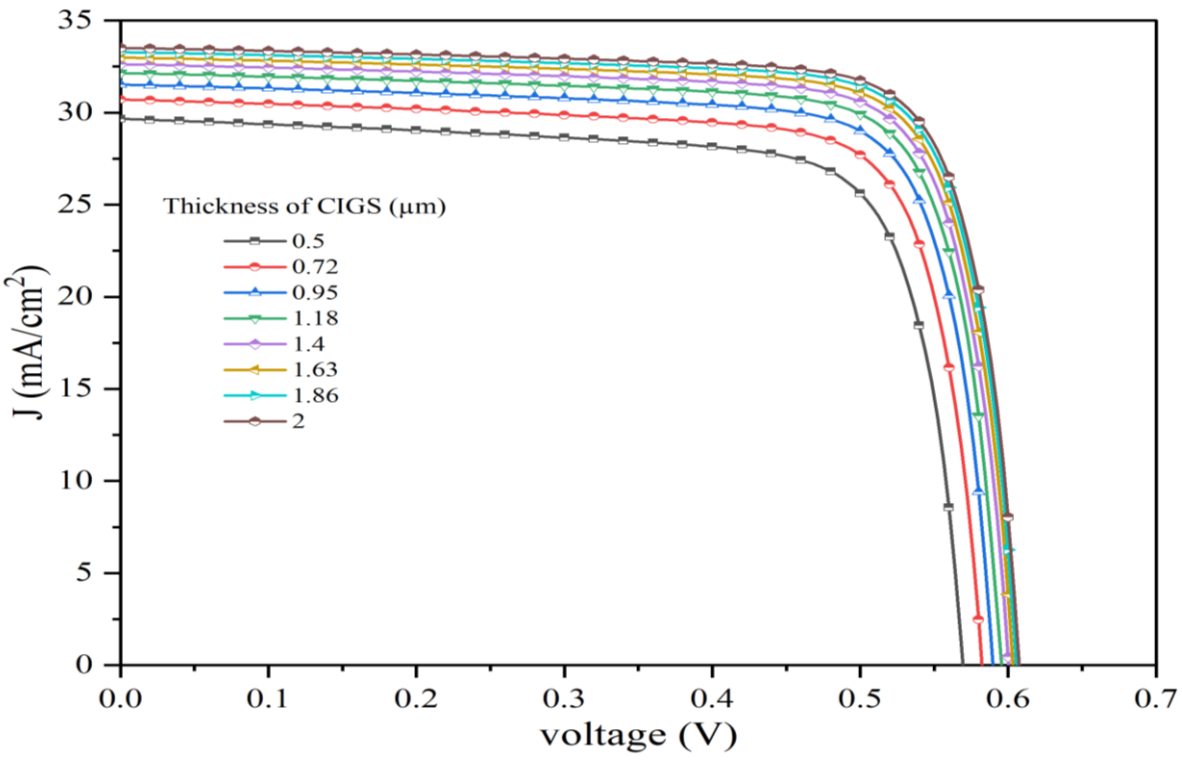

Figure III. 1: J-V characteristics of effect of thickness on CIGS layer

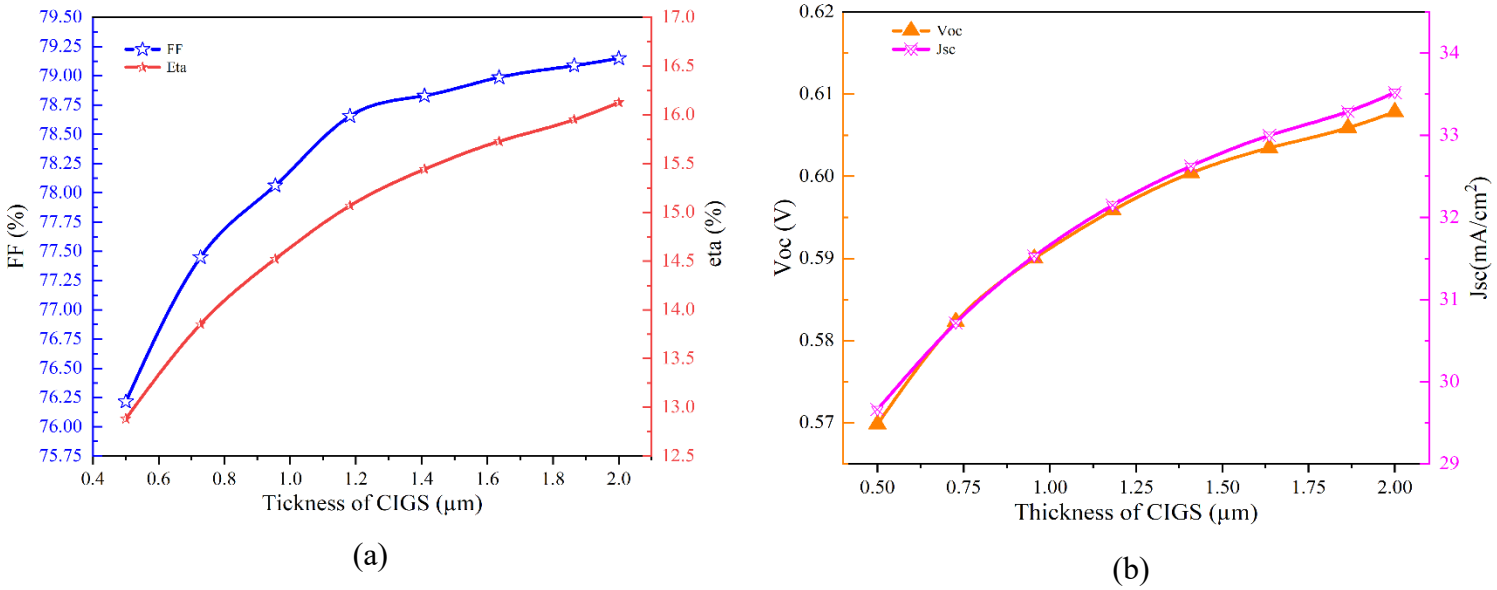

Figure III. 2: Effect of thickness on CIGS layer in thin film solar cell (a) effect of thickness on fill factor and efficiency (b) effect of thickness on V_{oc} and J_{sc}

By analysing the J-V graph in Figure III. 1, a clear observation can be made that increasing the thickness results in an increase in V_{oc} and J_{sc}. This correlation is further supported by Figure III. 2 (b) graph where it shows an increment in the V_{oc} and J_{sc}. Consequently, this leads to an overall improvement in the efficiency of the cell, as illustrated in Figure III. 2 (a), which displays an improvement in the efficiency coinciding with the increase in thickness. Additionally, the incrementation of thickness shows a positive correlation with the fill factor, as depicted in the same Figure.

The phenomenon can be elucidated by increasing the thickness of the active layer, known as CIGS, which leads to enhanced absorption of photons from the sun. As a result, a greater number of electron-hole pairs are generated within the absorber layer (CIGS). These pairs are subsequently collected due to the electrical field created by the p-n junction formed by the p-type CIGS and n-type CdS. The collected pairs are then transported to the electrodes for utilization by the consumer.

The transportation of charge carriers can be further explained by the significance of the thin, doped n-CdS layer, also referred to as the buffer layer. This layer efficiently facilitates the transport of electrons to the negative electrode end. Consequently, as more charges are generated, the likelihood of electrons reaching the n-ZnO layer and being collected by the electrode increases, resulting in the accumulation of electrical charges. This overall process leads to an augmented current density and V_{oc} output.

III.2.1.2. effect of band gap variation on absorber layer

This part will study the band gap (Eg) variation of the CIGS, the results are represented in the figures below, a typical band gap of CIGS is from 1 eV to 1.6 eV [1].

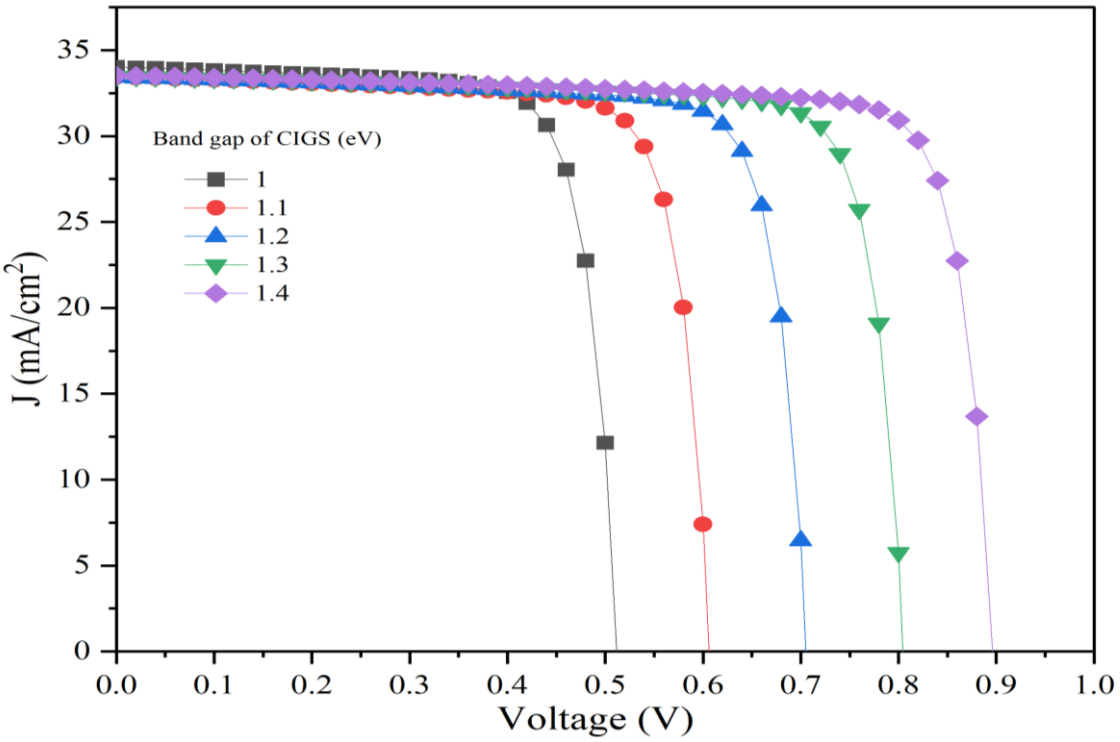

Figure III. 3: J-V characteristics due to variation of band gap

After the J-V characteristic, a detailed observation of the output parameters of the solar cell.

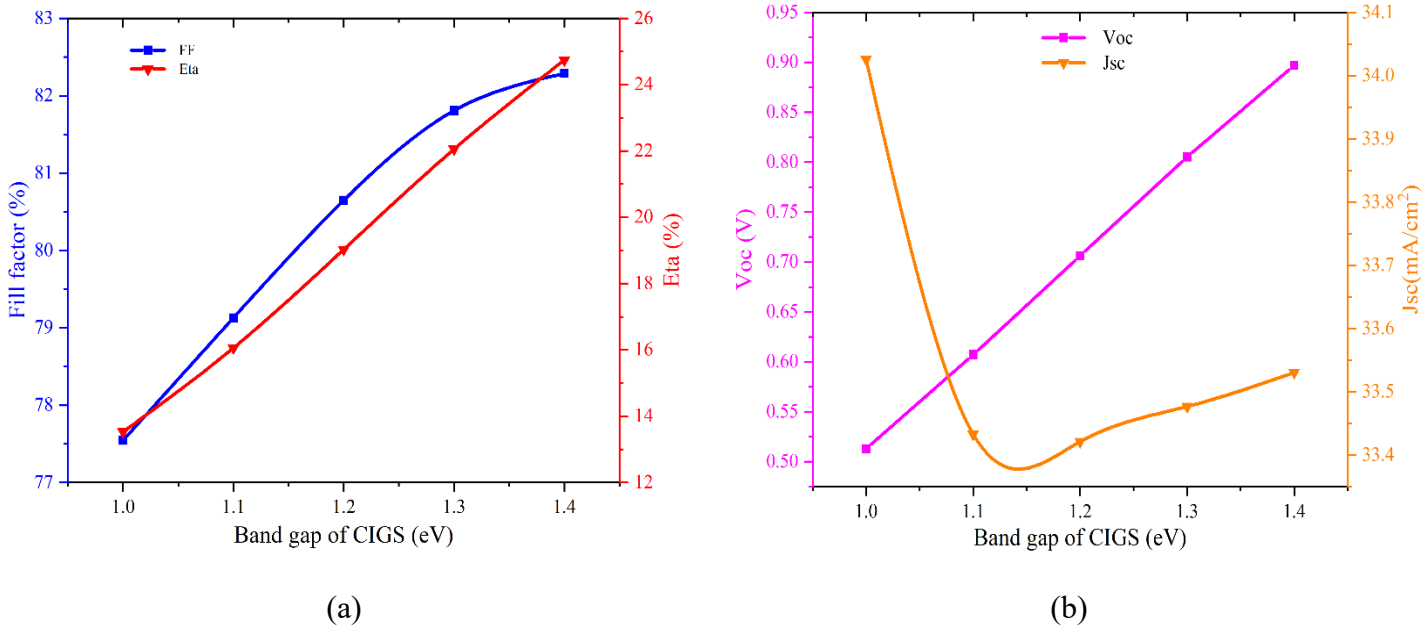

Figure III. 4: the effect of variation of the band gap of CIGS, (a) Fill factor and efficiency, (b) V_{oc} and J_{sc}

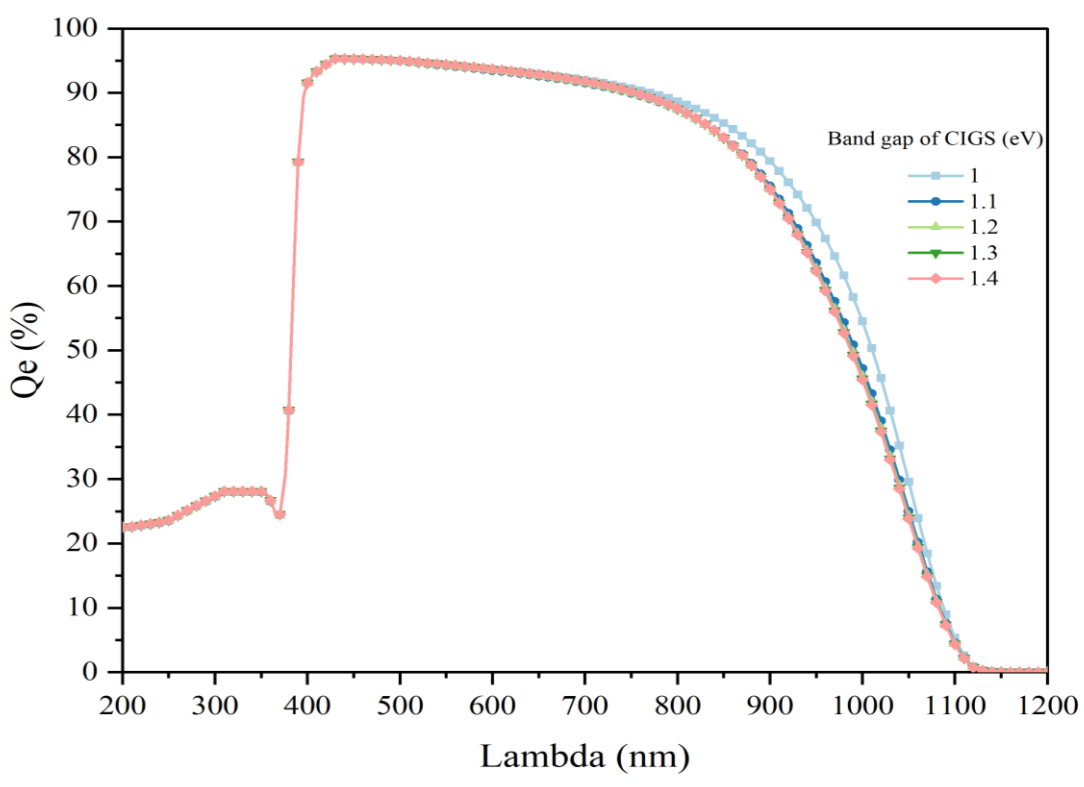

Figure III. 5: Quantum efficiency of the effect of band gap variation

By examining the J-V characteristics presented in Figure III. 3 , it becomes evident that altering the band gap of the absorber layer CIGS has an impact on both the V_{oc} and the J_{sc}.

Specifically, increasing the band gap results in an increase in V_{oc}, while simultaneously decreasing the J_{sc}, as represented in Figure III. 4 (b). Despite the decrease in J_{sc}, Figure III. 4 (a) shows the efficiency increases, along with an improvement in the fill factor.

The observed phenomenon can be explained by considering the energy requirements for electron excitation in the solar cell. Electrons need a certain amount of energy to transition from the valence band Ev to the conduction band Ec. As the band gap of the p-CIGS layer increases, the energy needed for electron excitation also increases. Consequently, photons with lower energies, particularly those in the red and infrared regions of the spectrum, do not possess sufficient energy to extract an electron from the valence band. This limited absorption of lower-energy photons leads to a decrease in the J_{sc} of the solar cell.

Furthermore, the widening of the band gap results in a higher potential for electrons to undergo the transition from the valence band to the conduction band. This increased potential difference across the Ev and Ec bands contributes to a higher V_{oc} in the solar cell. this is clearly demonstrated by the quantum efficiency (*Qe*) absorption in Figure III. 5 where we can notice a decrease in the absorption in wavelengths of about 800 to 1000 nanometres the increase of the band gap in the p-CIGS layer simultaneously influences the absorption regions in the solar spectrum.

III.2.1.3. The effect of dopage variation on absorber layer

simulating the dopage we will be able to study the effect closely and understanding this property's effect on the absorber will be essential for continuing the research.

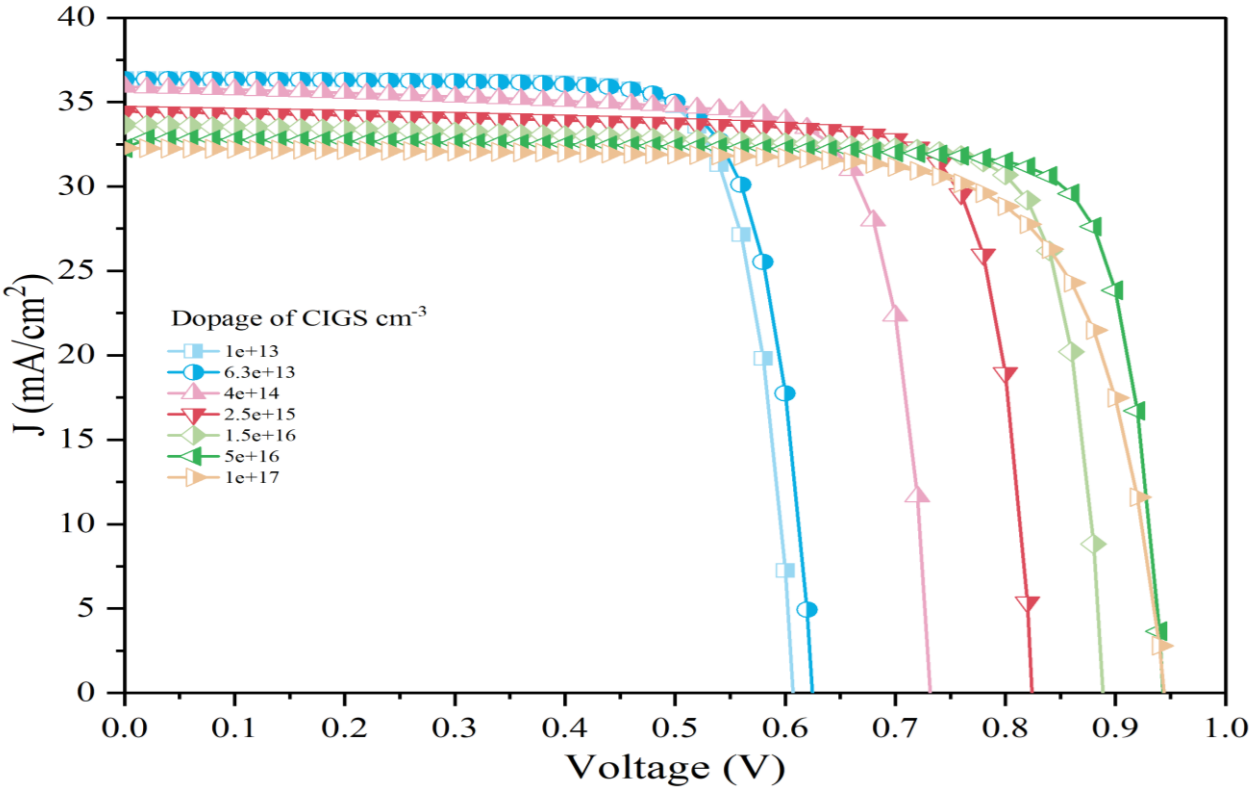

Figure III. 6: J-V characteristics of the effect of dopage on the CIGS layer

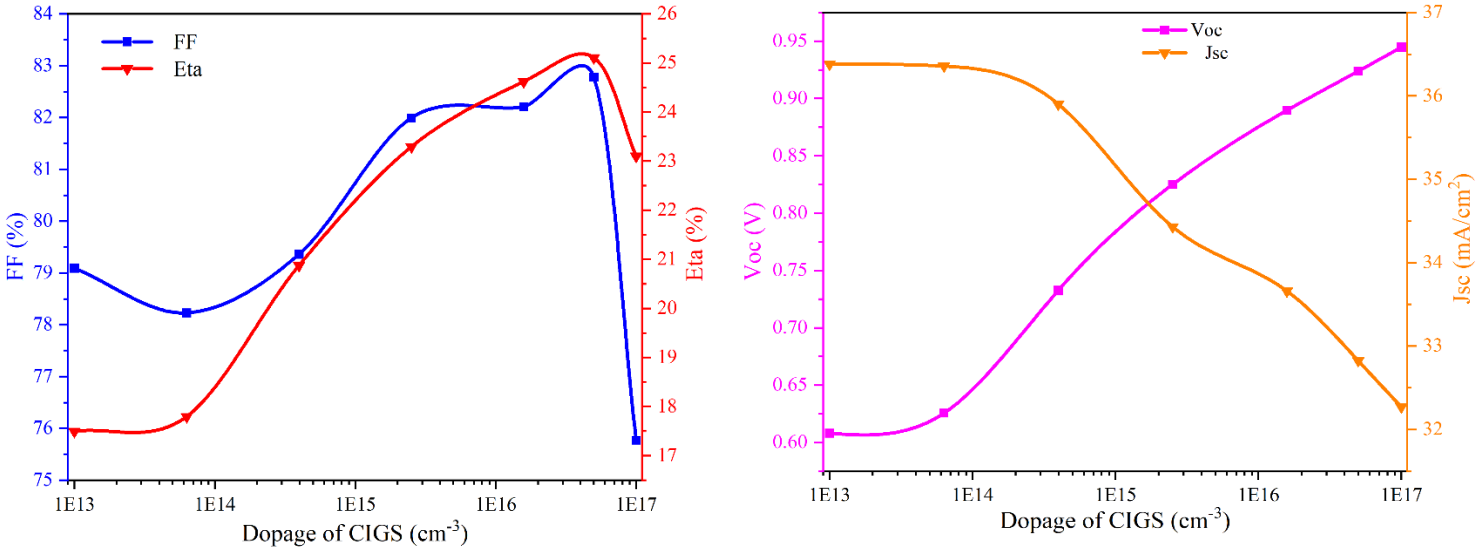

(a) (b)

Figure III. 7: Effect of variation of dopage of CIGS (a) represents efficiency and fill factor, (b) V_{oc} and J_{sc}

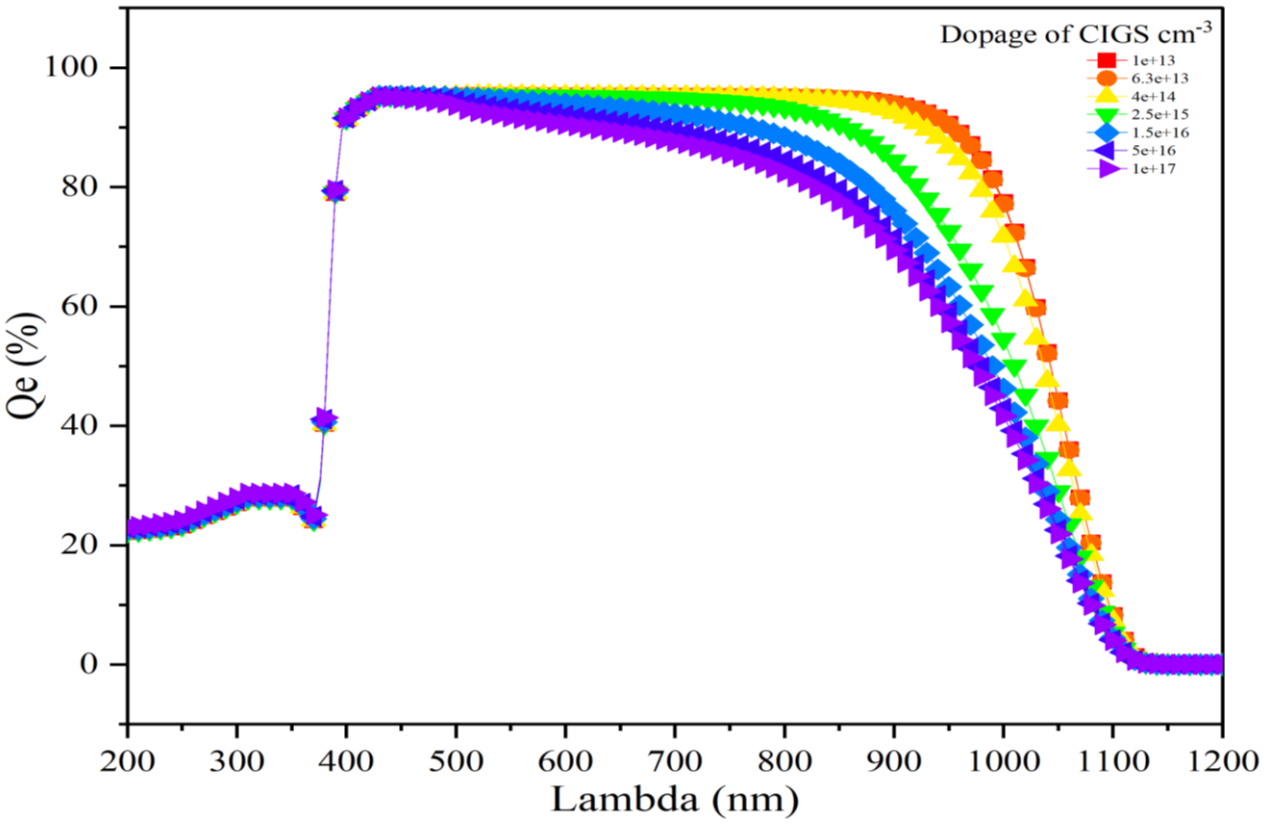

Figure III. 8: Quantum efficiency variation due to the variation of dopage of CIGS

Based on the analysis of the J-V characteristics presented in Figure III. 6, it can be observed that at the lower dopage levels result in higher J_{sc}, and to some extent, it has a low V_{oc}. by increasing the dopage a noticeable decrease in J_{sc} is evident, while V_{oc} increases, as depicted in Figure III. 7 (b). Additionally, the efficiency rises until a max point of about 5e16 cm^{-3} and then it shows a decline, along follows the fill factor with a rise and a reduction as demonstrated in Figure III. 7 (a).

We can explain this phenomenon based on the dopage levels in the p-CIGS layer of our solar cell. When the dopage levels are low, such as a concentration of 1e13 cm^{-3}, or low carrier concentration allows for efficient electron-hole generation with low recombination thus the hight J_{sc}. However, the limited charge extraction resulting from the low carrier concentration leads to a low V_{oc}. Additionally, arriving at 5e16 cm^{-3} the peak efficiency point of the dopage where nearly all parameters are at a high point including V_{oc} where the augmentation of doping leads barrier augmentation, therefor the barrier increase so the charges needs more potential energy to pass thus the augmentation of V_{oc} . the high quantum efficiency observed at lower carrier concentrations can be attributed to the high conversion

and generation with low recombination of photons into electron-hole pairs, as demonstrated in Figure III. 8.

III.2.2. Studding the effects on n-CdS layer

The high bandgap of CdS makes this section unsuitable. for bandgap studies, because absorption of photons on that layer would be negligible.

III.2.2.1. Effect of thickness

As mentioned before the thickness is an important propriety, we will simulate it this time on the buffer layer and analyse the results.

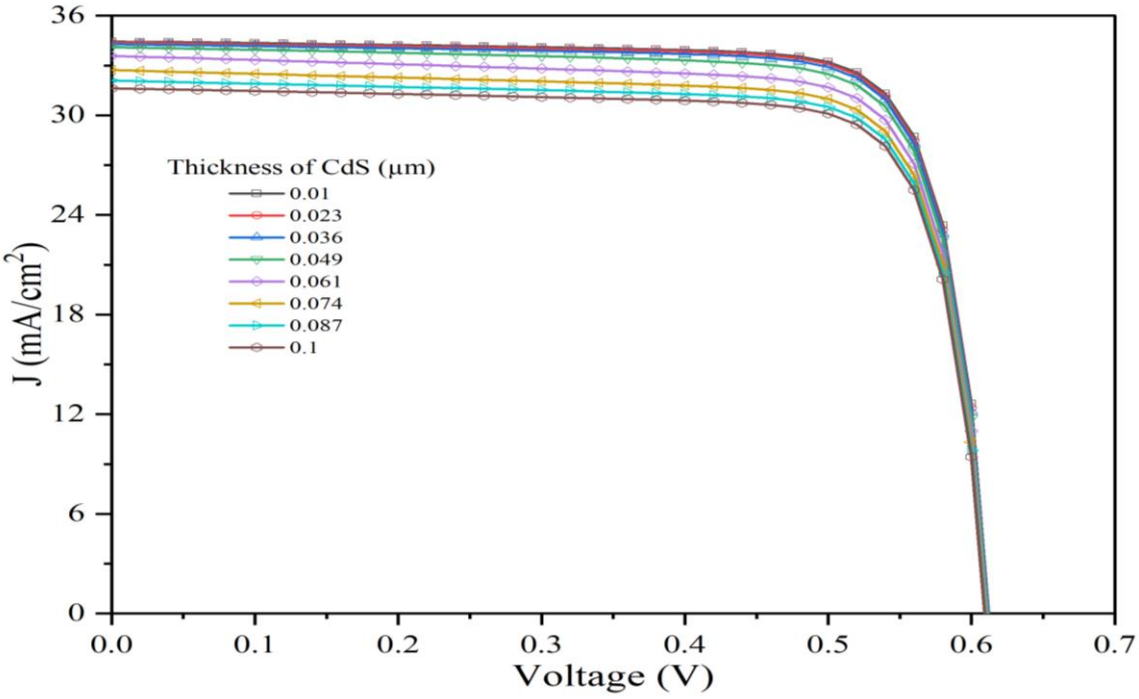

Figure III. 9: J-V characteristics of the effect of thickness on CdS layer

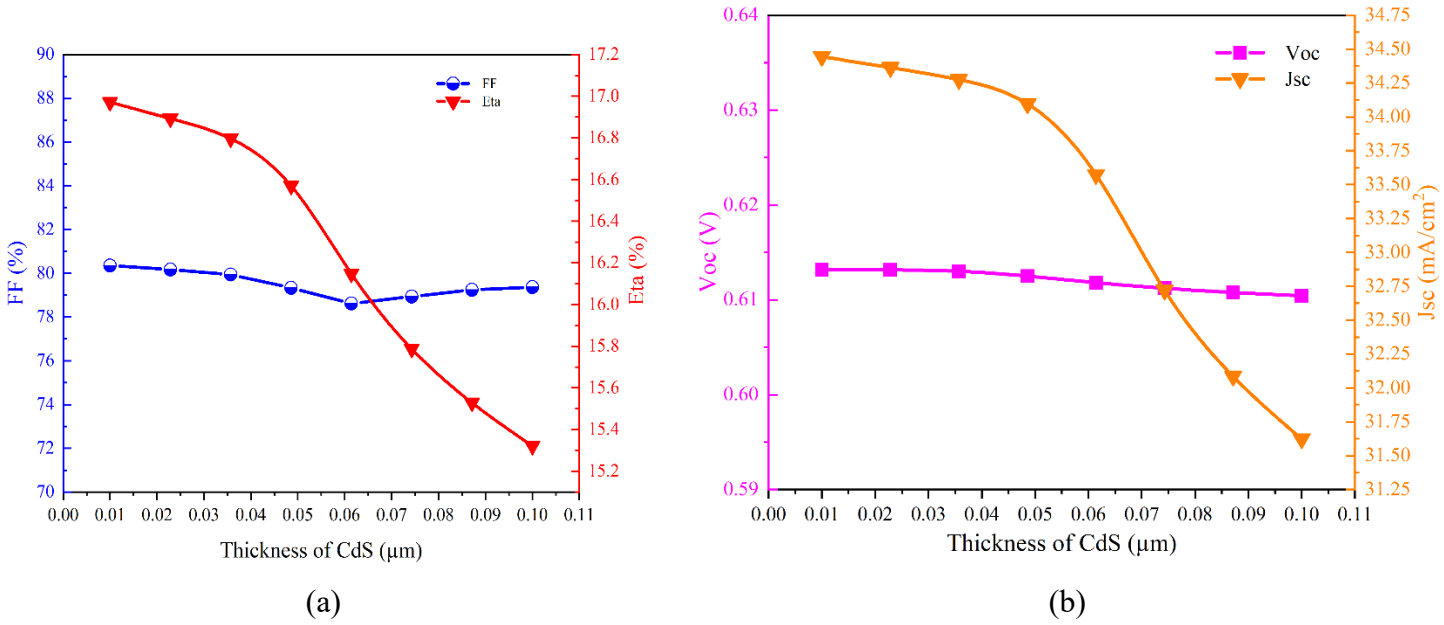

Figure III. 10: effect of variation of thickness of CdS, (a) represents fill factor and efficiency, (b) J_{sc} and V_{oc}

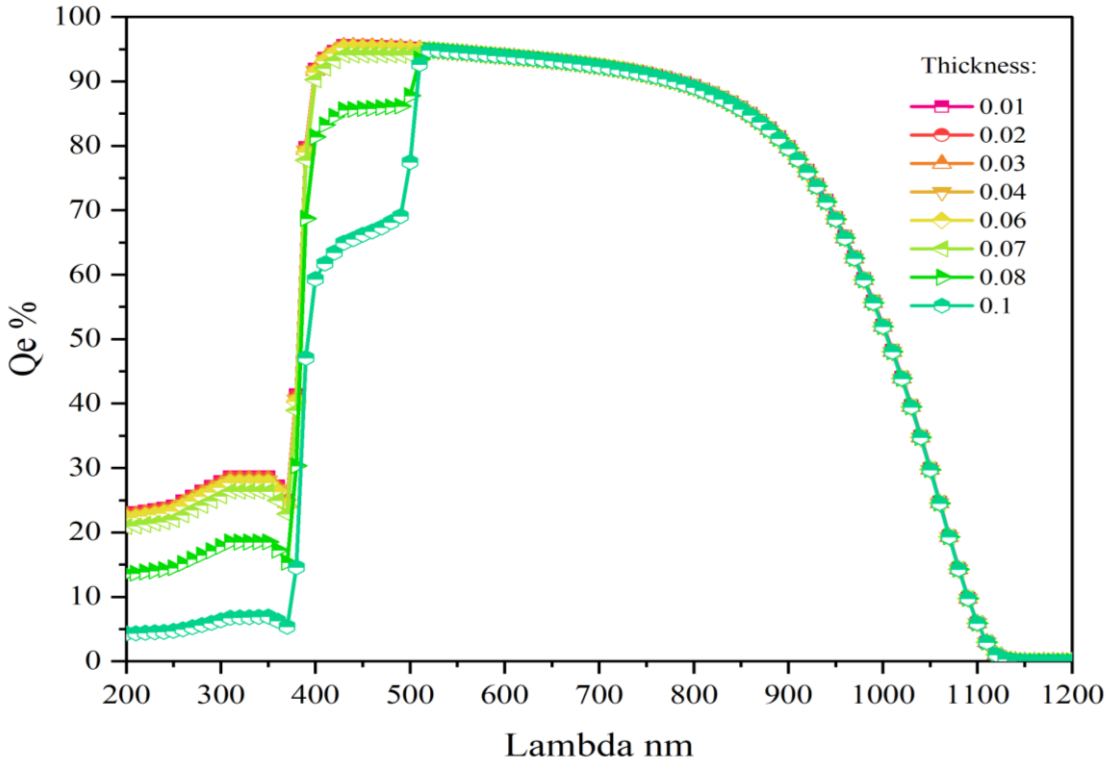

Figure III. 11: Quantum efficiency variation due to the variation of thickness of CdS

The performance of the solar cell is influenced by the thickness variation of CdS. By analysing the J-V characteristics in Figure III. 9, it becomes evident that increasing the thickness of CdS results in a slight decrease in J_{sc}, as depicted in Figure III. 10(b). This decrease can be attributed to the fact that a higher thickness can create traps for electrons,

leading to increased recombination. In other words, the electron lifetime becomes smaller than the thickness of CdS. On the other hand, although there seems to be a decrease in V_{oc} as shown in Figure III. 10(b), the decrement is not significant, indicating its stability.

The decrease in J_{sc} consequently leads to a reduction in the overall efficiency of the solar cell, as observed in Figure III. 9 (a). This decrease in efficiency is directly influenced by the decrease in J_{sc}. This observation is further supported by the analysis of the quantum efficiency graph in Figure III. 11, where a lower absorption in the near blue region is observed. This is due to the high band gap of CdS, which contributes to absorption in the ultraviolet region. Additionally, the increased thickness of CdS affects the transmission of light to the absorber layer, further impacting the overall performance of the solar cell negatively.

III.2.2.2. Effect of dopage variation of the CdS layer

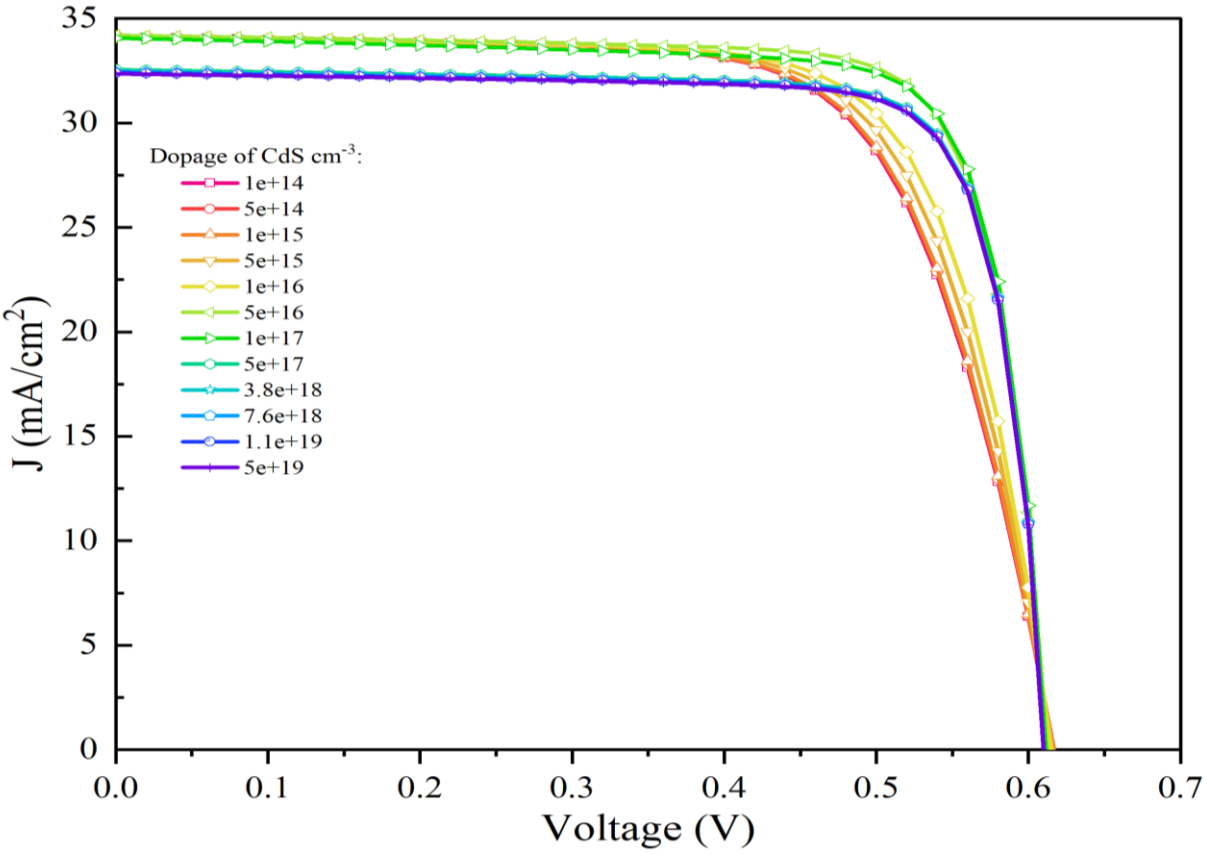

Figure III. 12: J-V characteristics of the effect of dopage variation on CdS layer

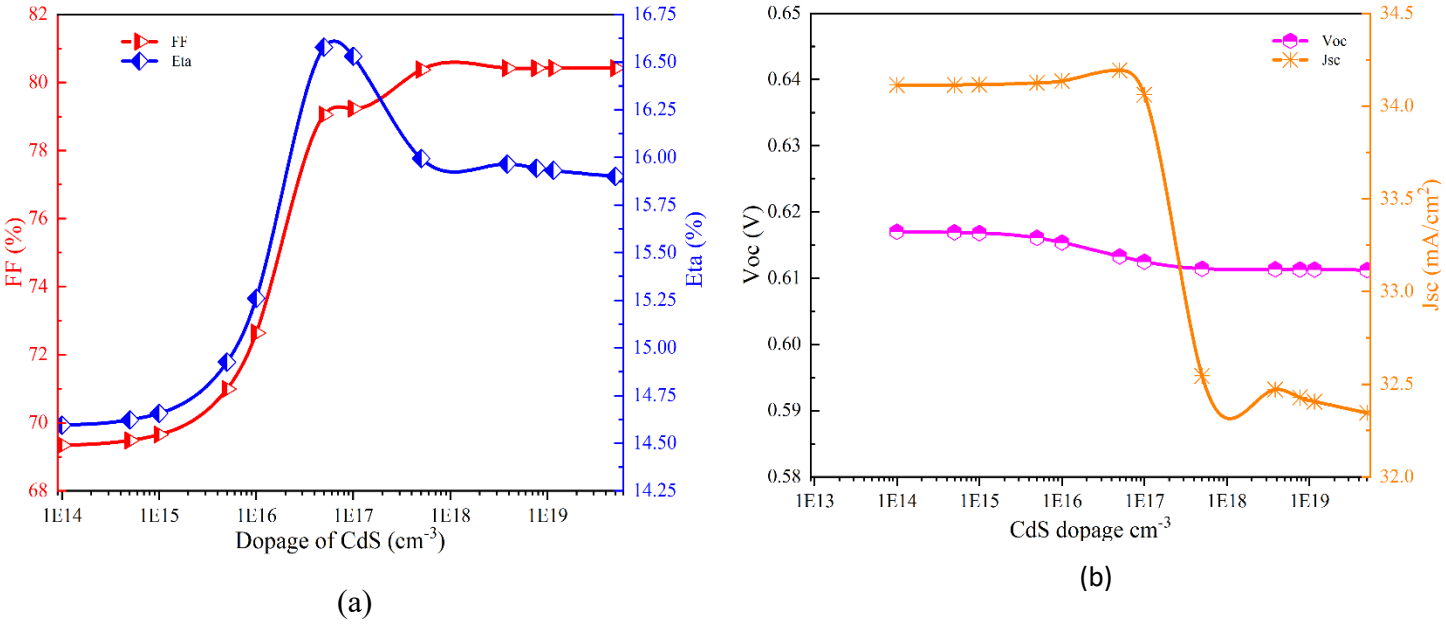

Figure III. 13: Effect of variation of dopage of CdS, (a) performance of fill form, (b) performance of J_{sc} and V_{oc}

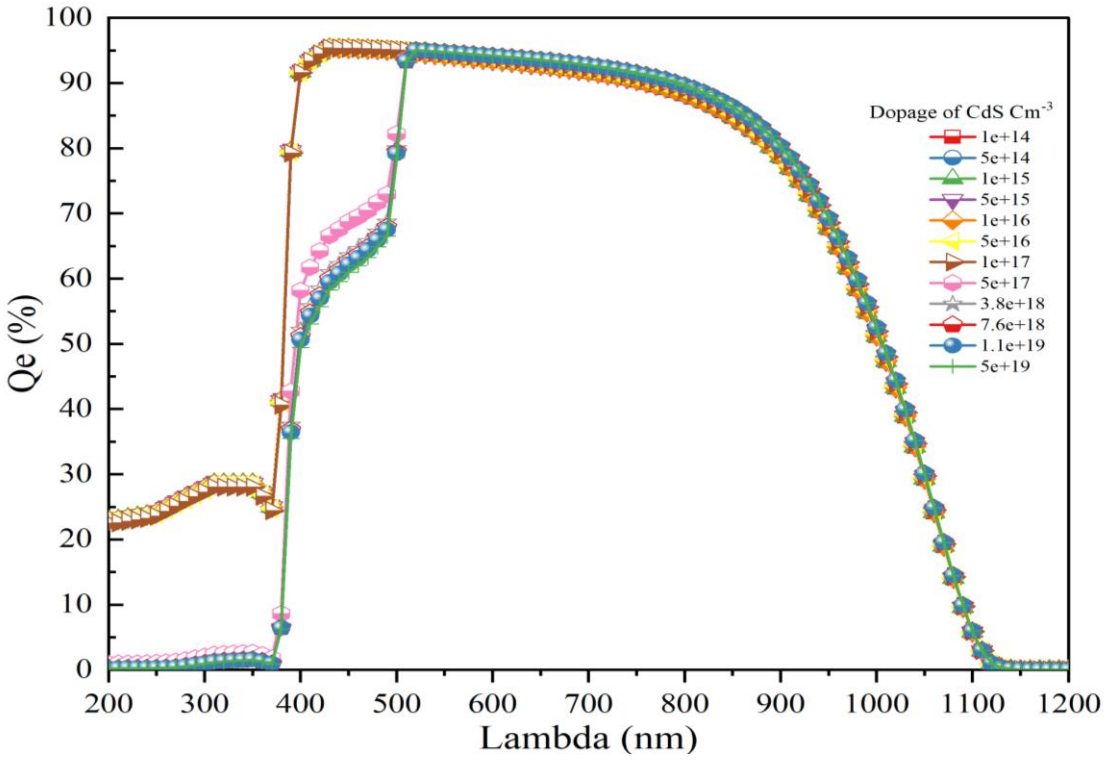

Figure III. 14: Effect of dopage variation of CdS on Quantum efficiency

Upon analysing the J-V characteristics presented in Figure III. 12, a slight increase in J_{sc} is observed. However, beyond a threshold of approximately 5e15 cm^{-3}, there is a noticeable abatement in J_{sc}. This threshold also corresponds to a minor reduction in V_{oc}, as depicted in Figure III. 13 (a). Although this reduction can be considered negligible,

indicating stability. Consequently, there is an enhancement in efficiency up to the aforementioned threshold, followed by a decline in efficiency as the fill factor increases.

The analysis reveals that doping has a dual effect on the CdS layer in the p-CIGS/n-CdS/n-ZnO solar cell structure. On one hand, higher doping concentrations negatively impact the optical absorption, particularly in the blue region, as demonstrated in Figure III. 14 where the quantum efficiency exhibits a decrease in blue wavelengths. This reduction in absorption subsequently leads to a decrease in the generation of J_{sc}, resulting in a decline in efficiency.

On the other hand, the analysis also indicates a positive impact of doping on the CdS layer. Specifically, at lower doping concentrations, there is an increase in J_{sc}, which contributes to an enhancement in efficiency during the early stages before reaching a threshold.

Furthermore, the characteristics of the doping variation phenomenon shed light on its effect on carrier mobility. The introduction of doping at higher concentrations introduces scattering centres, which can impede carrier mobility and introduce additional resistivity. This directly affects charge transportation within the device, resulting in a drop in efficiency, as depicted in Figure III. 13 (a), where the efficiency decreases from the optimal doping level. Conversely, lower doping concentrations lead to insufficient charge generation, resulting in lower efficiency.

III.2.3. Optimal parameters of the solar cell

The optimal parameters used in this simulation are the following:

Table III. 1: optimal parameters for the (p-CIGS/n-CdS/n-ZnO) solar cell

Properties	p-CIGS	n-CdS
Thickness (µm)	2	0.4
Band gap (eV)	1.4	2.4
Dopage (cm^{-3})	5e16	1e17

This optimization has given these results, that will allow the represent J-V characteristics also the output parameters.

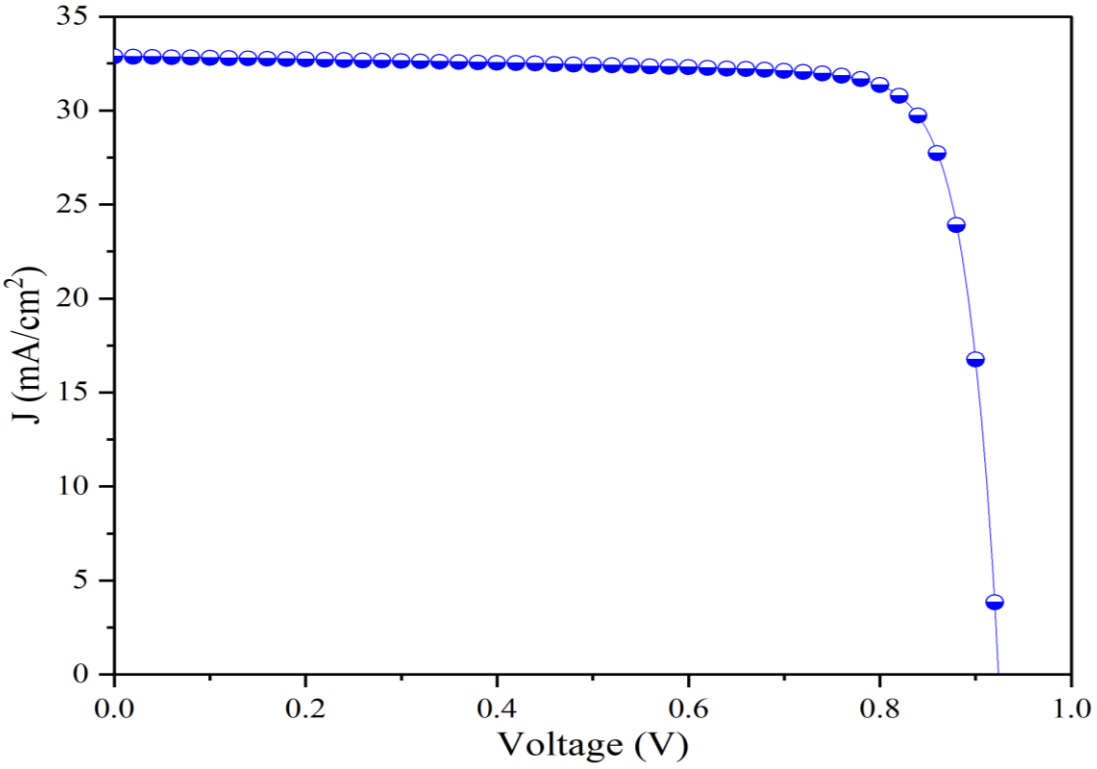

Figure III. 15: J-V characteristics for optimal configuration of solar cell

The table below will display a more detailed view on the collar cell.

Table III. 2: parameters of the optimized solar cell

Parameters	Results	Units
V_{oc}	0.92	Volts
J_{sc}	32.88	mA/cm^2
FF	83.08	%
Efficiency	25.24	%

For achieving an efficiency of 25.24 % it required careful optimization of multiple parameters like thickness and the band gap and the dopage of multi-layer. Further research efforts can focus on fine-tuning other parameters, exploring novel materials, and improving device architectures to push the efficiency even higher.

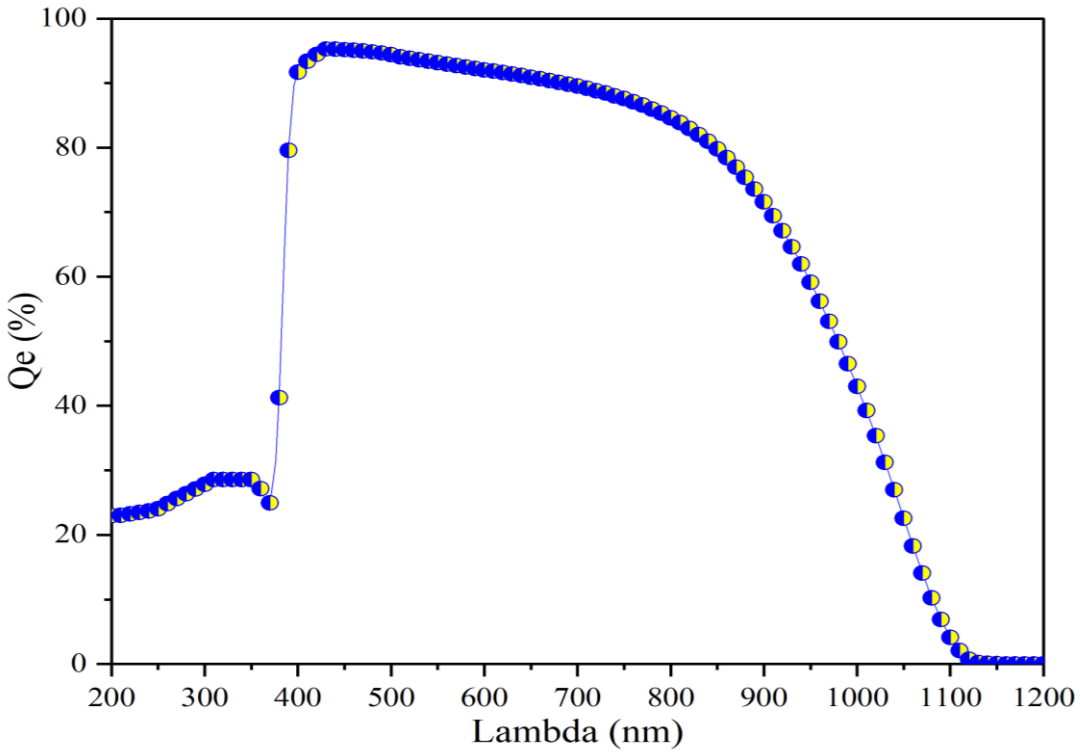

Figure III. 16: Quantum efficiency for the with optimal properties

The absorption of this optimized solar cell shows that the absorption is best at near blue regions, then that of the red region this can be explained with the band gap of 1.4 eV in the absorber layer.

III.3. Effect of introducing new absorber layer (p-CZTSe)

The two main types of thin film solar cells are the CdTe i.e. Cadmium Telluride, and the CIGS category namely Copper Indium Gallium, Sulphide. But there are drawbacks to both these technologies. While Cadmium is regarded as hugely toxic, Indium and Tellurium are considered as scarce elements in nature and very volatile in cost. In addition, one can note that Tellurium is as scarce as gold. Indium is not that scarce but has a demand for multiple other uses. One can also note the price volatility of both elements between 2003 and 2009 [47] [48].

So, the introduction of CZTSe (Copper Zinc Tin Selenide) will lower these toxic materials. Considering our structure it will consists of two absorbers, so we must carefully select the optimal options from the graph in Figure III. 2 (a) to allow sufficient space for integrating the second absorber while maintaining the thin film structure. In this situation, with a CIGS Thickness of 1.0 µm (Salmane et al) [39] following the research of Dr. Naceur

Salmane, he found that the incrementation rate slows down significantly beyond this point, indicating that further thickness increase would have minimal impact on efficiency or power generation. Therefore, selecting a CIGS Thickness of 1.0 µm ensures effective utilization of space while permitting the introduction of the new absorber layer, and permitting us to make further enhancements to the solar cell to arrive to a desirable performance in our thin film solar cell structure [49].

III.3.1. Study of different effects on CZTSe

The main effects that will be studied are the variation of Thickness, band gap and the dopage and seeing their effect on the solar cell over all, in this part we chose to take the band gap of CIGS about 1.2 eV so as not to lower the efficiency.

III.3.2. Optimizing the dopage and band gap of the p-CZTSe layer

As mentioned, before we will continue from the research of (Salmane et al.) In their study, they used a thickness of 1.0 µm for the CIGS layer and 0.9 µm for the CZTSe layer. In our simulation, we will vary the doping and band gap in a matrix to achieve optimal outcomes. Subsequently, we will compare the thicknesses of CIGS and CZTSe using the same method for the double absorber layer solar cell. The results will be presented in the form of a heat map and contour profile, which I will briefly explain.

III.3.2.1. Study of the effect of CZTSe as a double absorber layer in our solar cell variation of dopage with band gap

The following figures will give an insight of the best dopage and band gap that can be given to this solar cell to achieve even higher efficiency then the previous structure.

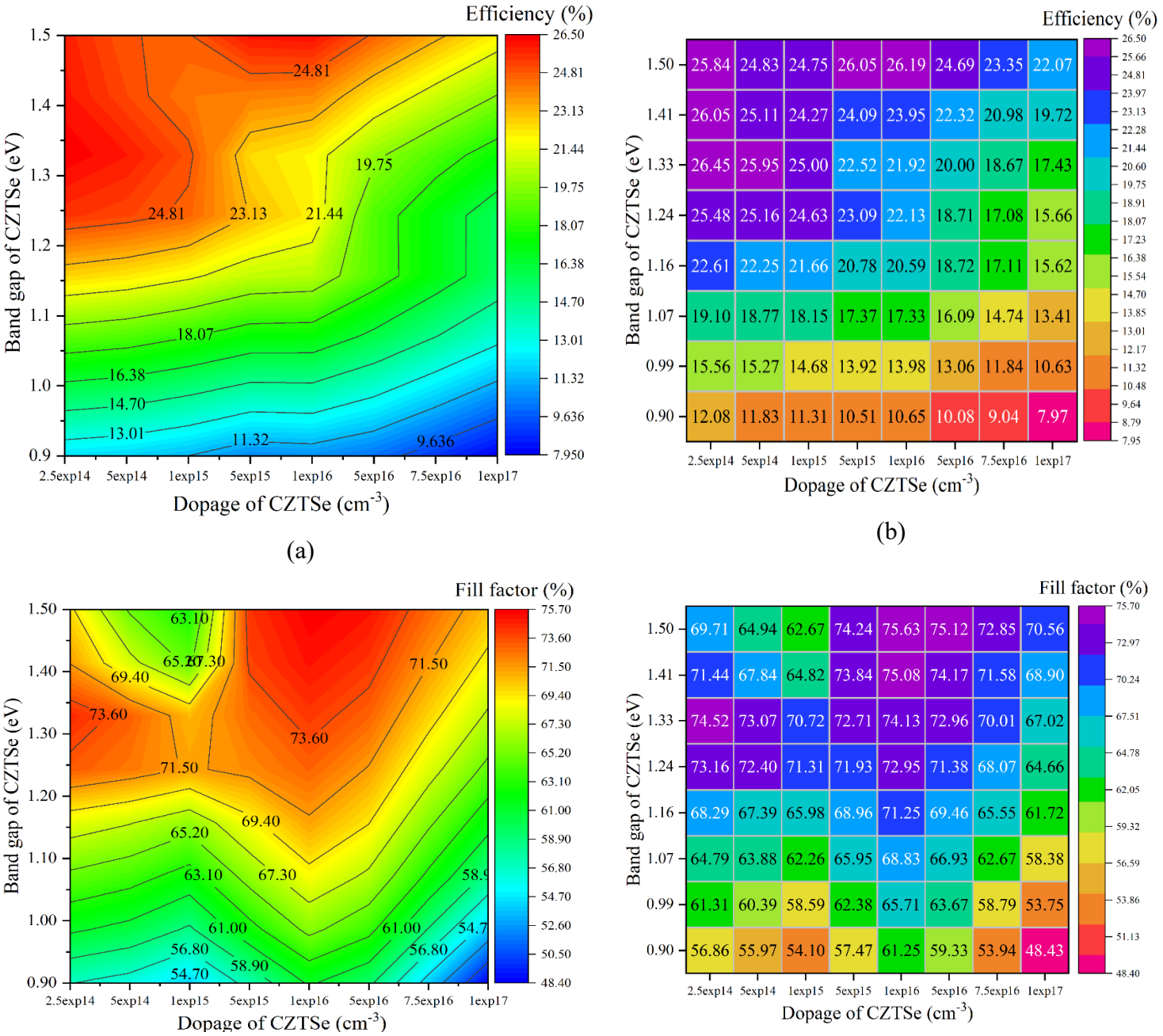

Figure III. 17: heatmap and contour presentation of the variation of dopage and band gap, (a)efficiency contour, (b) efficiency heatmap, (c) fill factor contour, (d) fill factor heatmap

After analysing the heatmap of efficiency and fill factor we can conclude that the best dopage band gap ratio for CZTSe we found the best dopage is: 2.5e14 cm^{-3}, band gap is: 1.33 eV.

With this parameter we will achieve a high efficiency of 26.45 %. Thus, simulating J-V characteristics to understand the comportment of the new variation.

As mentioned before in paragraph III.3.1, we had to shoes a lower CIGS band gap than the optimal achieved because when the band gap of the CZTSe which is on the top, when its lower than the band gap of CIGS our efficiency had dropped significantly because the CZTSe will be absorbed most of the spectrum combined with low thickness the efficiency will drop.

III.3.2.2. Simulation of optimal values between dopage and band gap of CZTSe

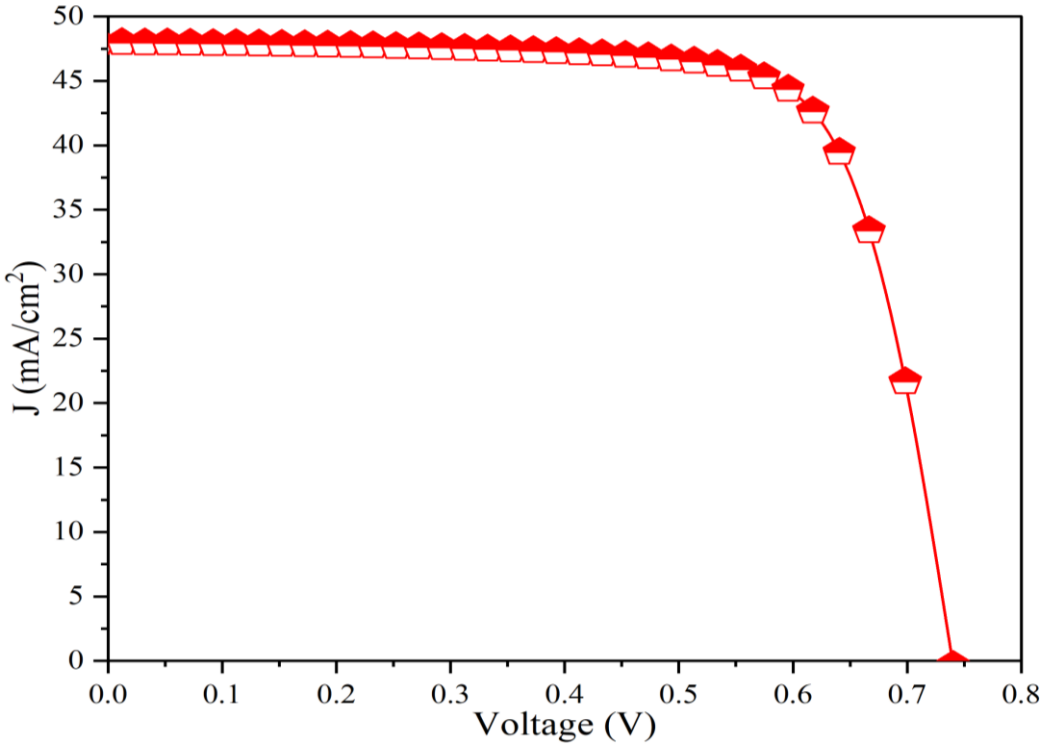

Figure III. 18: J-V characteristics after optimization of the second absorber layer CZTSe

The table below shows the parameters of the best out come from the previous simulation.

Table III. 3: output parameters of the optimized second absorber layer

Parameter	Renault	Unit
V_{oc}	0.739787	Volt
J_{sc}	47.98405	mA/cm²
FF	74.5139	%
Eta	26.4509	%

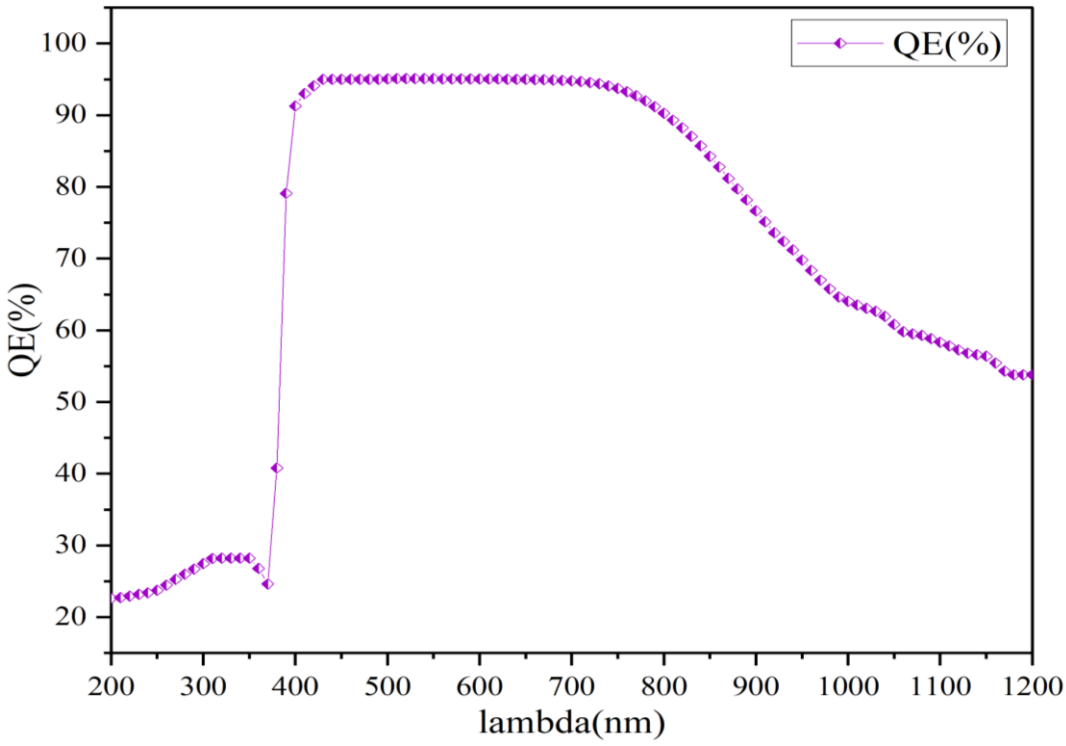

Figure III. 19: Quantum efficiency after optimization of the second absorber layer CZTSe

After analysing the J-V characteristics in Figure III. 18, it is evident that the J_{sc} exhibits a significant increase. This augmentation can be attributed to the enhanced absorption of the solar spectrum represented in Figure III. 19 the absorption in near red regions have augmented highly resulting from the optimization of crucial parameters ultimately showing the power of double absorber layers, giving the opportunity to have a tenable band gap thus resulting in a higher efficiency. Additionally, V_{oc} is observed to re ach approximately 0.74 volts, which can be attributed to the variation in doping levels and band gap, as previously mentioned. It is important to note that there exists a direct correlation between the doping levels, band gap, J_{sc}, and V_{oc}.

III.3.2.3. Optimizing the thickness of the p-CZTSe layer and p-CIGS

After optimizing the dopage and band gap of the CZTSe absorber layer we will try to enhance it farther more by optimizing the thickness of the p-CIGS absorber with p-CZTSe absorber layer:

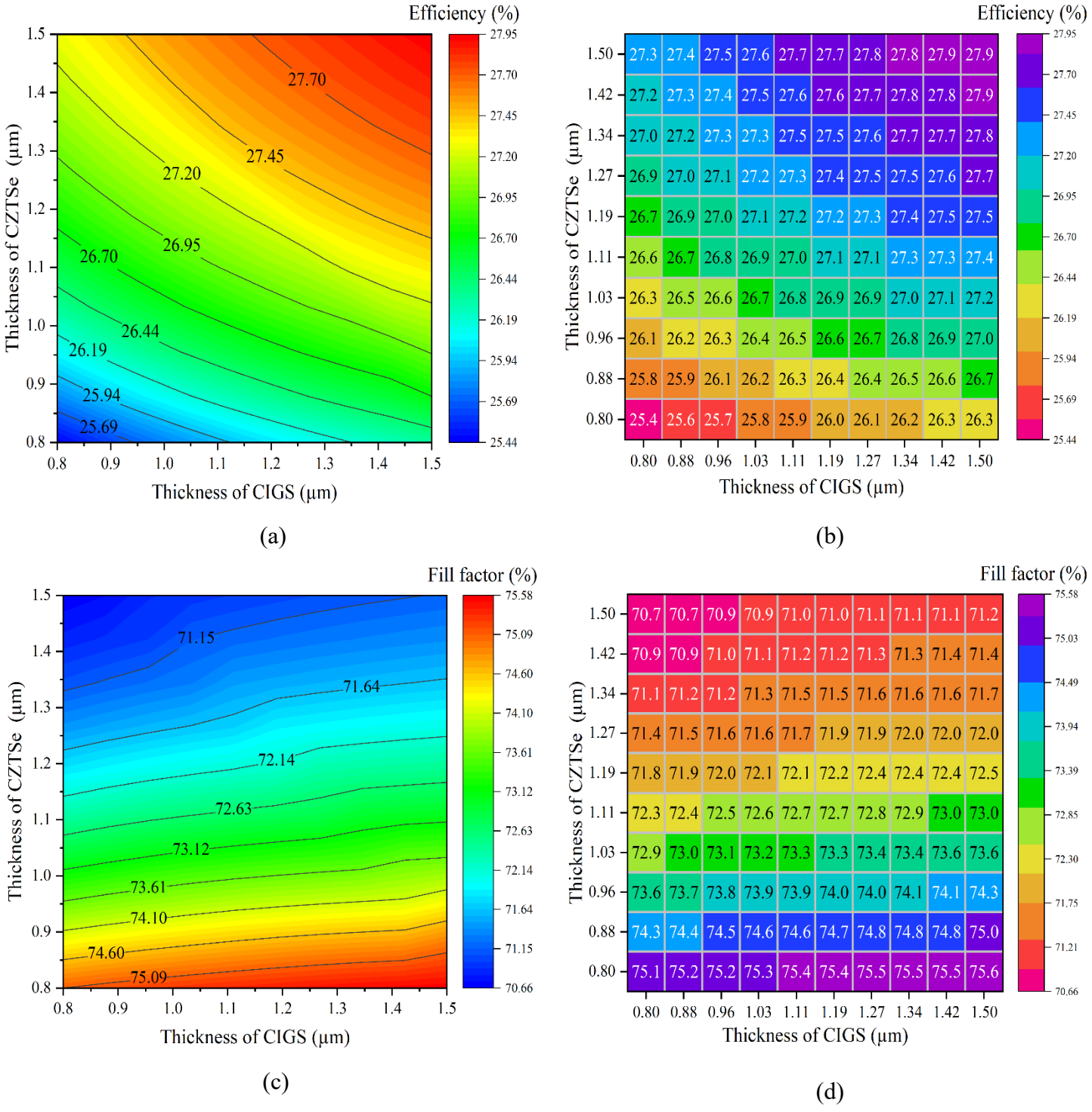

Figure III. 20: heatmap and contour presentation of the variation of the thickness of double absorber layer (p-CIGS) and (p-CZTSe), (a)efficiency contour, (b) efficiency heatmap, (c) fill factor contour, (d) fill factor heatmap

Therefore, based on our findings, it can be inferred that there exists a positive relationship between thickness and efficiency. By increasing the thickness of both absorber layers, we can achieve an efficiency of 27.9%. Specifically, when utilizing a thickness of 1.5 µm for both CIGS and CZTSe layers, this desired efficiency can be obtained.

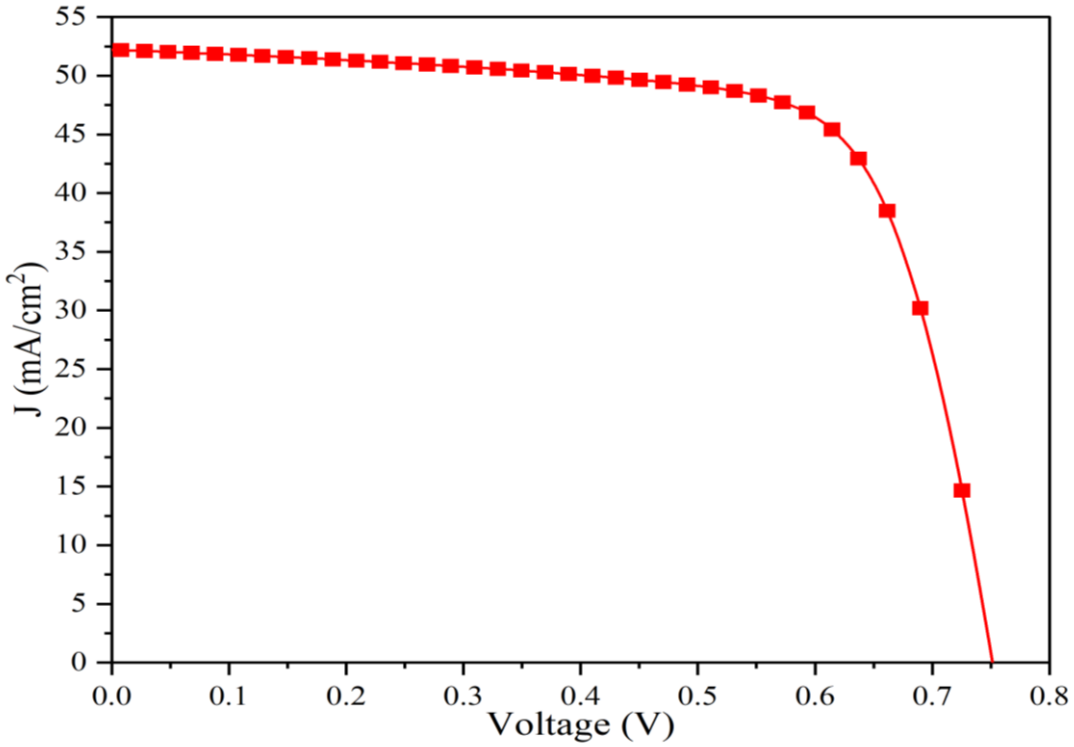

Figure III. 21: J-V characteristics of the optimal thicknesses in the CZTSe layer and CIGS layer of the double absorber solar cell

We can notice a slight increase of the V_{oc} and J_{sc} with choosing optimal parameters of the thickness.

Table III. 4: output parameters of the thickness optimized double layer solar cell

Parameters	Results	Unit
V_{oc}	0.752117	Volt
J_{sc}	52.206	mA/cm2
FF	71.1651	%
Eta	27.943	%

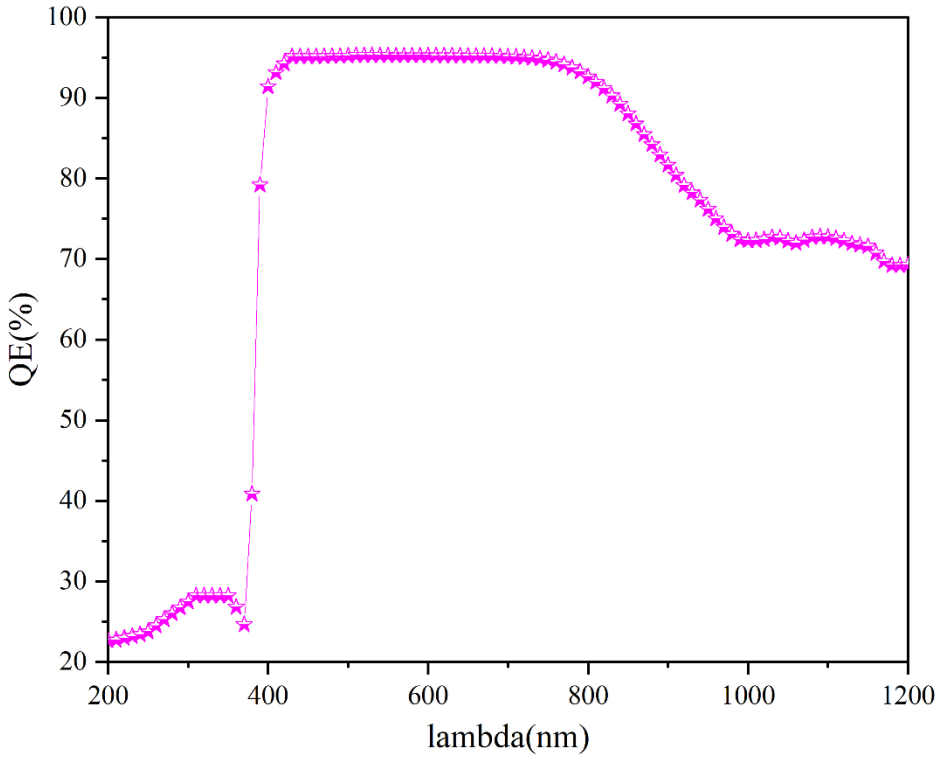

Figure III. 22: Quantum efficiency of the optimal of thickness of CZTSe layer and CIGS layer

In our analysis of the J-V characteristics presented in Figure III. 26, we consistently observed an increase in the J_{sc}, and furthermore, a slight increase in the open-circuit voltage V_{oc}. These trends can be attributed to the correlation between the augmentation of thickness led to an increase in the absorption process in high wavelength compared to before.

III.4. Tandem solar cell:

In this phase of our simulating pr$_{oc}$ess, we will begin by presentation the collected data from our study on a tandem solar cell. Additionally, we will carefully consider this data, taking into account various factors influencing the performance of the solar cell. With a thorough understanding of the data, we will then strive towards the achievement of an optimal and reliable configuring for the solar cell. Throughout this process we will consider the feedback and insights gained from previous research in the field. Furthermore, we will explore alternative approaches and potential modifications to further enhance the solar cell's efficiency. Ultimately, our aim is to derive meaningful conclusions and recommending based on the data analysis, contributing to the advancing of tandem solar cell technology.

It is worth noting that in tandem solar cells, the top sub-cell should consistently have a higher band gap compared to the bottom sub-cell. This principle is rooted in the well-established knowledge that perovskite materials typically possess a relatively high band gap. It is important to highlight that our analysis primarily focuses on situations where the band gap of the bottom sub-cell is lower than that of the top sub-cell, also these variations were made with previous studies.

However, it is crucial to acknowledge that our study does not take in consideration later in the simulation scenarios where the band gap of the bottom sub-cell exceeds that of the top sub-cell. This exclusion is attributed to the limitations of the SCAPS 1d script program designed to be used for tandem solar cell calculations. Since this program is still in its early stages of development, its main purpose is to facilitate mathematical computations. This program does a simulation of each sub-cell alone rather than doing the simulation of the tandem at once. The selection of results is through understanding of the physical phenomime, the Jsc and J_{mp} that where selected is of the sub-cell with the minimum output [50].

By acknowledging these factors and understanding their implications, we can gain a better comprehension of the scope and limitations of our research findings within the context of tandem solar cell simulations also the thickness and band gap of CIGS were mentioned in page 48.

III.4.1. Examining the Impact of Deferent Effects on Tandem Solar Cells

III.4.1.1. The effect of thickness variation on the CZTSe layer and the perovskite layer

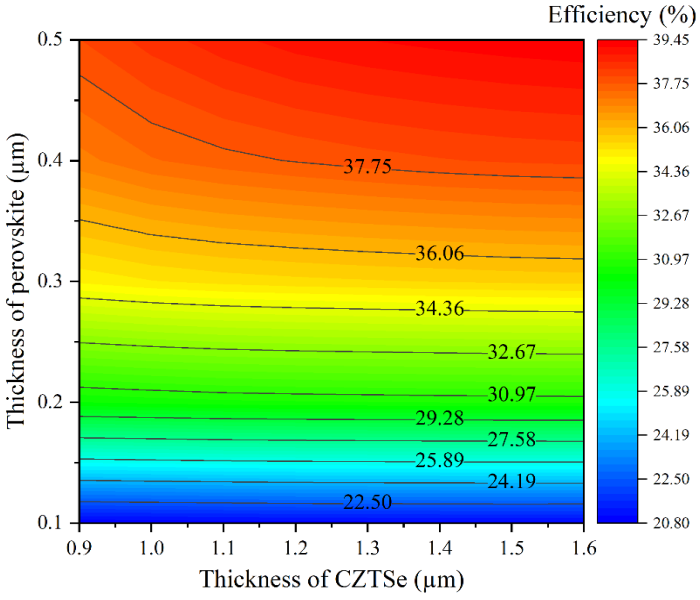

(a)

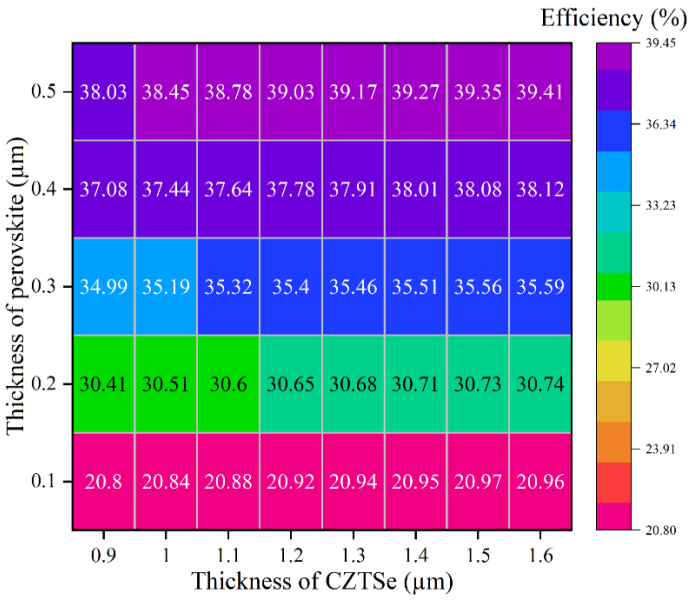

(b)

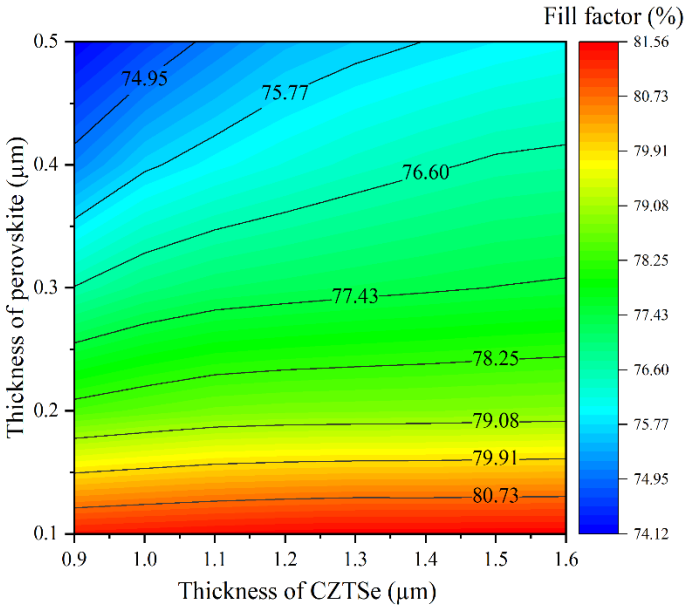

(c)

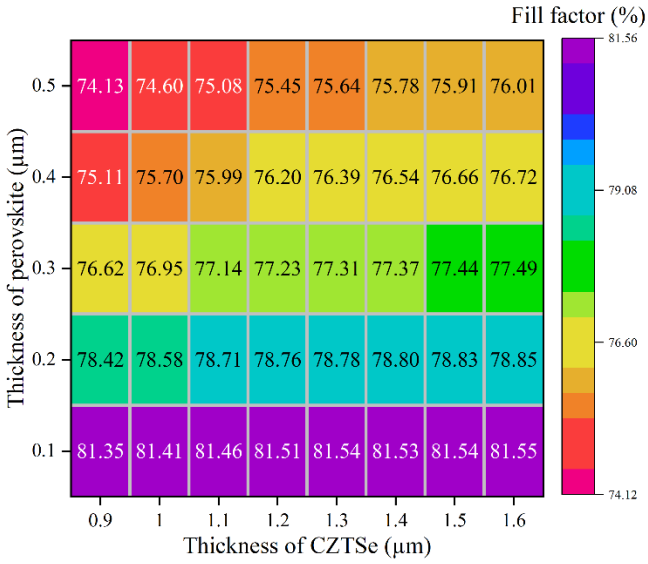

(d)

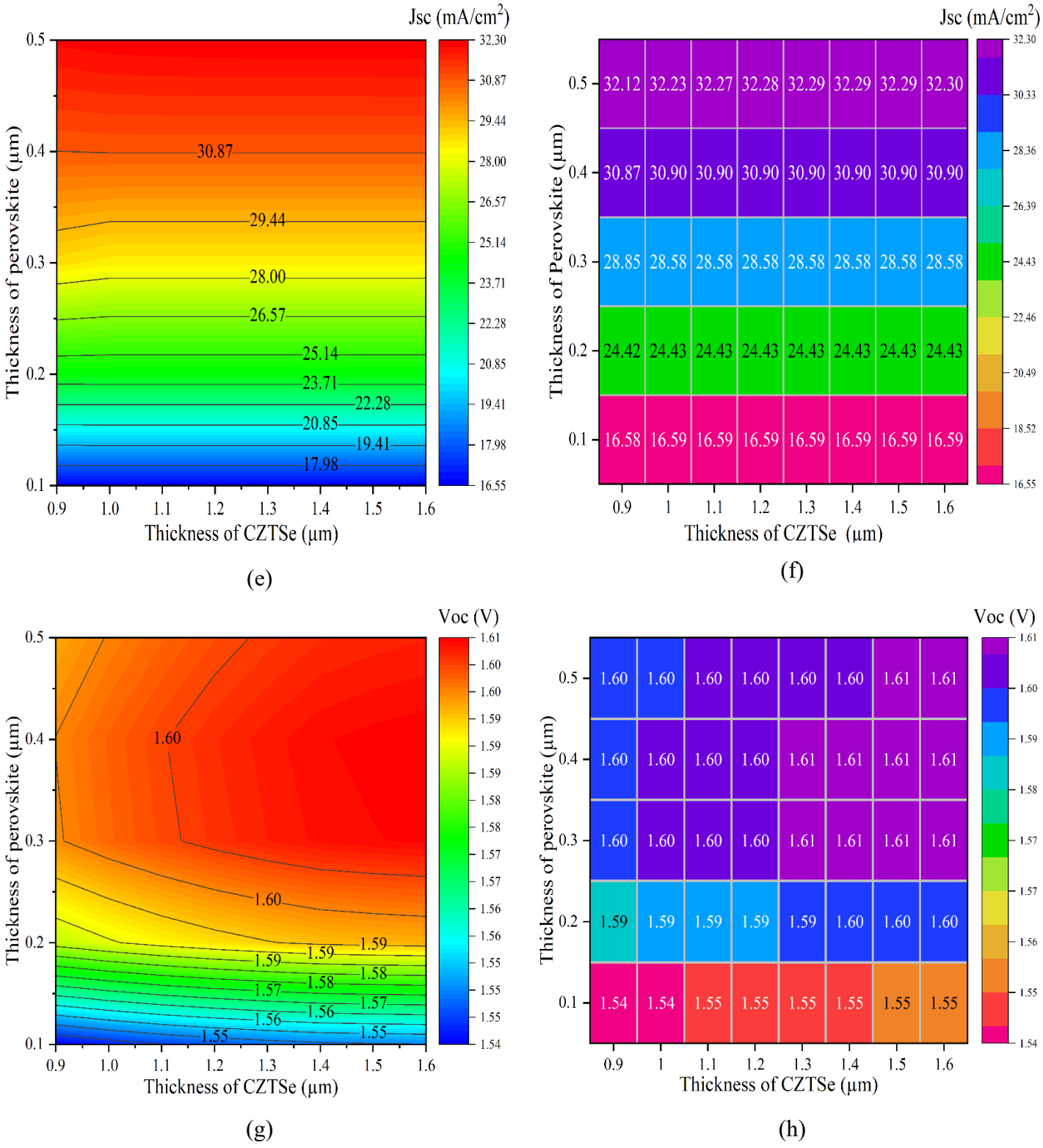

Figure III. 23 the variation of thickness of CZTS and the perovskite sub-cells representer using contour profile and heatmap, (a) shows the efficiency contour, (b) efficiency heatmap (c) shows the fil factor, (d) fill factor heatmap, (e) shows the J_{sc} contour, (f) shows the J_{sc} heatmap, (g) V_{oc} contour, (h) V_{oc} heatmap.

Upon detailed examination of the heatmap and contour profile illustrating the thickness variation of both CZTSe and perovskite layers in Figure III. 23 (a) and (b), a clear

pattern emerges. It becomes apparent that an increase in thickness directly corresponds to a higher efficiency in the tandem solar cell. This observation can be attributed to the enhanced absorption of the solar spectrum which leads higher generation that occurs with thicker layers, and the high mobility of the perovskite permits the carriers to arrive to the exterior electrodes without recombination. although there is augmentation in the V_{oc} as shown in the Figure III. 23 (g) and (h) but it is not noticeable. because the built in voltage is at saturation, but it is worth mentioning that the tandem solar cells are 2 terminal cells stacked on top of each other in series so the voltage of the top will be added to the bottom as a series battery.

This correlation is further validated by the J_{sc} heatmap depicted in Figure III. 23 (e) and (f). Notably, as the thickness increases, the J_{sc} values also exhibit a corresponding rise. It is worth highlighting that the variation in J_{sc} is mainly influenced by the thickness of the perovskite layer. As it will be explained in following sections, the current density within the tandem solar cell is primarily controlled by the sub-cell with lower current. After examining

Taken together, these findings highlight the significance of thickness optimization in achieving higher efficiency levels in the tandem solar cell. The subsequent sections will explore into the implications of these results and discuss their broader implications for tandem solar cell design and performance.

III.4.1.2. The effect of band gap variation of the CTSe and the perovskite

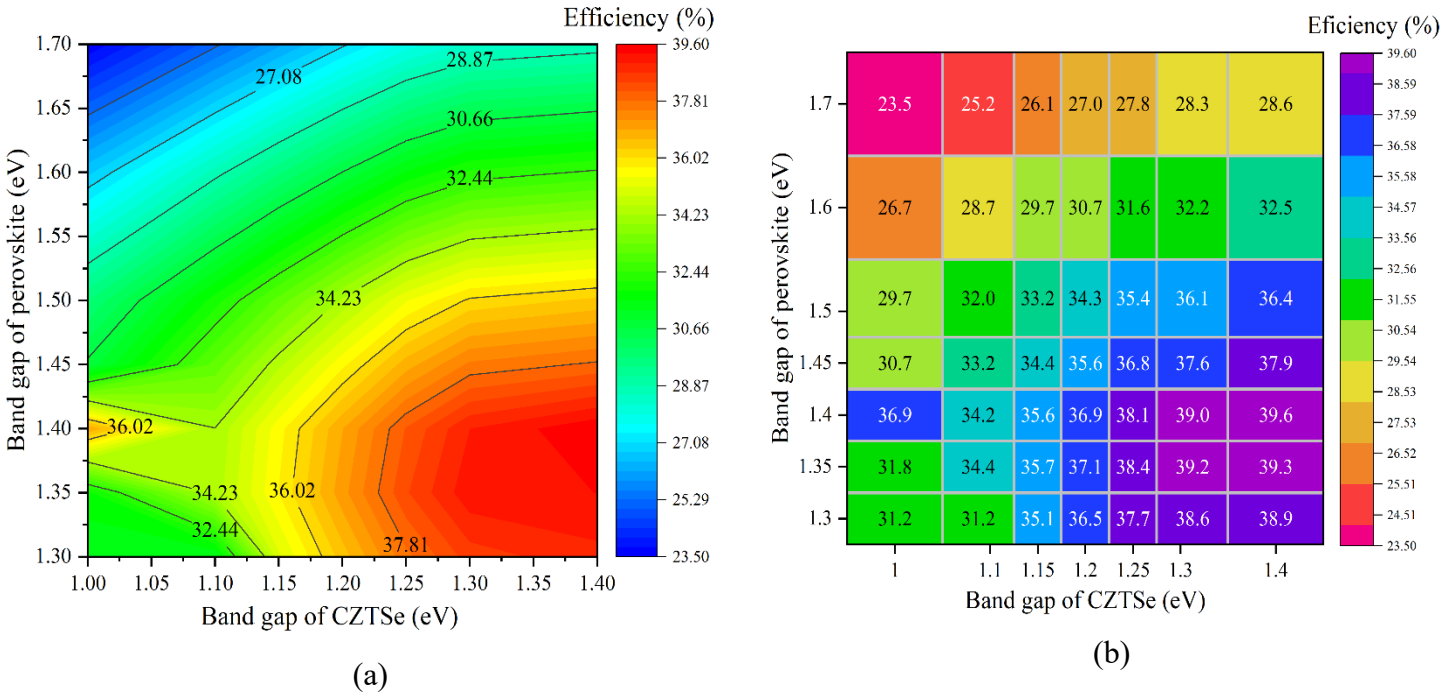

(a) (b)

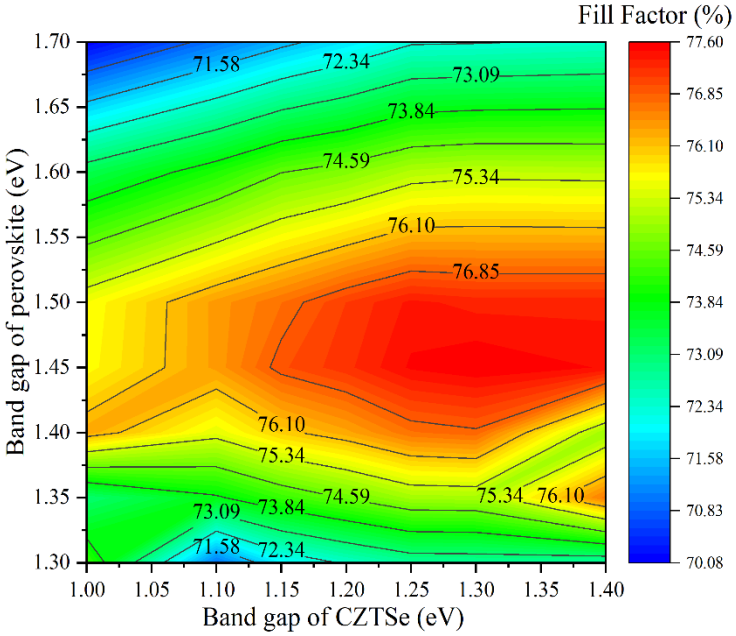
Fill Factor (%)
Band gap of perovskite (eV)
Band gap of CZTSe (eV)
71.58
72.34
73.09
73.84
74.59
75.34
76.10
76.85

(c)

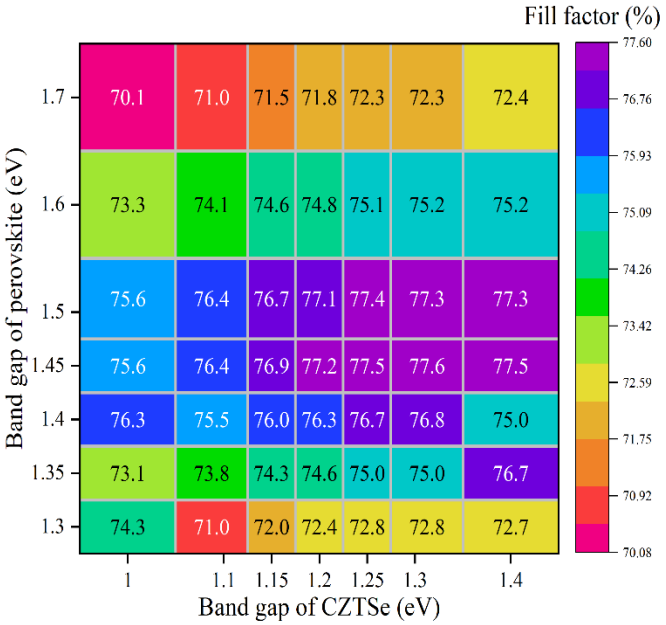
Fill factor (%)
Band gap of perovskite (eV)
Band gap of CZTSe (eV)
70.1 71.0 71.5 71.8 72.3 72.3 72.4
73.3 74.1 74.6 74.8 75.1 75.2 75.2
75.6 76.4 76.7 77.1 77.4 77.3 77.3
75.6 76.4 76.9 77.2 77.5 77.6 77.5
76.3 75.5 76.0 76.3 76.7 76.8 75.0
73.1 73.8 74.3 74.6 75.0 75.0 76.7
74.3 71.0 72.0 72.4 72.8 72.8 72.7

(d)

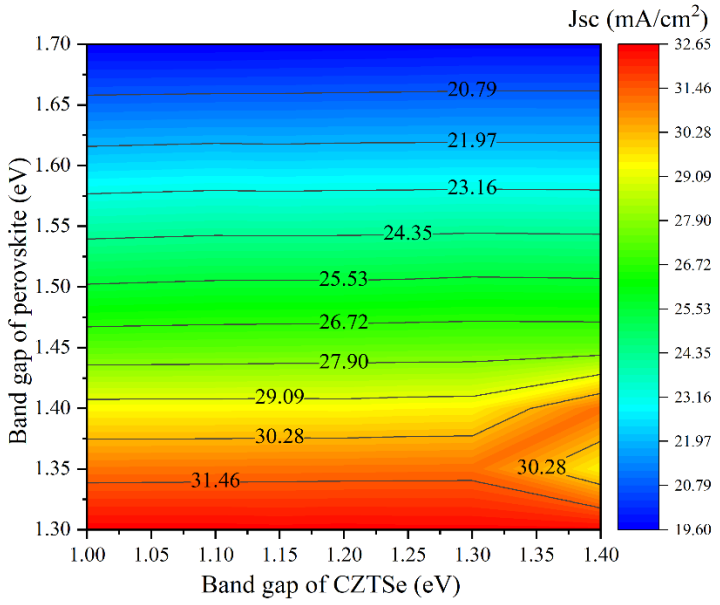
Jsc (mA/cm²)
Band gap of perovskite (eV)
Band gap of CZTSe (eV)
20.79
21.97
23.16
24.35
25.53
26.72
27.90
29.09
30.28
31.46

(e)

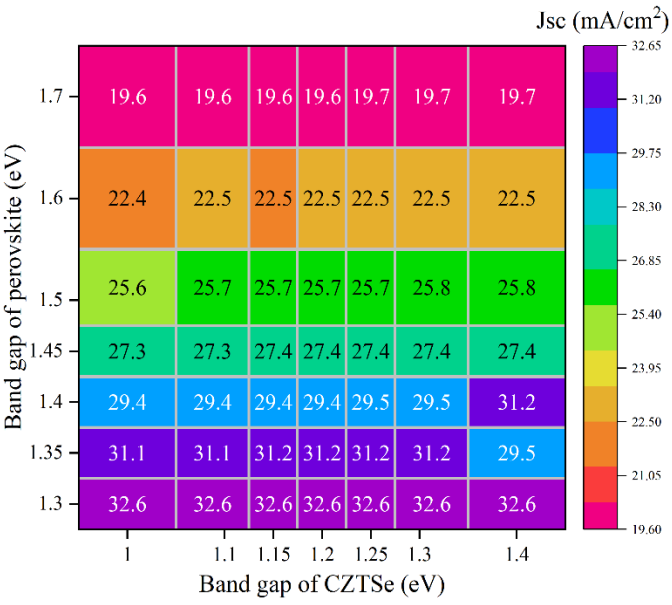
Jsc (mA/cm²)
Band gap of perovskite (eV)
Band gap of CZTSe (eV)
19.6 19.6 19.6 19.6 19.7 19.7 19.7
22.4 22.5 22.5 22.5 22.5 22.5 22.5
25.6 25.7 25.7 25.7 25.7 25.8 25.8
27.3 27.3 27.4 27.4 27.4 27.4 27.4
29.4 29.4 29.4 29.4 29.5 29.5 31.2
31.1 31.1 31.2 31.2 31.2 31.2 29.5
32.6 32.6 32.6 32.6 32.6 32.6 32.6

(f)

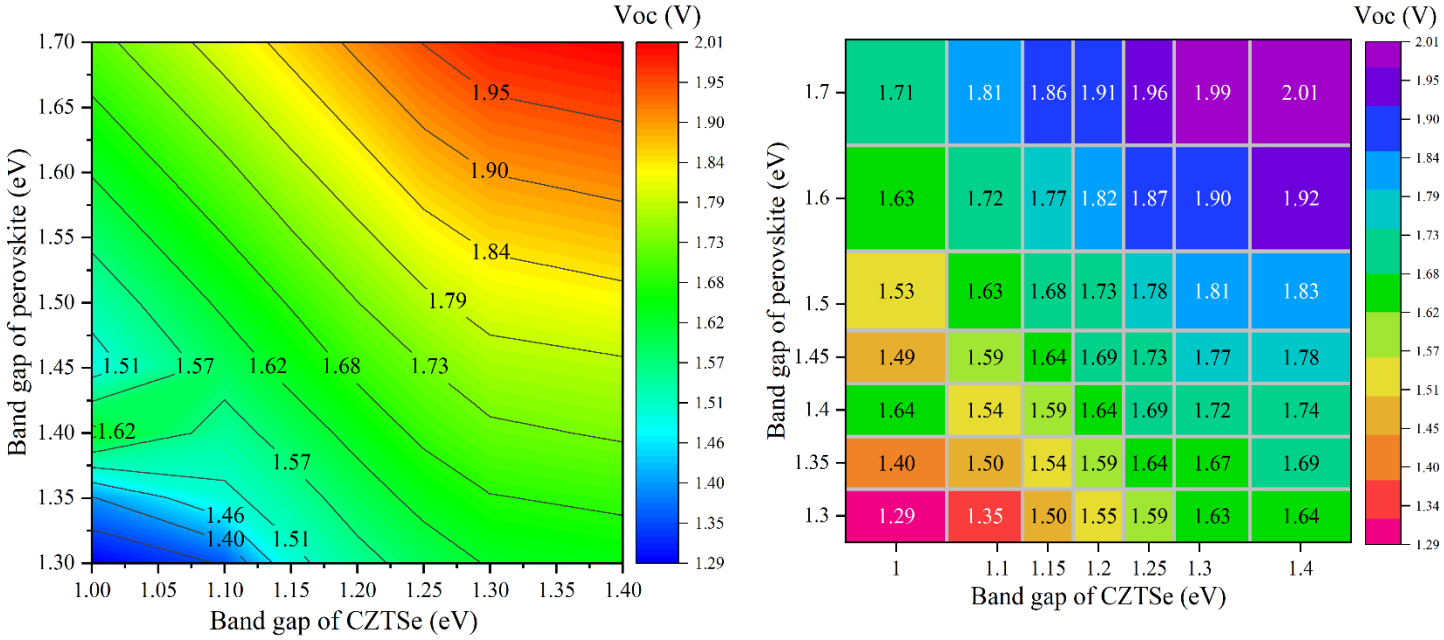

Figure III. 24: Variation of band gap of CZTSe and the perovskite sub-cells representer using contour profile and heatmap, (a) shows the efficiency contour, (b) efficiency heatmap (c) shows the fil factor, (d) fill factor heatmap, (e) shows the J_{sc} contour, (f) shows the J_{sc} heatmap, (g) V_{oc} contour, (h) V_{oc} heatmap.

Upon careful examination of the efficiency contour and heatmap showcasing the variation of band gap in Figure III. 24 (a) and (b), a clearer understanding emerges. It becomes apparent that the optimal combination for achieving the highest efficiency lies in a perovskite band gap of 1.4 eV and a CZTSe band gap of 1.25 eV. However, it is important to exercise caution and reserve conclusive decisions until we consider the final results. Additionally, as mentioned earlier on page 73, we don't take into account situations where the band gap of the lower sub-cell surpasses that of the higher sub-cell.

Moving forward with our analysis, it is noticeable that there is no direct positive correlation between efficiency and band gap. This can be attributed to the observation that higher band gaps correspond to lower J_{sc}, as evident in Figure III. 24 (e) and (f). Consequently, a higher band gap requires more energy from photons, particularly in the blue and ultraviolet regions, resulting in a reduced generation rate. Conversely, when considering V_{oc} as shown in Figure III. 24 (g) and (h), there exists a direct correlation with band gap, as the built-in voltage aligns with the absorber layer's band gap.

By elucidating these findings, we gain a deeper understanding of the intricate relationship between band gap, J_{sc}, and V_{oc}, shedding light on the complexities inherent in optimizing the performance of tandem solar cells.

III.4.2. Simulating tandem solar cell with optimal configurations

Once the finest parameters of a tandem solar cell have been obtained, we will proceed with simulating an optimal solar cell, incorporating the most advantageous configurations. In this segment, we aim to showcase the J-V characteristics.

Table III. 5: Optimal parameters of the tandem solar cell

Parameters	CZTSe	Perovskite	CIGS
Thickness	1.6 µm	0.5µm	1.2 µm
Band gap	1.25 eV	1.4 eV	1 eV

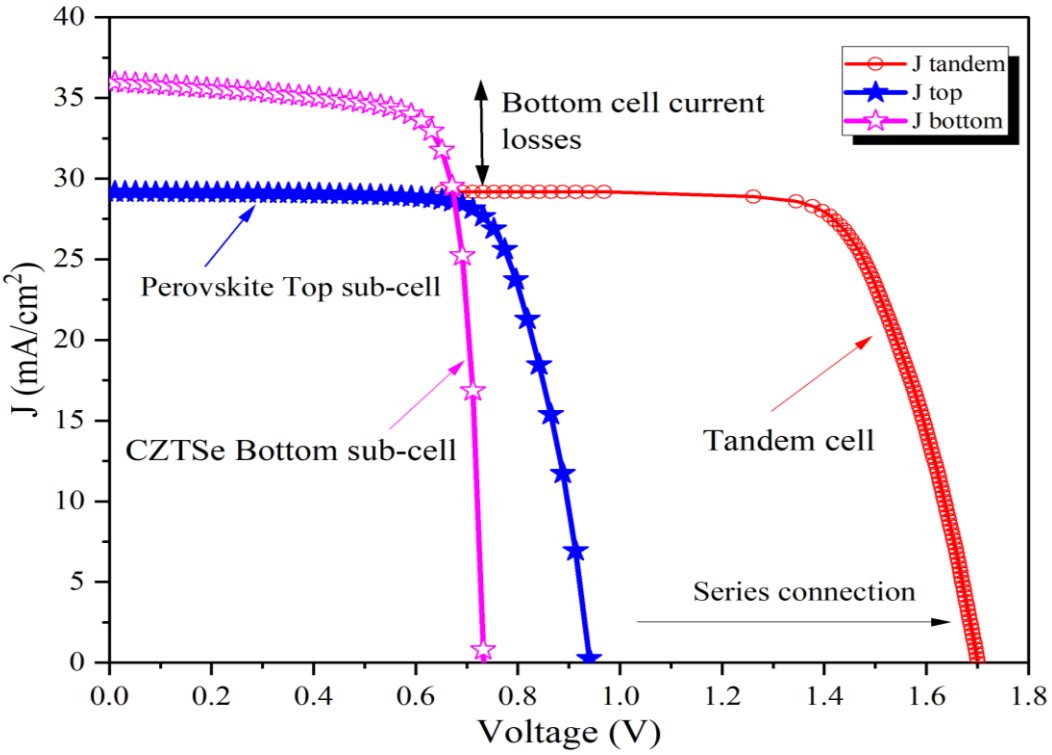

Figure III. 25: J-V characteristics for the tandem solar cell with optimized parameters

The following Table shows the parameter obtained after optimization:

Table III. 6: Output parameters of the optimal tandem solar cell

Parameter	Values	Unit
Efficiency	39.10	%
V_{oc}	1.70	Volts
J_{sc}	29.50	mA/cm2
FF	77.93	%

Upon examining the J-V characteristics depicted in Figure III. 25, it becomes evident that the tandem solar cell commences with a J_{sc} originating from the perovskite sub-cell that is characterized by its high band gap it generates the lowest current among the sub-cells. Additionally, a distinct observation arises as the voltage of the sub-cell is added to each other across the tandem structure, similar to connecting batteries in series, resulting in an augmented tandem Vo, although the J_{sc} is lowered due to perovskite sub-cell, the efficiency was compensated with the augmentation of V_{oc}.

III.5. Conclusion:

After conducting an extensive simulation using the SCAPS 1d software, a novel solar cell structure consisting of multiple layers stocked in tandem configuration has been examined in this study. The aim was to optimize the performance of the thin film solar cell and explore the potential benefits of incorporating additional absorber layers.

Throughout the examination, various modifications were made to the cell's structure, and additional materials were introduced to enhance its efficiency. The results have led us to conclude that the most favorable outcomes are achieved when the p-CIGS layer is kept within the range of 1.4-1.5 µm even enabling us to go lower in a double-layered configuration. This configuration not only ensures an optimal performance but also overcomes the limitations associated with excessive thickness.

Furthermore, it is crucial to mention the optimized configuration for the bottom cell, where a p-CZTSe layer with a thickness of 1.6 µm. The selection of the band gap has also been a crucial consideration, with the double-layered bottom cell requiring a value of 1.33 eV for optimal performance, while in a tandem structure necessitates a lower band gap of about 1,2 eV to meet the established regulations for the tandem structure.

Moreover, it is worth noting that the perovskite configuration follows a similar approach to the CZTSe layer, but with a distinctively designed structure. The band gap was tailored to 1.4 eV for the $RbGeI_3$ to ensure optimal functioning of the tandem structure. Additionally, a thickness of 0.5 µm was found to achieve high efficiency.

With these valuable findings, which have contributed to the enlarging knowledge in the field of thin film solar cells, our study demonstrates that the novel structure proposed in this research outperforms previously conducted studies. In comparison to a simple CIGS/Perovskite tandem solar cell that outcome an efficiency of 35.36% [51], our optimized structure has achieved an impressive efficiency. This remarkable result not only highlights the significant advancements made in the field but also offers promising possibilities for future research and development.

General conclusion

\

General conclusion:

In this study, we delve into the realm of solar cell innovation, exploring a novel structure that promises remarkable efficiency. Our study centres around a core configuration consisting of p-CIGS/n-Cds/n-ZnO layers. To further enhance the structure's potential, we introduce a CZTSe layer and meticulously optimize its parameters through a series of simulations, although the high efficiency, the possibility of addition of another cell to create a tandem cell with the $RbGeI_3$, that has the ability to achieve the pinnacle of efficiency was tempting.

Through the utilization of SCAPS 1d software, we embark on a simulation journey that encompasses a solar cell composition comprising p-CIGS /n-CdS/n-ZnO this simulation led us to elevate the efficiency of the single junction cell till about 25%, the question after that was how to enhance even more.

Thus, introducing an absorber layer CZTSe over the exciting CIGS. The inclusion of the CZTSe absorber layer is driven by its abundance of components, which enables the reduction in the thickness of the costly CIGS layer without sacrificing solar cell performance a vital consideration in cost-effective production. The effects of layer thicknesses and doping concentrations are subjected to meticulous optimization in order to yield a solar cell boasting outstanding performance parameters: an efficiency rating of 28%, VCO of 0.75 V, J_{SC} of 52.2 mA/cm2, and FF of 71.1%. The optimized values for layer thickness are as follows, CZTSe at 1.5 µm, and CdS buffer layer at 0.5 µm, while maintaining CIGS has been lower by 500 nm up to 800 nm in a tandem configuration.

The inclusion of the RbGeI3 perovskite layer brings about a significant improvement in the solar cell's efficiency, ultimately yielding an impressive 39% efficiency rating. This remarkable enhancement demonstrates the potential of this novel solar cell structure in harnessing solar energy more effectively.

Moreover, the integration of the RbGeI3 perovskite layer offers additional benefits beyond efficiency gains. The tandem enables the use of thinner layers of cheap materials while maintaining or even improving cell performance.

The incorporation of the RbGeI3 perovskite tandem cell in the solar cell structure, along with the optimized core configuration and CZTSe absorber layer, represents a significant breakthrough in solar cell technology. The findings from this study provide

crucial insights into the development of high-efficiency, cost-effective, and environmentally friendly solar cells. With a 39% efficiency rating, this novel solar cell structure holds great promise for advancing the utilization of solar energy and accelerating the transition to sustainable power sources.

Bibliography

[1] Leonid A. Kosyachenko, *Solar Cells New Approaches and Reviews*. AvE4EvA, 2015.

[2] Zekai Şen, *Solar Energy Fundamentals and Modeling Techniques : Atmosphere, Environment, Climate Change and Renewable Energy*. London: Springer-Verlag, 2008.

[3] J. Bisquert, *The Physics of Solar Cells: Perovskites, Organics, and Photovoltaic Fundamentals*. 2017. doi: 10.1201/b22380.

[4] Serdouk Mohammed Ridha, "Etude par simulation numérique des propriétés électriques d'une cellule solaire en silicium amorphe hydrogéné (a-Si:H)," MAGISTER, Université Mohamed Khider – Biskra, 2015.

[5] A. Kavaz *et al.*, *Solar Tree Project*. 2014.

[6] Ben Aicha Amina, Cherifi Souad, Frioua Chaima, "Simulation numérique d'une cellule solaire tandem à couche mince," MASTER ACADEMIQUE, Université Echahid Hamma Lakhdar El-Oued, Algerie.

[7] Gilles Poulain, "Procédés laser pour la réalisation de cellules photovoltaïques en silicium à haut rendement," HAL, France, 2014.

[8] Jošt, M *et al.*, "Subcell operation and long-term stability analysis of perovskite-based tandem solar cells using a bichromatic LED light source," 2021, [Online]. Available: https://www.researchgate.net/

[9] Hans Joachim Moller, *Semiconductors for solar cell applications*, vol. 35. Great Britain.: Pergamon Press, 1991.

[10] D. K. Prasad, *Designing with Solar Power: A Source Book for Building Integrated Photovoltaics (BiPV)*. Images Publishing, 2005.

[11] A.Mouhoub, "technique et systeme photovoltaique," Oct. 24, 2022.

[12] D. Mesquita, J. Lucas de Souza Silva, H. Moreira, M. Kitayama da Silva, and M. Villalva, *A review and analysis of technologies applied in PV modules*. 2019. doi: 10.1109/ISGT-LA.2019.8895369.

[13] "Polycrystalline silicon solar cell," *Science Photo Library*. https://www.sciencephoto.com/media/571070/view/polycrystalline-silicon-solar-cell (accessed Jun. 03, 2023).

[14] "Innovation: Thin Film Solar Cells at MX2016," *MaterialDistrict*, Jan. 02, 2016. https://materialdistrict.com/article/innovation-thin-film-solar-cells-at-mx2016/ (accessed Jun. 03, 2023).

[15] M. S. Alvar, "DEVICE PHYSICS OF PEROVSKITE SOLAR CELLS," DISSERTATION, MAX-PLANCK INSTITUTE FOR POLYMER RESEARCH AND JOHANNES GUTENBERG UNIVERSITY OF MAIN, MAX-PLANCK INSTITUTE FOR POLYMER RESEARCH AND JOHANNES GUTENBERG UNIVERSITY OF MAIN.

[16] G. Li, R. Zhu, and Y. Yang, "Polymer solar cells," *Nature Photon*, vol. 6, no. 3, Art. no. 3, Mar. 2012, doi: 10.1038/nphoton.2012.11.

[17] H. Cotal *et al.*, "III–V multijunction solar cells for concentrating photovoltaics," *Energy & Environmental Science*, vol. 2, no. 2, pp. 174–192, 2009, doi: 10.1039/B809257E.

[18] F. Dimroth and S. Kurtz, "High-Efficiency Multijunction Solar Cells," *MRS Bulletin*, vol. 32, no. 3, pp. 230–235, Mar. 2007, doi: 10.1557/mrs2007.27.

[19] H. Baig, K. C. Heasman, and T. K. Mallick, "Non-uniform illumination in concentrating solar cells," *Renewable and Sustainable Energy Reviews*, vol. 16, no. 8, pp. 5890–5909, Oct. 2012, doi: 10.1016/j.rser.2012.06.020.

[20] Mohammad, "Device physics of perovskite solar cells," DISSERTATION, Max-Planck institute for polymer research, Mayence, 2020.

[21] M. Sajedi Alvar, P. W. M. Blom, and G.-J. A. H. Wetzelaer, "Device Model for Methylammonium Lead Iodide Perovskite With Experimentally Validated Ion Dynamics," *Advanced Electronic Materials*, vol. 6, no. 6, p. 1900935, 2020, doi: 10.1002/aelm.201900935.

[22] "Solar Cell I-V Characteristic and the Solar Cell I-V Curve," *Alternative Energy Tutorials*, Feb. 16, 2021. https://www.alternative-energy-tutorials.com/photovoltaics/solar-cell-i-v-characteristic.html (accessed Jun. 03, 2023).
[23] R. Strandberg, "Analytic JV -Characteristics of Ideal Intermediate Band Solar Cells and Solar Cells With Up and Downconverters," *IEEE Transactions on Electron Devices*, vol. 64, no. 5, pp. 2275–2282, May 2017, doi: 10.1109/TED.2017.2686359.
[24] S. Ishraq and K. Hossain, "Assessment on flexible solar cells and their applications," Jun. 2017, doi: 10.13140/RG.2.2.31416.44805.
[25] Victor Karpov, Diana Shvydka, *Physics of Thin-Film Photovoltaics*. USA: John Wiley & Sons, 2022.
[26] Xiao-Yu Yang, *Photoenergy and Thin Film Materials | Wiley Online Books*. Scrivener Publishing LLC, 2019. Accessed: Jun. 03, 2023. [Online]. Available: https://onlinelibrary.wiley.com/doi/book/10.1002/9781119580546
[27] E. Ghorbani *et al.*, "Hybrid-Functional Calculations on the Incorporation of Na and K Impurities into the CuInSe and CuIn Solar-Cell Materials," *J. Phys. Chem. C*, vol. 119, no. 45, pp. 25197–25203, Nov. 2015, doi: 10.1021/acs.jpcc.5b07639.
[28] "What is epitaxy?," *Molecular Beam Epitaxy Research Group*, Aug. 22, 2014. https://uwaterloo.ca/molecular-beam-epitaxy/about/what-epitaxy (accessed Jun. 03, 2023).
[29] K. L. Chopra and S. R. Das, *Thin Film Solar Cells*. Boston, MA: Springer US, 1983. doi: 10.1007/978-1-4899-0418-8.
[30] P. Bras, "Sputtering-based processes for thin film chalcogenide solar cells on steel substrates," 2017, Accessed: Jun. 03, 2023. [Online]. Available: https://urn.kb.se/resolve?urn=urn:nbn:se:uu:diva-329778
[31] Shahzada Ahmad, Samrana Kazim, and Michael Gratzel, *Perovskite Solar Cells: Materials, Processes, and Devices*. Germany: WILEY-VCH GmbH, 2022.
[32] Q. Wali, N. K. Elumalai, Y. Iqbal, A. Uddin, and R. Jose, "Tandem perovskite solar cells," *Renewable and Sustainable Energy Reviews*, vol. 84, pp. 89–110, Mar. 2018, doi: 10.1016/j.rser.2018.01.005.
[33] Marc Burgelman and Marc Burgelman ,Koen Decock, Alex Niemegeers, Johan Verschraegen, Stefaan Degrave, *SCAPS manual*. 'Belgium: University of Gent, 2021.
[34] Grishma Pindolia , Satyam M. Shinde , Prafulla K. Jha b, "Optimization of an inorganic lead free RbGeI3 based perovskite solar cell by SCAPS-1D simulation," *Elsevier Ltd*, Mar. 2022, [Online]. Available: www.elsevier.com/locate/solener
[35] Khursheed Parrey, Tamkeen Farooq,Shakeel Ahmad Khandy, Apurva Gupta, "First principle studies on structure, magneto-electronic and elastic properties of photovoltaic semiconductor halide (RbGeI3) and ferromagnetic half metal oxide (RbDyO3)." https://www.researchgate.net/publication/331854713_First_principle_studies_on_structure_magneto-electronic_and_elastic_properties_of_photovoltaic_semiconductor_halide_RbGeI3_and_ferromagnetic_half_metal_oxide_RbDyO3 (accessed Jun. 04, 2023).
[36] Pia Dally, "Cellules Solaires à base de Matériaux Pérovskites : De la caractérisation des matériaux à l'amélioration des rendements et de la stabilité," Dissertation, HAL, France, 2020.
[37] J. S. Shaikh *et al.*, "Perovskite solar cells: In pursuit of efficiency and stability," *Materials & Design*, vol. 136, pp. 54–80, Dec. 2017, doi: 10.1016/j.matdes.2017.09.037.
[38] N. Bakr, Z. Khodair, and S. Mundher, "Effect of Substrate Temperature on Structural and Optical Properties of Cu 2 ZnSnS 4 (CZTS) Films Prepared by Chemical Spray Pyrolysis Method," *Research Journal of Pharmaceutical, Biological and Chemical Sciences*, vol. 5, pp. 51–61, Oct. 2015.
[39] N. Selmane, A. Cheknane, F. Khemloul, M. Helal, and H. Hilal, "Cost-saving and performance-enhancement of CuInGaSe solar cells by adding CuZnSnSe as a second absorber," *Solar Energy*, vol. Volume 234, pp. 64–80, Feb. 2022, doi: 10.1016/j.solener.2022.01.072.

[40] L. Sravani, S. Routray, M. Courel, and K. P. Pradhan, “Loss mechanisms in CZTS and CZTSe Kesterite thin-film solar cells: Understanding the complexity of defect density,” *Solar Energy*, vol. 227, pp. 56–66, Oct. 2021, doi: 10.1016/j.solener.2021.08.052.
[41] S. Delbos, “Këwhile thin films for photovoltaics: A review,” *European Physical Journal Plus*, vol. 3, p. 35004, Aug. 2012, doi: 10.1051/epjpv/2012008.
[42] Jiaxiong Xu, Junhui Lin, Chunan Zhuang, “Analysis of the open-circuit voltage of Cu2ZnSn(S, Se)4 thin film solar cell”.
[43] Shahin Enayati Maklavani and Shahram Mohammadnejad, “Reduction of interface recombination current for higher performance of p+-CZTSxSe(1-x)/p-CZTS/n-CdS thin-film solar cells using Kesterite intermediate layers,” *Solar Energy*, vol. 204, pp. 489–500, Jul. 2020, doi: 10.1016/j.solener.2020.04.096.
[44] T. Jesper Jacobsson, Adam Hultqvist, Sebastian Svanström, Lars Riekehr, and Ute B. Cappel, “2-Terminal CIGS-perovskite tandem cells: A layer by layer exploration”, [Online]. Available: https://www.sciencedirect.com/science/article/pii/S0038092X20306472
[45] D.K. Sarkar, M. Mottakin, A.K Mahmud Hasan, V. Selvanathan, K. Sobayel, “A comprehensive study on RbGeI3 based inorganic perovskite solar cell using green synthesized CuCrO2 as hole conductor,” 2023, [Online]. Available: https://www.sciencedirect.com/science/article/abs/pii/S1010603023000886
[46] Tongha-Mary Ekwu, Eli Danladi, Nicholas Tasie, Rita C Obasi, “A qualitative theoretical study of inorganic HTM-Free RbGeI3 based perovskite solar cells using SCAPS 1D as a pathway towards 3.601% efficiency,” Mar. 2023. https://www.researchgate.net/publication/368958459_A_QUALITATIVE_THEORETICAL_STUDY_OF_INORGANIC_HTM-FREE_RbGeI3_BASED_PEROVSKITE_SOLAR_CELLS_USING_SCAPS-1D_AS_A_PATHWAY_TOWARDS_3601_EFFICIENCY?enrichId=rgreq-c1e742df20040c78abeefdb4ab4e8ce4-XXX&enrichSource=Y292ZXJQYWdlOzM2ODk1ODQ1OTtBUzoxMTQzMTI4MTEyMzkyNDkwNEAxNjc3ODM2NDE1MzE4&el=1_x_3&_esc=publicationCoverPdf (accessed Jun. 07, 2023).
[47] Niclas D. Weimar, “CZTS Solar Cells,” *sinovoltaics*, Jun. 01, 2023. https://sinovoltaics.com/learning-center/solar-cells/czts-solar-cells/
[48] Naceur Selmane, Ali Cheknane, Michel Aillerie, and Hikmat S. Hila, “Effect of ZnO-Based TCO on the Performance of a-Si H(n)/a-Si H(i)/c-Si H(p)/Al BSF(p+)/Al Heterojunction Solar Cells,” 2018, [Online]. Available: wileyonlinelibrary.com
[49] Naceur Selmane, Ali Cheknane, and Hikmat S. Hilal, “Optimization of Al-Doped ZnO Transparent Conducting Oxide and Emitter Layers for Enhanced Performance of Si Heterojunction Solar Cells,” *Journal of Electronic Materials*, 2020.
[50] F.Jain, “lecture 14 and 13,” University of Connecticu (UCONN), Storrs., 216AD.
[51] M. M. Salah, A. Zekry, A. Shaker, M. Abouelatta, M. Mousa, and A. Saeed, “Investigation of Electron Transport Material-Free Perovskite/CIGS Tandem Solar Cell,” *Energies*, vol. 15, no. 17, Art. no. 17, Jan. 2022, doi: 10.3390/en15176326.

Abstract :

This research focuses on addressing the challenges associated with indium-based CuInGaSe (CIGS) solar cells by proposing a novel solar cell structure. The objective is to maintain the benefits of CIGS structures while reducing the use of costly and hazardous elements. The proposed structure involves the addition of a CuZnSnSe (CZTSe) layer to the core configuration (p-CIGS/n-Cds/n-ZnO) and optimizing it to achieve high efficiency. Through optimization of parameters such as layer thickness, doping concentration and band gap while maintaining a reduced CIGS layer thickness. The results demonstrate that adding a CZTSe layer will increase the efficiency of the cell from 25% until 28%, this is while lowering some toxic materials and adding environmentally friendly martials. In continuation of the research, the proposed solar cell structure with the CZTSe double absorber layer demonstrates promising performance enhancements. Building upon this progress, an additional novel feature is introduced by incorporating a rubidium germanium triiodide ($RbGeI_3$) perovskite layer to form a tandem solar cell configuration. The perovskite layer, placed on top of the CZTSe/CIGS double absorber layer, aims to further enhance the efficiency of the solar cell and also holds the potential to achieve efficiencies nearing 40%.

Keywords: CIGS, CZTSe, Perovskite, $RbGeI_3$, Tandem, Double absorber

Résume :

Cette recherche vise à relever les défis associés aux cellules solaires CuInGaSe (CIGS) à base d'indium en proposant une nouvelle structure de cellule solaire. L'objectif est de maintenir les avantages des structures CIGS tout en réduisant l'utilisation d'éléments coûteux et toxique. La structure proposée implique l'ajout d'une couche de CuZnSnSe (CZTSe) à une configuration fondamentale (p-CIGS/n-Cds/n-ZnO) et son optimisation pour atteindre une efficacité élevée. Grâce à l'optimisation de paramètres tels que l'épaisseur de couche, la concentration de dopage et la bande interdite tout en maintenant une épaisseur de couche CIGS réduite. Les résultats démontrent que l'ajout d'une couche de CZTSe augmentera l'efficacité de la cellule de 25% jusqu'à 28%, tout en réduisant certains matériaux toxiques et en ajoutant des matériaux martiaux respectueux de l'environnement. Dans la continuité de la recherche, la structure de cellule solaire proposée avec la double couche d'absorbeur CZTSe démontre des améliorations de performances prometteuses. S'appuyant sur ces progrès, une nouvelle fonctionnalité supplémentaire est introduite en incorporant une couche de pérovskite de triiodure de rubidium-germanium ($RbGeI_3$) pour former une configuration de cellule solaire en tandem. La couche de pérovskite, placée au-dessus de la couche à double absorbeur CZTSe/CIGS, vise à améliorer encore l'efficacité de la cellule solaire et a également le potentiel d'atteindre des rendements proches de 40 %.

Mots clés : CIGS, CZTSe, Pérovskite, RbGeI3, Tandem, Double absorbeur

ملخص:

يركز هذا البحث على معالجة التحديات المرتبطة بالخلايا الشمسية CuInGaSe (CIGS) القائمة على الإنديوم من خلال اقتراح هيكل خلية شمسية جديد. الهدف هو الحفاظ على فوائد هياكل CIGS مع تقليل استخدام العناصر المكلفة والخطرة. يتضمن الهيكل المقترح إضافة طبقة CuZnSnSe (CZTSe) إلى التكوين الأساسي (p-CIGS / n-Cds / n-ZnO) وتحسينها لتحقيق كفاءة عالية. من خلال تحسين المعلمات مثل سماكة الطبقة وتركيز المنشطات وفجوة النطاق مع الحفاظ على سماكة طبقة CIGS مخفضة. أظهرت النتائج أن إضافة طبقة CZTSe ستزيد من كفاءة الخلية من 25% الى 28%، وذلك مع تقليل بعض المواد السامة وإستعمال مواد صديقة للبيئة. استمرارًا في البحث ، يوضح هيكل الخلايا الشمسية المقترح مع طبقة امتصاص مزدوجة CZTSe تحسينات واعدة في الأداء. بناءً على هذا التقدم ، تم تقديم ميزة جديدة إضافية من خلال دمج طبقة بيروفسكايت ($RbGeI_3$) لتشكيل تكوين ترادفي للخلايا الشمسية. تهدف طبقة البيروفسكايت ، الموضوعة فوق طبقة الامتصاص المزدوجة CZTSe / CIGS ، إلى زيادة تعزيز كفاءة الخلية الشمسية ولديها أيضًا إمكانية تحقيق كفاءات تقترب من 40٪.

الكلمات الرئيسية:CIGS, CZTSe, Perovskite, $RbGeI_3$, Tandem, Double absorber